Customised hydrogel matrices for osteoclast differentiation and culture

A thesis submitted to the University of Manchester for the degree of

Doctor of Philosophy

in the

Faculty of Biology, Medicine and Health

2022

Mattia Vitale

The School of Biological Sciences

Division of Cell Matrix Biology and Regenerative Medicine

Contents

Word count: 42223

List of figures

Chapter 1

Figure 7 Formation of the Fmoc-FF peptide hydrogel structure. The peptide spontaneously organises into β-sheets with anti-parallel orientation (**A**). Due to π–π interactions between the Fmoc groups, these β-sheets then come together (**B**). The interlocking Fmoc groups act like a zipper to create a cylindrical structure (**C** and **D**). Adapted from R. V Ulijn and Smith, 2008.

Figure 8 Fmoc-based peptide hydrogels with tuneable stiffness to mimic different human tissues for TE applications. Soft hydrogels (0.8-1.1 kPa, left) can be used to mimic very soft tissues such as brain; medium soft (3-4 kPa, middle) and stiff hydrogels (8-9.2 kPa, right) can be used for harder musculoskeletal tissues such as muscle, cartilage of bone. Adapted from Biogelx.co.uk.

Chapter 2

Figure 9. Schematic illustration of the protocol to prepare hydrogels for cell culture.

Figure 10 Photo image of Raw 264.7 morphology at low and high cell density. Figure adapted from ATCC (ATCC, 2018).

Figure 11 F-actin staining of Raw 264.7 cells cultured on a TCPS surface (**A**) and Fmoc-based hydrogels (**B**). Raw 264.7 cells cultured on hydrogels maintain the same physiological shape, diameter and spreading as those on TCPS (N=2), up to 96 h post culture. The cells are clearly visible and spread on each of the hydrogel formulations tested. Elongated pseudopodia are clearly observable in green (Alexa Fluor 488 phalloidin). Nuclei are stained with Hoechst 33342 (blue). Scale bars on each panel indicate 20 µm.

Figure 12 Live/Dead assay of Raw 264.7 cells cultured on Fmoc-FF/S hydrogel at different time points. Calcein AM (green) and Ethidium homodimer-1 (red) were used to assess viable and dead cells respectively. Scale bars on each panel indicate 100 µm.

Figure 13 Live/Dead assay of Raw 264.7 cells cultured on Fmoc-FF/S/RGD hydrogels at different time points. Staining and scale bars as in Figure 12.

Figure 14 Molecular structure of the three building blocks Fmoc-FF, Fmoc-S, Fmoc-RGD. The Fmoc-FF/S is made from Fmoc-FF and Fmoc-S in a 1:1 ratio. The Fmoc-FF/S/RGD hydrogel is made from these two peptides plus Fmoc-RGD in a 1:0.5:0.5 ratio.

Figure 15 (**A**) Schematic representation of the optimised protocol used to incorporate the Hap nanopowder within hydrogels. (**B**) Pre-gel and hydrogel vials images with or without addition of Hap.

Figure 16 Effect of Hap nanoparticle concentration on the storage moduli (1 Hz frequency, 0.1% shear strain) of Fmoc-FF/S and Fmoc-FF/S/RGD decorated hydrogels.

Figure 17 Homogeneous distribution of Hap nanoparticles within the hydrogel network. (**A**) Image stack of Fmoc-FF/S/RGD hydrogel showing calcein-stained Hap (conc. 1mg/ml) homogenously distributed within the gel network. (**B**) Cumulative release fit of Hap from Fmoc-FF/S/RGD hydrogel over time. Data were obtained using the same method described above to label the Hap nanoparticles.

Figure 18 Analysis of hydrogel microstructure by AFM and distributions of fibre widths as measured on the AFM images (**A**-**D**). Hydrogel nanotopography of Fmoc-FF/S (**A**) and Fmoc-FF/S/RGD (C) without added Hap, and Fmoc-FF/S (**B**) and Fmoc-FF/S/RGD (**D**) after incorporation of Hap (Scan size 2 μm^2 , Scale bar 400 nm).

Figure 19 Size distribution of Hap nanoparticles. (**A**) AFM image of Hap nanoparticles (concentration 1 μg/ml) on a 2 μm^2 scan size region of polylysine–coated mica. (**B**) Size distribution of Hap nanoparticles when alone (grey bars), and on the Fmoc-FF/S/RGD hydrogel fibres (black bars).

Figure 20 Topography of Hap-decorated Fmoc-FF/S/RGD hydrogels. (**A**) 2 μm^2 AFM images of Fmoc-FF/S/RGD incorporating Hap in a repeating pattern. (**B**) Enlarged AFM image of the area outlined in **A** showing Hap nanoparticles decorating the Fmoc-FF/S/RGD fibres. (**C**) Corresponding height profile of the linear scan indicated by the white dotted arrow in B. (**D**) Schematic model of a hydrogel fibre incorporating Hap nanoparticles. Scale bar for A is 400 nm. Scale Bar for B is 200 nm.

Figure 21 (**A**) Frequency sweep rheology measurements (0.1-100 Hz 0.1 % strain) of Fmoc-FF/S and Fmoc-FF/S/RGD hydrogels, with and without Hap incorporation. (**B**) Photographs of the spheroids of Fmoc-FF/S (I), Fmoc-FF/S + Hap (II), Fmoc-FF/S/RGD (III) and Fmoc-FF/S/RGD + Hap (IV) used for the rheology experiments, evidencing dimensional stability for all the formulations. All measurements were performed at least 3 times at 25 °C.

Figure 22 Comparison of the storage and loss moduli of each hydrogel formulation at 1 Hz, 0.1% strain. (Data are shown as mean ± SD; ∗∗∗p -value < 0.001; ∗∗p -value < 0.05).

Figure 23 Analysis of Raw 264.7 cell culture and differentiation on 15 mM Fmoc-FF/S and Fmoc-FF/S/RGD hydrogels with and without Hap. (**A**) F-actin staining of Raw 264.7 cells after seven days culture on the different hydrogels (green: F-actin, Alexa Fluor 488 phalloidin; blue: Nuclei, Hoechst 33342; scale bars 20 μm). (**B**) Measurements of cell diameter (data shown as mean ± SD, N = 43, ∗∗p < 0.05). (**C**) Analysis of multinucleation by a violin distribution plot (data shown as number of nuclei per cell, N = 100). (D) SEM images of Raw 264.7 cells cultured on Fmoc-FF/S/RGD with or without incorporated Hap. White arrow shows elongated pseudopodia of Raw 264.7-derived OC. (Data are shown as mean ± SD; ∗∗∗p -value < 0.001; ∗∗p -value < 0.05).

Figure 24 F-actin staining of Raw 264.7 cultured on Fmoc-FF/S/RGD with Hap in presence/absence of αvβ3. Cells treated with the antibody (right panel) showed rounded morphology with minimal or no focal adhesion. Untreated cells are spread with prominent pseudopodia interacting with the gel matrix.

Figure 25 (**A**) Analysis of viability of Raw 264.7 cells cultured on Fmoc-FF/S/RGD + Hap at different time points using a LIVE/DEAD assay (green: viable cells, calcein AM; red: dead cells, ethidium homodimer-1; scale bar 100 μm). (**B**) PicoGreen fluorescence quantification of dsDNA of Raw 264.7 cells cultured on Fmoc-FF/S/RGD + Hap at different time points (24 h values were used as baseline control).

Figure 26 (**A**) Immunofluorescence staining of TRAP (green: F-actin, Alexa Fluor 488 phalloidin; red: TRAP, anti-TRAP mAb conjugated Alexa Fluor 594). (**B**) Relative TRAP immunofluorescence intensity of cells cultured on Hap-decorated Fmoc-FF/S/RGD hydrogels compared to the naked Fmoc-FF/S/RGD (fluorescence intensity was measured from at least N = 100 cells and corrected against the background). (**C**) Gene expression of TRAP relative to GAPDH by Raw 264.7 cells (n = 3) after three (D3) and seven (D7) days culture on Hap-decorated Fmoc-FF/S/RGD hydrogel. (Data shown as mean ± SD; ∗∗∗p < 0.001; ∗∗p < 0.05).

Chapter 3

Figure 27 Domain architectures, sequence lengths and thermal stability of recombinant collagen constructs. The darker-hue green Col domain in EPclA represents a bacterial triple

helical collagen domain, whereas the yellow Colα2 domains represent varying lengths of human type 2 collagen sequence. The light green Col domain in DCol1 is a shorter collagen sequence made up of two 30 amino-acid blocks flanking the GFPGER integrin binding site. DCol1 sequence design was guided by the amino acid preferences of EPclA. The Tm values show the denaturation temperatures of the respective collagen domains. PfN (red) – phage fibre N terminal capping domain; PfC (blue) – phage fibre C terminal capping domain; PCoil (orange) – coiled-coil domain forming a trimeric helix (Ghosh et al., 2012); H – terminal 6xHis tags, which can be N or C terminal. The green stars show GFPGER integrin binding sites.

Figure 28 Collagen protein characterisation. (**A**) SDS-PAGE analysis of the purification of DCol1. Lane compositions: M, molecular weight markers; FT, flow through; 1–2, wash fractions with 60 mM imidazole; 3–4, elution fractions with 250 mM imidazole; 5–8 elution fractions with 1 M imidazole. (**B**) CD spectra at 4°C of RTC (grey), DCol1 (blue) and GFOGER (red). The vertical axis measures the mean residue ellipticity θ in degrees cm^2 $dmol^{-1}$. CD data were collected between 190 and 260 nm.

Figure 29 Schematic representation of the optimised protocol used to incorporate proteins within hydrogels. Protein of interest were diluted up to the desired concentration in the well plate. Fmoc-FF/S pre-gel solution was then pipetted into the protein containing solution to form a spheroid like to allow protein incorporation.

Figure 30 Analysis of spheroid-shaped hydrogels under visible (I) and UV (II) light. All spheroids show dimensional stability indicating a self-supporting structure consistent with a successful hydrogel self-assembling mechanism. Spheroids of hydrogels modified with eGFP and GFOGER show fluorescence under UV light, indicating successful protein and peptide incorporation (see main text).

Figure 31 SDS-PAGE of GFOGER peptide labelled with NHS-Fluorescein under normal and UV light. Lane composition is: M, molecular weight; 2-3, 5-6, 8-9, NHS-Fluorescein labelled-GFOGER.

Figure 32 SDS-PAGE analysis of (**A**) protein incorporation into the hydrogel spheroids, and (**B**) retention inside the hydrogels over time. The GFOGER bands are obtained from fluorescence after UV exposure of the gels. Panel (**A**) Lanes: M, molecular weight markers; 1, protein stock solution; 2, protein incorporated into the hydrogel spheroid; 3, remaining protein into the well solution. Panel (**B**) Lanes: **M**, molecular weight markers; **24**, **48**, **72 h**, protein

retention over time. Arrows indicate the different protein bands and their corresponding molecular weights.

Figure 33 Fluorescence spectroscopy spectra of Fmoc-FF/S peptide (grey), collagen (red) and Fmoc- FF/S-collagen solutions (blue) prepared in PBS (pH = 7.4). Excitation wavelength 280 nm; emission wavelength recorded within the 300–400 nm range.

Figure 34 Scanning electron microscopy images showing the outer (left) surface morphology of Fmoc-FF/S and the collagen-modified hydrogels at lower and higher magnification and a cross section showing the inner (right) surface morphology at higher magnification. Low magnification scale bar is 50 µm; high magnification scale bar is 5 µm.

Figure 35 Rheological amplitude sweep test (shear strain range of 0 – 100 % 1 Hz) of Fmoc-FF/S hydrogels after protein incorporation. Measurements were repeated for each modified hydrogel at three different protein concentrations (1, 50, 100 µg/ml). Line blue represents the storage modulus (G') whereas the red line illustrates the loss modulus (G").

Figure 36 Analysis of the mechanical properties of the Fmoc-FF/S hydrogels after incorporation of proteins at different concentrations. (**A**) Storage and loss moduli (0.02% strain, 1 Hz) of Fmoc-FF/S hydrogels with and without collagen or eGFP at different concentrations (1, 50, 100 µg/mL). (**B**) Photographs of spheroids of Fmoc-FF/S modified with different collagen of eGFP proteins.

Figure 37 HT1080 cell adhesion and cell spreading. (**A**) F-actin staining of HT1080 cells after 24 h culture on the different collagen hydrogels (green: F-actin, Alexa Fluor 488 phalloidin; scale bars 100 µm, inset 50 µm) with and without pre-incubation with mAb13 (anti β_1) antibody. (**B**) Analysis of cell adhesion on the different collagen-modified hydrogels without (blue bars) and with (grey bars) pre-incubation with mAb13 antibody. (**C**) Spread HT1080 cells show a mean aspect ratio above 1 while rounded shaped cells are reflected by an aspect ratio 1. Data shown as mean ± SD, n = 43, */# $p < 0.05$, ns (not significant). Significance for each group is relative to Fmoc-FF/S (*), with the exception of groups shown in the grey columns which are in comparison to their respective blue columns (#).

Chapter 4

Figure 38 X-ray crystal structure of human OSCAR ectodomain in complex with a collagen triple helical peptide. Ribbon diagram of OSCAR (green) showing the two Ig domains D1 and

D2 in a semi-transparent surface. The collagen triple helical peptide is shown as three chains coloured blue, yellow and magenta. Adapted from Haywood *et al.*, 2016.

Figure 39. Domain architectures of the recombinant proteins OCol1, DCol1 and the parent recombinant collagen EPclA (Ghosh *et al.*, 2012a). Key to domain names and colors: **PfN** (red) – phage fiber N terminal capping domain; **PfC** (blue) – phage fiber C terminal capping domain; **PCoil** (orange) – phage trimeric coiled-coil domain; **H** – hexa-histidine tag (His_6). The red and yellow stars indicate approximate positions of OSCAR and integrin binding sites.

Figure 40 CD spectra at 4°C (black line), 70°C (red line) and 4°C after denaturation (green dashed line) for OP1, OP1* and OCol1. The vertical axis measures mean residue ellipticity θ in degrees cm2 dmol−1. CD data were collected between 190 and 260 nm.

Figure 41 Thermal denaturation of the OP1, OP1* and OCo1, monitored by CD at 220 nm as a function of increasing temperature between 4°C and 70°C, with a protein concentration of 0.5 mg/ml in CD Buffer pH 7.4, and a heating rate of 1°C/min.

Figure 42 SPR multi-cycle kinetic analysis of OSCAR-OP1 interaction. OSCAR was immobilised onto a CM5 sensor chip surface and OP1s was flowed over the surface in assay running buffer of 10 mM PBS, 150 mM NaCl, 0.05% Tween20, pH 7.4.at a concentration series 5000 – 0 nM . Sensograms were analysed using the Langmuir 1:1 model and relative responses shown (red) with theoretical fit (black) overlaid. Experiments were performed in duplicate and sensograms presented representative of data obtained.

Figure 43 SPR multi-cycle kinetic analysis of OSCAR-OP1* interaction. Panel A shows sensograms of OSCAR-OP1*, analysed using the Langmuir 1:1 model and relative responses shown (red) with theoretical fit (black). Panel B showed steady state analysis as a measure of affinity vs OP1* concentration.

Figure 44 TRAP straining of Raw 264.7 cells cultured for up to 5 days on OP1/OP1* coated 24-well plate. Different concentrations (0-100 ng/ml) of hRANKL were used.

Figure 45 Gene expression of TRAP and OSCAR relative to GAPDH by Raw 264.7 cells (n = 3) after 24h and five (d5) days cultured on OP1 and OP1* with different concentration of hRANKL (0-100 ng/ml). (Data shown as mean ± SD; $***p < 0.001$; $**p < 0.05$).

Figure 46 OCol1 incorporation into Fmoc-FF/S/RGD with and without Hap. Panel **A** shows SDS-PAGE of OCol1 incorporated into hydrogels. Lane composition (from left to right): Molecular weight markers; 3, 4, 5 and 10, 11, 12 protein stock solution; protein incorporated into the hydrogel; remaining protein into the well, respectively. Panel **B**, photograph of Fmoc-FF/S/RGD with and without Hap incorporating OCol1.

Figure 47 Fmoc-FF/S/RGD with and without Hap incorporating OCol1.

Figure 48 (**A**) Analysis of Raw 264.7 cells after seven days culture on FF/S/RGD and OSCAR-collagen modified hydrogels (green: F-actin, Alexa Fluor 488 Phalloidin; blue: Nuclei, Hoechst 33342; scale bars 20 μm). (**B**) Analysis of multinucleation by a violin distribution plot (data shown as number of nuclei per cell, N = 100). (**C**) Measurements of cell diameter (data shown as mean ± SD, N = 43, $**p < 0.05$). (**D**) Table summarising the mean diameter of the cells cultured on the OSCAR modified hydrogels.

Figure 49 Analysis of viability of Raw 264.7 cells cultured on OSCAR modified Fmoc-FF/S/RGD at day 3 and day 7 using a LIVE/DEAD assay (green: viable cells, Calcein AM; red: dead cells, ethidium homodimer-1).

Figure 50 Gene expression of TRAP and OSCAR relative to GAPDH by Raw 264.7 cells (n = 3) after day three (d3) and seven (d5) days cultured on OSCAR-modified hydrogels with different concentration of 10ng/ml of hRANKL. (Data shown as mean ± SD; $***p < 0.001$; $**p < 0.05$).

List of tables

Chapter 1

Chapter 2

Chapter 3

Chapter 4

List of abbreviations

2D	Two Dimensional
3D	Three Dimensional
AFM	Atomic Force Microscopy
BMMs	Bone Marrow Isolated Macrophages
BMP	Bone Morphogenetic Protein
BSA	Bovine Serum Albumin
BTE	Bone Tissue Engineering
CAP	Calcium-Phosphate
CD	Circular Dichroism
CFU-GM	Colony Forming Unit Granulocyte–Macrophage Progenitor
CLP	Collagen-Like Peptides
CPD	Critical Point Dryer
CSFs	Colony Stimulating Factors
CTSK	Cathepsin K
D	Aspartic Acid
DAPI	4’6’-Diamidino-2-Phenylindole
DCLs	Dendritic Cells
dDH_2O	Double Deionised Water
DMEM	Dulbecco’s Modified Eagle’s Medium
DNA	Deoxyribonucleic Acid
PBS	Dulbecco’s Phosphate Buffer
ECM	Extra Cellular Matrix
EDC	1-Ethyl-3-(3-Dimethylaminopropyl)-Carbodiimide
EGFP	Enhanced Green Fluorescent Protein
EHEC	Enterohaemorrhagic *Escherichia coli*
EPCLPs	EHEC Prophage Collagen-Like Proteins
ETHD-1	Ethidium Homodimer-1
ETOH	Ethanol

F	Phenylalanine
FBS	Foetal Bovine Serum
FCRγ	Fc Receptor Common Γ
FGF	Fibroblast Growth Factor
Fmoc	Fluorenyl methoxycarbonyl
G’	Storage Modulus
G’’	Loss Modulus
GAPDH	Glyceraldehyde 3-Phosphate Dehydrogenase
GM-CSF	Granulocyte-Macrophage Colony-Stimulating Factor
HA	Hyaluronic Acid
Hap	Hydroxyapatite
HEMA	Hydroxyethyl Methacrylate
HPLC	High Performance Liquid Chromatography
HSC	Hematopoietic Stem Cell
IL-1	Interleukin-1
ITAM	Immunoreceptor Tyrosine-Based Activation Motif
K	Lysine
M-CSF	Macrophages Colony-Stimulating Factor
MMP-9	Matrix Metalloproteinase-9
NFATC1	Nuclear Factor Of Activated T Cells 1
NF-Kβ	Nuclear Factor-Kβ
NHS N-	Hydroxysuccinimide
Ni-NTA	Nickel-Nitrilotriacetic
O	4-hydroxyproline.
OBs	Osteoblasts
OCps	Osteoclast Precursor Cells
OCs	Osteoclasts
OP	OSCAR Peptides
OPG	Osteoprotegerin
OSCAR	Osteoclast–Associated Receptor

P4H	Prolyl-4-Hydroxylase
PBMCs	Human Peripheral Blood Mononuclear Cells
PEG	Polyethylene Glycol
PLGA	Poly(Lactic-co-Glycolic) Acid
PSA	Penicillin-Streptomycin-Amphotericin B
PTH	Parathyroid Hormone
qPCR	Quantitative Polymerase Chain Reaction
RA	Rheumatoid Arthritis
RANK	Receptor Activator of Nuclear factor Kappa-B
RANKL	Receptor Activator Of Nuclear Factor Kappa-B Ligand
RGB	Red Green Blue
RGD	Arginine-Glycine-Aspartic Acid
RNA	Ribonucleic Acid
RT	Room Temperature
RTC	Rat Tail Collagen
S	Serine
SAPHs	Self-Assembled Peptide-Based Hydrogels
SEM	Scanning Electron Microscopy
SPR	Surface Plasmon Resonance
SSA	Steady State Analysis
TCPS	Tissue Culture Polystyrene
TE	Tissue Engineering
TGF-β	Transforming Growth Factor
TNF	Tumour Necrosis Factor
TRAF6	TNF Receptor Associated Factor 6
TRAP	Tartrate-Resistant Acid Phosphatase

Abstract

Bone is a highly dynamic tissue that constantly undergoes remodelling to ensure correct turnover over time. Bone homeostasis is finely balanced by osteoclasts, that resorb bone, and osteoblasts that lay down new bone matrix. Most studies are focused on the osteoblasts role in bone formation while osteoclasts are often overlooked. Yet, the role of osteoclasts is pivotal for bone homeostasis and aberrant osteoclast activity has been reported in several pathological diseases, such as osteoporosis and bone cancer. Therefore, it is important to develop cell culture platforms for the study of osteoclast function and their interactions with the surrounding matrix. As such the overall aim of this work is to develop customised hydrogel-based materials for use as substrates to study osteoclast differentiation and function *in vitro*. Hydrogels are water-swollen networks with great potential for tissue engineering applications. However, their use in bone regeneration has often been hampered by insufficient mechanical properties and lack of mineralization. Here are presented data on the modification of self-assembling peptide hydrogels with both minerals and matrix proteins which demonstrate the improved performance of the modified hydrogels as platforms for cell culture and differentiation. Hydroxyapatite was used in order to create a nanocomposite hydrogel with enhanced mechanical properties as well as improved bioactivity. Atomic force microscopy confirmed that hydroxyapatite nanoparticles were successfully incorporated within Fmoc-based hydrogels without disrupting the self-assembling mechanism while providing a superior scaffold with improved mechanical properties. Interestingly, the newly developed nanocomposite supported the viability and differentiation of pre-osteoclasts *in vitro*. This was confirmed by the presence of typical mature osteoclasts features (e.g. multinucleation and actin ring) and expression of typical osteoclast genes. A new protocol to incorporate collagen intro self-assembly peptide hydrogels was

also developed. Hydrogels were modified through a passive diffusion protocol in which collagen molecules of different sizes were successfully incorporated and retained over time. SDS-PAGE showed that these collagens interact with the hydrogel fibres without affecting the overall mechanical properties of the composite hydrogels. Furthermore, the collagen molecules incorporated into the hydrogels were still biologically active and provided sites for adhesion and spreading of human fibrosarcoma cells through interaction with the α2β1 integrin. Finally, the effect of collagen as costimulatory pathway during osteoclastogenesis *via* OSCAR, a well-known osteoclast associated receptor, was investigated. Different proteins containing the OSCAR-collagen binding domain and their binding to OSCAR, were characterised by circular dichroism and surface plasmon resonance, respectively. OSCAR-peptides were incorporated into the previously developed hydroxyapatite-decorated hydrogel. Resulting scaffolds were tested to assess their capability of trigger the differentiation of osteoclast compared to the unmodified hydrogels. As expected, collagen peptides containing the OSCAR-binding domain, that were incorporated into hydroxyapatite modified hydrogels, enhanced the differentiation of osteoclast precursors compared to the unmodified hydrogels.

This work laid the foundation for generating new bone-mimicking substrates that can be used as a platform to generate mature osteoclasts which can be progressed to help study the pathological mechanisms associated with their over activation during bone disease.

List of publications

- *"Role of OSCAR Signalling in Osteoclastogenesis and Bone Disease"* Iva Nedeva, **Mattia Vitale**, Ari Elson, Judith A. Hoyland and Jordi Bella. 12 April 2021, Frontiers in Cell and Developmental Biology, 9, 641162. https://doi.org/10.3389/fcell.2021.641162

- "*Hydroxyapatite-decorated Fmoc-hydrogel as a bone-mimicking substrate for osteoclast differentiation and culture*" **Mattia Vitale**, Cosimo Ligorio, Bethan McAvan, Nigel W. Hodson, Chris Allan, Stephen M. Richardson, Judith A. Hoyland and Jordi Bella. 15 January 2022. Acta Biomaterialia 138 144-154. https://doi.org/10.1016/j.actbio.2021.11.011 .

- *"Incorporation of natural and recombinant collagen proteins within Fmoc-based self-assembling peptide hydrogels"* **Mattia Vitale**, Cosimo Ligorio, Ian P.Smith, Stephen M. Richardson, Judith A. Hoyland and Jordi Bella. 21 April 2022. Gels 8, 254. https://doi.org/10.3390/gels8050254.

Acknowledgements

After all these years, this fantastic journey called PhD has finally come to an end. Writing this dissertation gave me the opportunity to reflect on my progress, how much I have learnt and how I have improved during these years. Certainly, I couldn't have done it without the help of the many people I have met during my path…

First of all, I would like to begin by thanking my supervisory team.

To Prof Judith Hoyland, for her advice, her kindness and her support even when I had lots to learn. Thanks for giving me the possibility to work in your team and for making me feel always welcome since day one.

To Dr Jordi Bella, for introducing me in the marvellous world of collagen, for having taught me so many techniques but most importantly for his day-to-day guidance. Thanks for believing in me, for giving me trust with your students and for your support during tough times. I will never forget our conversations, our insightful meetings, and your fantastic cocktails.

To Dr Stephen Richardson for our stimulating conversation and precious advice. Thanks for your time and patience with me. I still remember your comments on my Literature review and during our first one-to-one meetings. After all, it is also because of them that I have improved. For this reason, thank you.

Thank you to Pauline Baird, for welcoming me with a smile every day in the lab, for your patience and your support. Thank you to Dr Nigel Hodson for his training and help with AFM. Also, I would like to thank all the people who I worked with throughout these years. It would be impossible to name you all, but it has been a pleasure working with you.

To all my students, I hope I managed to teach you something and that you will remember me with the same smile as I remember you.

Thanks to my colleague and close friend Dr Cosimo Ligorio. If I can consider myself something like a material scientist is thank to you. You taught me everything I know about peptide-hydrogels (and more…) with patience and perseverance. I will never forget our coffees in the tea rooms, our jokes, and our laughs.

To Matty, my coach, my friend, my brother. Thanks for teaching me the sweet science. You have been fundamental during these past two years. You were there at my best but most importantly at my worst. Thanks for making me a better person.

Thanks to my friend and flatmate Ian. Our movie nights, our chats about boxing and jiu jitsu are the right break that we all need from science. Thanks for teaching me how to do deadlifts.

To my Hermano Carlos, for being always on my corner. You are the first person I met when I moved to Manchester, and I will never forget your support during my staying in WestPoint. You are a friend for life.

Above all, I would like to dedicate this thesis to my parents. I will be forever grateful to you for teaching me the respect and care of others and for providing me a good education. You have always been there for me, backing up my decisions and pushing me to my best even when I did not believe in myself. I would not be the person I am now without you therefore, Grazie Mamma e Papá.

To my beloved sister Elena for guiding me and protecting me from above… I hope that, wherever you are, you will be always proud of your big brother. If I kept fighting …it is also thanks to you.

To my Nonna Rosa for her prayers, her love, and her delicious food.

Lastly, I would like to thank Ludovica, you came into my life as a thunder in a sunny day and now we dance together in the rain. I cannot wait to see what the future holds for us.

Declaration

No portion of the work referred to in the thesis has been submitted in support of an application for another degree or qualification of this or any other university or other institute of learning.

Copyright statement

I. The author of this thesis (including any appendices and/or schedules to this thesis) owns certain copyright or related rights in it (the "Copyright") and s/he has given The University of Manchester certain rights to use such Copyright, including for administrative purposes.

II. Copies of this thesis, either in full or in extracts and whether in hard or electronic copy, may be made only in accordance with the Copyright, Designs and Patents Act 1988 (as amended) and regulations issued under it or, where appropriate, in accordance with licensing agreements which the University has from time to time. This page must form part of any such copies made.

III. The ownership of certain Copyright, patents, designs, trademarks and other intellectual property (the "Intellectual Property") and any reproductions of copyright works in the thesis, for example graphs and tables ("Reproductions"), which may be described in this thesis, may not be owned by the author and may be owned by third parties. Such Intellectual Property and Reproductions cannot and must not be made available for use without the prior written permission of the owner(s) of the relevant Intellectual Property and/or Reproductions.

Further information on the conditions under which disclosure, publication and commercialisation of this thesis, the Copyright and any Intellectual Property and/or Reproductions described in it may take place is available in the University IP Policy (see http://documents.manchester.ac.uk/DocuInfo.aspx?DocID=24420), in any relevant Thesis restriction declarations deposited in the University Library, The University Library's 14 regulations (see http://www.library.manchester.ac.uk/about/regulations/) and in The University's policy on Presentation of Theses.

Chapter 1- General Introduction

1.1 Thesis organisation

The first chapter of this thesis provides a general introduction to the general features of the bone, with a particular focus on its structure and function and the bone-specific cells, osteoblasts, and osteoclasts. Current therapies to tackle bone diseases are discussed next, as well as the use of biomaterials to treat bone defects, with particular attention to the use of hydrogels as scaffolds for bone tissue engineering (BTE), their advantages and disadvantages.

The second chapter of this thesis presents work on Fmoc-based RGD-functionalised peptide hydrogels that have been modified with hydroxyapatite (Hap) nanopowder as nanofiller, to create nanocomposite hydrogels for osteoclast culture and differentiation. Characterization of the new biomaterials is presented, as well as their capability to support differentiation of pre-osteoclast cells (osteoclastogenesis).

The third chapter describes the development of a protocol to incorporate natural and recombinant collagen proteins into Fmoc-hydrogels without any covalent crosslinking. It presents data on the biochemical, mechanical (rheology), and functional characterization of the resulting blended hydrogels.

Finally, in the fourth chapter the knowledge and expertise obtained in the second and third chapters was exploited to incorporate collagen-based peptides specific to the OSCAR receptor, which has been shown to act as co-stimulatory agent during osteoclastogenesis, into Hap-decorated, Fmoc-based hydrogels. These combined data show that the hydrogels modified with both Hap and OSCAR-binding collagen peptides have a positive effect on the differentiation of osteoclasts compared to the unmodified hydrogels.

1.2 Bone Structure and composition

The human skeleton represents 20% of human total weight, and the adult human body is made of a total of 206 bones (Steele and Bramblett, 1990). Skeletal segments are made of bone tissue (also known as osseous tissue) which is a dense connective tissue that has a rigid structure which provides the typical bone rigidity. The main structural components of the bone are the cortical bone and the trabecular bone (**Figure 1**). Cortical bone is the outer layer of the bone, and it forms a dense, low surface area, which surrounds the bone marrow cavity. It is the hardest layer of the bone and provides the characteristic compactness and white colour. Cortical bone is formed of concentric lamellae of bone tissue (osteon or *Haversian system*) that form an envelope around the blood vessels. This region is responsible for the main function of the bone of supporting the whole body and protecting the organs from damage. Cortical bone is covered by a membrane that covers all the bones, called the periosteum, and by the

endosteum on its inner surface (Young, Woodford and O'Dowd, 2014). The inner layer of the bone is called trabecular or spongy bone. This layer is much softer and less dense than the cortical layer, with a porous network that provides flexibility to the bone. The trabecular bone is highly vascular and it contains the red bone marrow where haematopoiesis occurs (Ralston, 2013).

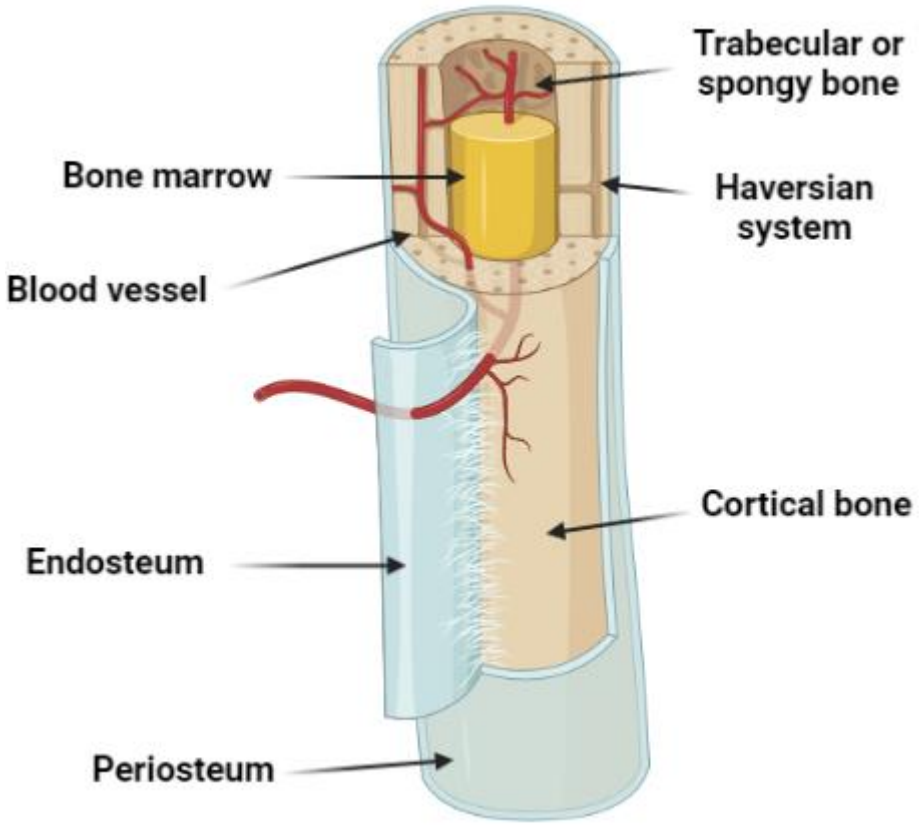

Figure 1 Schematic illustration of the bone structure, showing the gross anatomical features of a typical long bone section. From the outer to the inner region the bone section is formed by the periosteum and endosteum, thin membranes that wrap up the bone. The outer region of the bone called cortical bone surrounds the inner bone marrow that fills the trabecular or spongy bone. This is an intensive vascularised area. Figure made using BioRender.

Bone tissue is composed of an organic component (flexible matrix, 30-40%) and a mineralized component (60-70%). The former is mainly made of collagen type I (~ 95%), which is a triple helical fibrillar protein made of two collagen α1 chains and one α2 chain. The remainder 5-10% is called ground substance and consists of elastin, hyaluronic acid, chondroitin sulphate and non-collagenous proteins such as osteocalcin, osteopontin or bone sialoprotein (Weiner and Traub, 1992). Fibrillar collagen confers to the bone its characteristic tensile strength. On the other hand, the mineralised component is mainly made of microscopic crystals of hydroxyapatite (70% of bone in weight), calcium carbonate (12%), magnesium phosphate (1.5%), magnesium fluoride (0.5%) and traces of iron oxide. The organic part of the bone guarantees its good resistance to mechanical stress, whilst the mineralized component gives it its characteristic hardness.

1.2.1 Types of bone

There are five types of bone in the human body: long, short, flat, sesamoid and irregular (**Figure 2**) (Ralston, 2013). Long bones (*ossa longa*) are characterised by a long portion called diaphysis and a rounded head at each edge called epiphysis. Due to their size and shape, they are mainly made of compact bone at the diaphysis, with the majority of spongy bone localised at the edges. Examples of this type of bone are the femur, tibia, finger bones, etc. Short bones (*ossa brevia*) present only a thin layer of compact bone surrounding a spongy interior. Examples of this type of bone are the wrist and ankle bones. Flat bones (*ossa*

plana) are “sandwich-like” bones with two thin parallel layers of compact bone and a layer of spongy bone in between. Examples of flat bones are the parietal, frontal or occipital bones from the skull. Sesamoid bones (*ossa sesamoidea*) like the patella are bones surrounded by tendons. Finally, irregular bones (*ossa irregularia*), have similar structure to the short bones but, as their name suggests, are irregularly shaped. Examples are the vertebrae, the temporal bone, or the sphenoid bone.

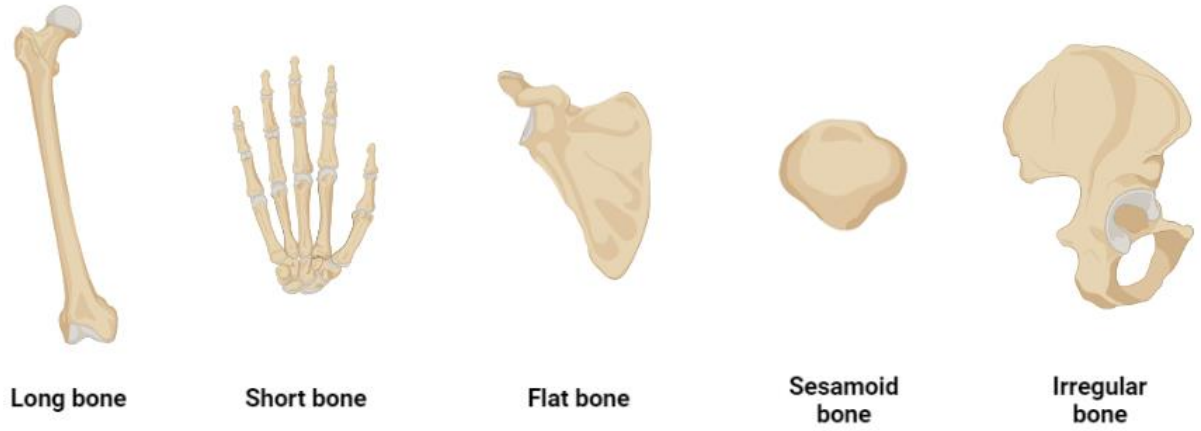

Figure 2 The most common types of bone. Based on their shape and structure they can be classified as long bones, short bones, flat bones, sesamoid bones and irregular bones. Figure made with BioRender

1.3 Bone function

Bones have three main functions: mechanical, synthetic, and metabolic (Von Euw *et al.*, 2019).

1. **Mechanical**

   All the bones in the body form the skeleton. Altogether they form a structural frame that sustains the body and reduces the weight of the body on the tendons and ligaments, while protecting the organs and preventing any damage to the internal structures (Von Euw *et al.*, 2019). Because of its structure, bone has an extraordinarily high compressive strength (~170 MPa), poor tensile strength (104–121 MPa), and a quite low sheer stress strength (51.6 MPa) (Turner, Wang and Burr, 2001). This means that, although the bone is a hard tissue, it can easily break whilst maintaining a significant degree of elasticity, mainly due to its collagen component (Viguet-Carrin, Garnero and Delmas, 2006).

2. **Synthetic**

   As previously mentioned, the spongy bone contains the bone marrow. This is where haematopoiesis occurs and, as a result, red blood cells, platelets and white blood cells are generated within this section of the bone (Florencio-Silva *et al.*, 2015). Moreover, defective or aged blood cells are destroyed in the bone marrow (Young, Woodford and O'Dowd, 2014).

3. **Metabolic**

   The bone acts as a reservoir of important minerals for the body such as calcium and phosphorus (Doyle and Jan de Beur, 2008). Similarly, the bone marrow can release fat into the blood stream acting as a storage

reserve of fatty acids (Styner *et al.*, 2017). Bone is also an endocrine organ. In fact, by releasing fibroblast growth factor (FGF) it can control the phosphate metabolism acting on the kidney reabsorption (Shimada *et al.*, 2004). Finally, due to its high content in calcium, bones are responsible for maintaining the calcium-balance as the calcium released during bone remodelling is released into the systemic circulation (Copp and Shim, 1963).

1.4 Bone remodelling and bone cells

Despite its inactive aspect, approximately 10% of the bone tissue undergoes a continuous remodelling process every year throughout life. It is estimated that almost the entire amount of bone tissue in the human body is completely replaced within 10 years (Manolagas, 2000). This entire process allows for the correct turnover of the skeleton, preventing the accumulation of hyper-mineralised bone, ensuring the optimal repair of micro damage as well as maintaining mineral homeostasis (Kenkre and Bassett, 2018). Bone remodelling activity is finely coordinated by local and systemic factors that stimulate pathways leading to the activation of the two major cells of the bone: osteoclasts (OCs), which resorb bone, and osteoblasts (OBs), which deposit new bone matrix. A third cell type is also present in the bone microenvironment, osteocytes. Evidence suggests that the fine balance between OC and OB action relies on osteocytes acting as

mechanosensors and orchestrators of the bone remodelling process (**Figure 3)** (Bonewald, 2011; Sims and Vrahnas, 2014).

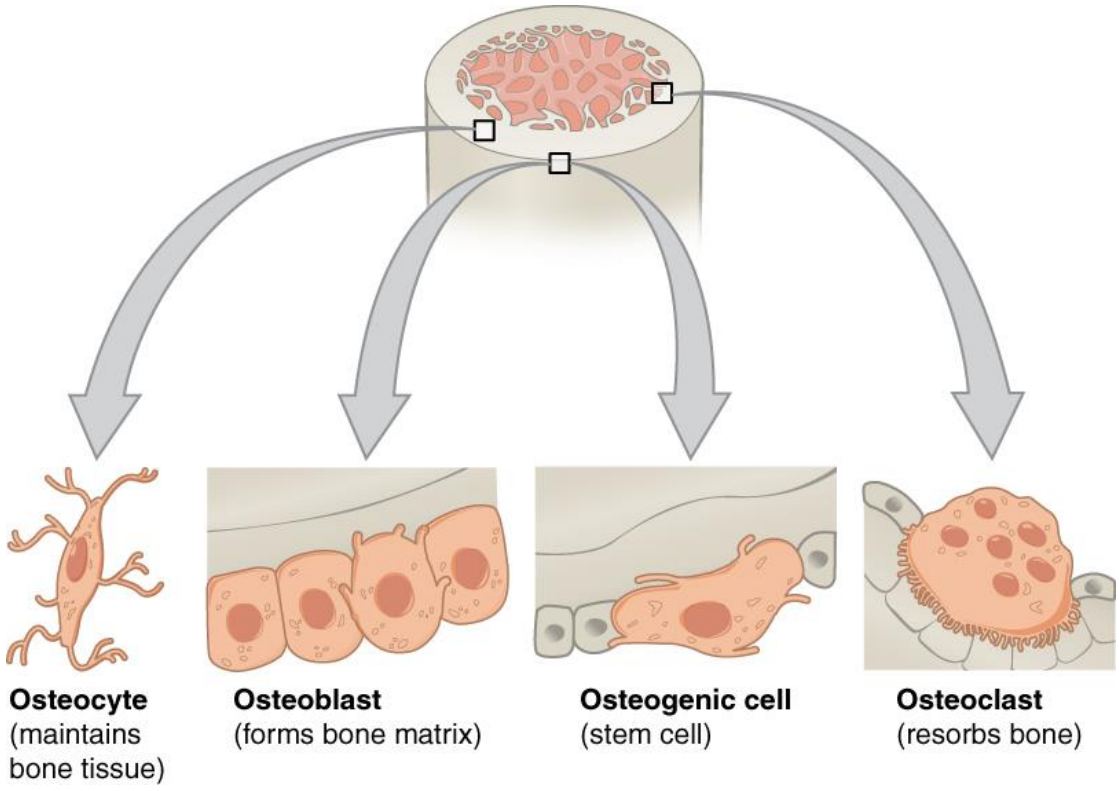

Figure 3 Different types of cells in the bone. Osteoprogenitors cells are cells that differentiate to osteoblasts, cells that deposit new bone. Osteoblasts remaining in the bone matrix are termed osteocytes. Osteoclasts are hematopoietically-derived and resorb bone. Adapted from https://open.oregonstate.education/aandp/chapter/6-3-bone-structure.

OBs are cuboidal mono-nucleated cells responsible for bone deposition. Located on the surface of the bone, they produce a mix of proteins called osteoid that, once mineralized, becomes bone (Kovacs, 2001). They have an abundant endoplasmic reticulum, enhanced Golgi apparatus, as well as numerous secretory vesicles due to their enhanced protein synthesis activity (Capulli, Paone and Rucci, 2014). On the other hand, OCs are terminally differentiated giant

multinucleated cells, which derive from mononuclear cells. Typically, a mature human OC has between five and twelve nuclei and can reach up to 100 µm in diameter. They are characterized by an abundant cytoplasm with a large number of lysosomes and vesicles filled with acid phosphatase. Yet, due to their enhanced enzymatic activity, they have poor rough endoplasmic reticulum and widespread Golgi complex (Väänänen *et al.*, 2000).

1.4.1 OCs function

Through the effect of parathyroid hormone (PTH) stimulation and local cytokine activity (IL-1, IL-6, IL-11…), immature mononucleated OCs are driven from the bone's crypt towards the bone resorption area, where they undergo a dramatic change in morphology and differentiation process. Once at the site of resorption, mature OCs can adhere to the bone and begin the bone remodelling process. Adhesion to the bone is facilitated by integrin receptors, such as $\alpha_v\beta_3$, via the specific amino acid motif Arg-Gly-Asp (RGD, where Arg is Arginine, Gly is Glycine, and Asp is Aspartate) present in bone matrix proteins such as osteopontin (Luxenburg *et al.*, 2007). When adhering to the bone OCs undergo a prominent rearrangement of the actin cytoskeleton, forming a very dense area of active podosomes (called ruffled border or sealing zone) that seals the cell membrane to the mineralised extracellular matrix (Lakkakorpi *et al.*, 1991).

The ruffled border is also important for OCs resorption activity. Through the action of a carbonic anhydrase, which catalyses the formation of bicarbonate ions $H_2O + CO_2 \rightarrow HCO_3^- + H^+$, hydrogen ions are released into the resorptive cavity acidifying and softening the matrix and hence helping with the degradation of the bone (Crockett *et al.*, 2011). Inserted into the ruffled border plasma membrane, there is a vacuolar-type proton ATPase (V-ATPase). Thanks to this pump, the large amount of acids that is needed to solubilise the mineralised matrix, is secreted into the sealing zone. To maintain electroneutrality, a simultaneous efflux of chloride anions is provided by a ClC family of chloride channels such as CLCN7 (Stenbeck, 2002)

At the same time, an intense traffic of intercellular vesicles brings enzymes, such as tartrate-resistant acid phosphatase (TRAP), cathepsin K (CTSK), and matrix metalloproteinase-9 (MMP-9), to the resorption pit to aid in the bone degradation process (Ramos *et al.*, 2016).CTSK (molecular weight 37 kDa) is synthesized as proenzyme and, after autocatalytic cleavage, it is transformed into the mature, active form of the enzyme (molecular weight ~27 kDa) (Inaoka *et al.*, 1995). The activity of this enzyme is crucial for the OCs function. In fact, CTSK reaches its optimal enzymatic activity in the acidic environment of the bone matrix, and after being released from the functional secretory domain of the OCs, it is responsible for the digestion of the main organic components of the bone such as collagen and elastin (Saftig *et al.*, 2000).

The MMPs, instead, are a family of endopeptidases whose activity involves metal ion cofactors such as zinc or cobalt. Also known as matrixins, they are involved in tissue remodelling in both healthy and diseased tissue. MMP-9 and MMP-13 are believed to be associated with OCs activation, migration and differentiation (Nagase H, Visse R, 2006). They are also involved in tumour metastasis, as they can promote malignant cell spreading into secondary tissues (Andersen *et al.*, 2004).

1.4.2 OCs ontogeny and differentiation

OCs were firstly identified by Kolliker in 1873, who observed the presence of giant cells in the periosteum of normal bone (Kölliker, 1873). OCs are hematopoietically-derived cells, originated by differentiation of monocytes/macrophages (**Figure 4**) (Nijweide, Burger and Feyen, 1986). They share a common hematopoietic stem cell (HSC) progenitor with lymphocytes, red blood cells as well as dendritic cells (DCLs) and mononuclear phagocytes. This HSC is able differentiate to a multinucleated bone resorbing cell upon stimulation by granulocyte macrophage colony-stimulating factor (GM-CSF) and macrophage colony-stimulating factor (M-CSF) (Bar-Shavit, 2007; Ono and Nakashima, 2018). However, it has been shown that, due to inflammatory stimuli, the DCLs could undergo a trans differentiation into OCs progenitor (Alnaeeli, Penninger and Teng, 2006). Moreover, recent advances in osteoclast biology have shown that they can be also derived by erythromyeloid progenitor (EMP) that

contributed towards the maintaining of the bone homeostasis and remodelling together with the "classic" differentiated OC (Yahara *et al.*, 2020). These data also suggest that EMP-derived OCs can be rescued in osteopetrosis condition and therefore modulate osteoclast activity *in vivo* (Jacome-Galarza *et al.*, 2019) .

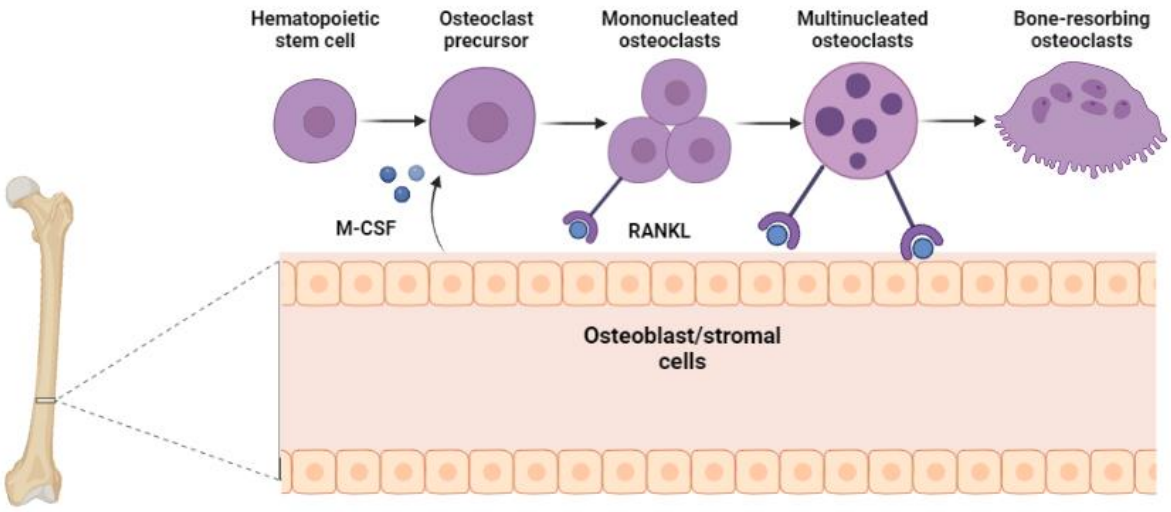

Figure 4 Mechanism of OC differentiation. Mature bone resorbing cells are derived from the fusion of mononucleated osteoclasts. They are generated from a hematopoietic stem cell and they are committed to osteoclastogenesis thanks to the the stimulation of two important cytokines: M-CSF and RANKL. Activated pre-osteoclasts merge then together to form mature bone-resorbing osteoclasts. Figure made with BioRender.

A major step forward of the last decades was the discovery of the Receptor Activator of Nuclear Factor Kappa-B Ligand (RANKL), a crucial cytokine for osteoclastogenesis (Yasuda, 2021). In fact, M-CSF has been known for a long time as the only cytokine required to form OCs. However, although M-CSF presence is pivotal during all the stages of OCs development, RANKL activation of its receptor RANK, "guides" the OC precursor cells (OCLPs) towards the final steps of the differentiation (Nakagawa *et al.*, 1998; Suda *et al.*, 1999).

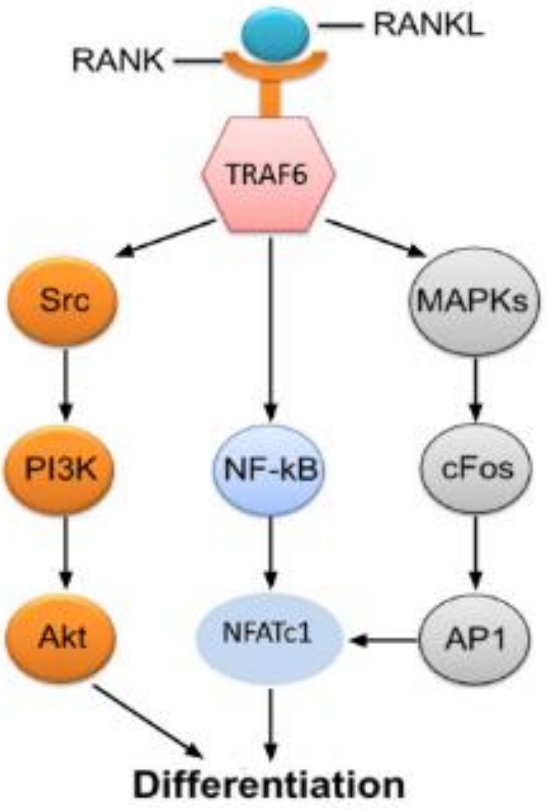

Figure 5 RANK-RANKL signalling in OCs differentiation. Upon binding of RANKL to its receptor RANK, there is an increased expression of NF-κB, AP1 and Src that in turn stimulates an increased expression of NFATc1, a key transcription factor regulating the expression of OC-specific genes that leads to the differentiation of mature OCs. Adapted from (Nedeva *et al.*, 2021).

RANKL is a type II membrane protein and is a member of the tumour necrosis factor (TNF) superfamily (Hanada *et al.*, 2011). Encoded by the TNFSF11 gene (Anderson *et al.*, 1997) the protein consists of 314 amino acids and it can be expressed in three different molecular forms: primary secreted form, truncated or trimeric transmembrane protein (Findlay and Atkins, 2011). As shown in **Figure 5**, upon binding to its receptor, RANKL causes the downstream activation of the nuclear factor-κβ (NF-κβ), Akt kinase and several mitogen factors which directly regulate the expression of nuclear factor of activated T cells 1 (NFATc1), a master

regulator of osteoclastogenesis (Park, Lee and Lee, 2017). NFATc1 upregulates the expression of TRAP, CTSK, the β3 integrin subunit and this eventually leads to OCs activation and differentiation (Boyce and Xing, 2007; Kim and Kim, 2016; Nedeva *et al.*, 2021). Src-mediated activation of the PI3K/Akt pathway downstream of the TNF receptor associated factor 6 (TRAF6) is also required for OCs production. RANKL signalling is pivotal for OCs differentiation and alteration in one of its components may cause impairments to OCs formation and therefore may lead to different pathologies. In fact, it has been demonstrated that depletion of RANKL can cause an uncontrolled bone deposition leading to increased risk in fractures and bone-shape defects. (Lo Iacono *et al.*, 2012). Similarly, overexpression of RANKL, as observed in tumour microenvironment or in the Paget's disease, could lead to an increased OCs activity where an uncontrolled bone degradation can cause bone pain, bone fragility and eventually bone fractures (Wada *et al.*, 2006).

For the reasons mentioned above, in order to maintain correct bone turnover and to prevent disease or injury, OCs and OBs activity must be finely regulated. RANKL/RANK signalling can be blocked by the action of osteoprotegerin (OPG). Secreted by the OBs, OPG is able to bind RANKL and impair the interaction with its receptor RANK, preventing OCs activation (Wada *et al.*, 2006; Boyce and Xing, 2007).

Furthermore, OCs are Ca^{2+}-sensitive and they can sense the local calcium concentration in the bone cavity whilst the resorption activity is ongoing (due to the hydroxyapatite being degraded) and self-regulate themselves during the process (Kajiya, 2012). Alternatively, mature OCs can undergo fission to generate daughter mononucleated cells called osteomorphs. Osteomorphs cells can then go back into the OC-differentiation cycle (McDonald *et al.*, 2021) Thanks to this fine regulation, the balance between bone resorption and bone deposition is safely maintained.

1.5 Bone disease

The term "bone disease" refers to any condition mainly related to a pathology or injury affecting the bones. The most common condition affecting the bone are fractures, followed by osteoporosis and cancer (*Muscle and Bone Diseases | NIAMS*, no date). The current incidence of bone disease in the worldwide population has steadily increased over the years, especially in the last couple of years due to the global pandemic situation (Disser *et al.*, 2020). It is estimated that almost 1.5 million people suffer from bone disease, with fractures and osteoporosis being the leading problem among the population older than 50 years. In fact, aging can be a risk factor coupled with increased obesity and poor physical activity. Although bone disease does not get the same attention as cancer, cardiovascular or infectious diseases, it is still a serious health problem as

they are common, costly, and can become a chronic burden for both the individuals and society.

Overall, bone diseases can be divided into four main groups:

1. **Osteoporosis:** This is one of the most prevalent bone conditions. It can affect over 3 million people in the UK and almost 500,000 people over their lifetime will receive treatments in hospital due to bone pain, fragility and fractures as a result of osteoporosis. Major causes of osteoporosis include abnormalities in bone mass as part of the normal process of ageing, obesity, use of steroids, excessive consumption of alcohol, and smoking. Osteoporosis can also be caused by a metabolic dysfunction such as mineral or vitamin deficiencies (e.g. calcium, phosphorus, vitamin D), hyperparathyroidism, menopause, or developmental bone disorders (NHS, 2019).
2. **Fractures:** Due to its composition, bone is a very hard tissue but as a result of poor tensile strength it can easily break. Common causes of fractures are accidents like a fall or by being hit by an object. Elderly people are more vulnerable to fractures due to balance issues, bones being more fragile etc.
3. **Bone cancer:** Primary bone cancer is a very rare condition, and it accounts for less than 1% of all new diagnosed cancers. Main types of bone cancer

are osteosarcoma, Ewing Sarcoma and chondrosarcoma, that affects young adults and adults differently (Ferguson and Turner, 2018).

4. **Secondary bone cancer**. Secondary bone cancer is a more frequent condition that occurs when the bone is not the primary site of tumour, but the malignant cells metastasise to bone. It can affect any of the bones of the body, but the most commonly affected areas are the spine, skull, pelvis, ribs, humerus or femur. For instance, breast, prostate and lung cancer and some types of blood cancer such as multiple myeloma or leukaemia are commonly known to spread to the bone (Weilbaecher, Guise and McCauley, 2011a) .

1.5.1 OCs involvement in Bone Disease

Although many cells can release matrix-degrading enzymes, OCs are the main cells involved in bone loss in osteolytic disease. In fact, deregulation in one or more steps of OC differentiation and/or function can cause an uncoupling in the balance between OBs and OCs, resulting in a more disruptive activity of the OCs (Helfrich, 2005; Tuck *et al.*, 2017; Veis Novack and Mbalaviele, 2017). Cytokine and growth factors can directly and indirectly interact with OCs and their precursors, encouraging their differentiation and having potent effect on OCs activity. Osteoporosis is an example of bone disease where the OCs-mediated bone loss is prominent (Teitelbaum, 2000). It has been shown that the aging process and lower levels of estrogen may contribute to a pro-inflammatory bone

environment where myeloid and T-cells are recruited and TNF-α and RANKL levels are increased (Cenci *et al.*, 2000; D'Amelio *et al.*, 2008). Similarly, autoimmune inflammatory diseases such as rheumatoid arthritis (RA) can lead to localised bone loss and increased risk of fractures (Weilbaecher, Guise and McCauley, 2011b). Again, a pro-inflammatory cascade signalling (TNF-α, IL-1 release) may be involved in the increased number of OCs that are generally found at the inflamed bone surfaces (Novack and Mbalaviele, 2016).

Moreover, as described in the previous section, solid malignant tumours can metastasize to the bone. Tumour microenvironments consist of complex interactions between cells *via* cytokine activity but skeletal-related events (e.g., osteolysis, fractures…) due to the increased activity of OCs, contribute to a higher tumour burden as well as a poor prognosis. In fact, it has been demonstrated that malignant cells can secrete microvesicles that can exacerbate the OCs activity, leading to bone pain, difficulties in walking and eventually bone fractures, worsening the prognosis of the patients (Raimondi *et al.*, 2015). Additionally, malignant cells may induce a higher presence of DCLs, which can differentiate into OCs (Alnaeeli, Penninger and Teng, 2006; Zhuang *et al.*, 2012). For this reason, blocking one or more of the main stages in OCs life such as differentiation, adhesion or cytokine release has become very important. The next section will discuss current common treatments to tackle bone defect and bone disease.

1.5.2 Current bone disease treatments

Similar to any other type of disease, prevention is by far the most effective way to prevent bone disease. Maintaining adequate levels of calcium and vitamin D as well as keeping an active lifestyle are key to limiting the impact of bone disease, promoting bone health and effective bone remodelling. However, when this is not possible, an initial assessment of the type and cause of bone disease is often the first step performed by a doctor. Bones are often imaged by radiography, which will give the clinician an idea of the seriousness of the problems. Similar techniques may include CT-scans and MRI scans, which may as well be used to investigate cancer (Ralston, 2018). Blood tests or bone biopsy can be also performed. According to the type of injury the bone is usually immobilised, and the patient is advised to rest and refrain from any physical activities. This can be followed by rehabilitation and/or physiotherapy.

Being the most common bone disease, there are several specific treatments for osteoporosis. Commonly, current therapies aim to tackle unbalances between bone resorption and bone deposition activity. In order to reduce the bone resorption, and therefore the bone loss, two types of drugs are used: the first are antiresorptive drugs that aim at reducing bone loss, while the second consists of the use of anabolic agents, which are drugs that promote the bone deposition. Examples of these types of drugs are bisphosphonates, oestrogen, calcitonin and a synthetic form of parathyroid hormone (U.S. Department of Health and Human

Services., 2004). Currently, bisphosphonates such as alendronate and zoledronic acid are anti-osteolytic agents commonly used to inhibit OCs resorption. Their mechanism of action aims at blocking the cytoskeleton rearrangement and the formation of the sealing zone (Russell *et al.*, 2007). Additionally, Anti-RANKL Monoclonal Antibodies (e.g., Denosumab) are currently used to block the RANKL/RANK/OPG axis (Bi *et al.*, 2017; Lu *et al.*, 2018). Different treatments can be used when a bone cancer is diagnosed, depending on its stage, prognosis, and symptoms. Current treatments include radiotherapy, chemotherapy and some forms of targeted therapy such as immunotherapy (Cancer Research UK, 2020). **Table 1** summarises the most common bone diseases where OCs are involved, and current therapies applied.

Table 1 Most common bone diseases related to osteoclast function, and current therapies.

Osteoclast-related bone diseases	Osteoclast formation and function	Unbalanced pathways	Current therapies and/or future targets
Osteoporosis	Excessive osteoclast formation and abnormal resorption activity	Oestrogen deficiency, increased level of RANKL leading to excessive osteoclast formation and increased bone resorption	Bisphosphonates, oestrogen replacement, RANKL antibody, calcitonin, PTH peptides
Osteopetrosis and bone mass gain	Inefficient osteoclast formation/reduced osteoclasts activity and abnormal resorption activity	Absence/Downregulation of RANKL leading to excessive bone deposition and bone mass gain	No treatment/ Hematopoietic stem cell transplantation
Rheumatoid arthritis	Excessive osteoclast formation and abnormal resorption activity	Overexpression of RANKL leading to excessive osteoclast formation MMP-9 and MMP-14 produced by osteoblasts	Immune inhibitors, TNF-α inhibitors. RANKL antibody
Bone tumours	Excessive osteoclast formation and abnormal resorption activity	Unbalanced equilibrium between bone resorption and bone deposition Increased bone disruption	Bisphosphonates, RANKL antibody
Paget's bone disease	Excessive osteoclast formation and abnormal resorption activity	High-RANKL expression leading to osteoclast hyperactivity	RANKL antibody

Alternatively, bone graft is now widely used to repair bone defects and bone damage (Laurencin, Khan and El-Amin, 2006; Amini, Laurencin and Nukavarapu, 2012). Bone graft implants can be divided into autograft or autologous bone transplant, and allograft or heterologous bone transplant. Nowadays, autologous bone transplant is the gold standard for bone grafts as the patient's own tissue can be used. Bone is usually harvested from the patient's iliac crest, thus ensuring that the implant is histocompatible and non-immunogenic and that it contains all the essential components to achieve osteoinduction, osteoconductividity and osteogenesis (Dimitriou *et al.*, 2011). However, autografts are very expensive and they may result in several comorbidities such as bleeding, infections, or scarring (Baldwin *et al.*, 2019). Heterologous transplants represent the second most used bone-grafting procedure. The bone graft is harvested either from a suitable donor bone tissue or from a cadaver. Allografts are also likely histocompatible, and they can be provided in different forms, depending on the host-site requirement. However, as they are pre-treated with UV and devitalised, they have reduced osteoinductive features (Delloye *et al.*, 2007; Moroi *et al.*, 2022). Although all the above-mentioned treatments are widely used nowadays and they have shown to improve bone regeneration, there are still some limitations such as high costs, biological concerns, limited access, and limited osteoinductive and angiogenic potentials.

1.6 Bone tissue engineering

Tissue engineering (TE) studies can offer an alternative solution to problems such as those listed above. This field has grown exponentially over the last decades, with hundreds of studies published on PubMed. As described before, bone is a highly dynamic tissue and the ultimate goal of BTE studies is to create a bone scaffold that aids bone repair and enhances bone regeneration (O'Keefe and Mao, 2011). Potential biomaterials for BTE applications should consider the following features: biocompatibility, as they should closely mimic the natural bone Extra Cellular Matrix (ECM); osteogenic, cells embedded within should be able to perform physiological activities such as bone deposition/bone degradation without minimal interference; osteoinductive potential, so that cell-biomaterial interactions could provide signals that help direct the cells to the correct phenotype (Petite *et al.*, 2000).

These systems could also incorporate functional motifs such as collagen, laminin or the tripeptide RGD, which could potentially improve cell adhesion, differentiation, maintenance and survival of bone cells at a reduced cost, more reliable results, and better future applications (Felding-Habermann and Cheresh, 1993; Knight *et al.*, 2000; Boateng *et al.*, 2005). Therefore, development of new culturing systems able to reproduce more realistically the natural host environment is an area of intense research activity. Additionally, optimized and

validated culture systems might, in the long term, bring a reduction to the need for animal experimentation.

Below are discussed the main classes of biomaterials used for BTE studies.

1. **Osteoinductive biomaterials**: They are classified as "smart" biomaterials due to their capability to induce bone formation by providing signalling to the surrounding *in vivo* environment. They have a great potential for bone regeneration (Blokhuis and Arts, 2011; Agrawal and Srivastava, 2020). Synthetic ceramics such as hydroxyapatite (Hap), their composites such as Hap/Poly(Lactic-co-Glycolic) acid (PLGA) and Calcium-phosphate (CaP)-based biomaterials have demonstrated a great osteoinductive activity due to the presence of calcium and phosphate ions which may influence cell differentiation into bone cells (Blokhuis and Arts, 2011; Xavier *et al.*, 2015; Jeong *et al.*, 2019).

2. **Hybrid materials**: These biomaterials are described as the combination of two of more different components with different characteristics. Hybrid materials can show synergic effects such as higher mechanical strength, enhanced osteoinductive properties or improved cell adhesion. Examples of these class of biomaterials are a PLGA and Polyglycolide co-polymer system (Ulery, Nair and Laurencin, 2011; Zhao *et al.*, 2021), PLGA-polyphosphazenes polymer blends (Baillargeon and Mequanint, 2014), or

polymer-ceramic composites containing Hap crystals and collagen fibres (Tsai *et al.*, 2020).

3. **Hydrogels**: Hydrogels are one of the most interesting biomaterials of the last decade. Also known as 'water-swollen' materials, they are able to build a 3D network of fibres by absorbing and retaining water to almost 95% of their weight (Ahmed, 2015). Due to their composition and cell-cell interaction within the polymer network, hydrogels can mimic the ECM whilst providing cell adhesion, and promoting cell-cell interaction and tissue regeneration (Lee and Mooney, 2001; Drury and Mooney, 2003; Slaughter and Fisher, 2009; Zhang *et al.*, 2021). Hydrogel-based scaffolds are currently used for bone studies because they can provide a realistic hydrophilic environment that supports OCs attachment, spreading, and new bone growth (Sabir, Xu and Li, 2009; Bai *et al.*, 2018).

1.6.1 Hydrogels

As mentioned above, hydrogels are usually defined as water entrapping materials made of polymeric fibres that assemble to form a self-supporting network (Slaughter and Fisher, 2009). Due to their high percentage of water, mechanical stiffness, flexibility, and nanofibrous architecture, hydrogels are ideally suited biomaterials for BTE (Amini, Laurencin and Nukavarapu, 2012). Hydrogels are usually composed of specific structures (called building blocks) that allow precise

dynamic control of the material final ultrastructure (e.g tapes, ribbons, etc.) (R. V Ulijn and Smith, 2008). Hydrogels can be divided into two major classes, depending on the nature of the interactions between the polymer fibres: physically cross-linked hydrogels (or physical hydrogels), or chemically cross-linked hydrogels (or chemical hydrogels). Physical hydrogels consist of polymers whose fibres interact by dynamic and reversible cross-links based on noncovalent hydrogen bonding, electrostatic or hydrophobic interactions. Chemical hydrogels are made of networks of fibres held together via chemical, covalent crosslinking (N. A. Peppas *et al.*, 2006). A different classification of hydrogels is based on the origin of their building blocks. These building blocks can be based on natural polymers such as hyaluronic acid (HA), alginate, collagen or chitosan, or they can be chemically produced as synthetic polymers. Natural polymer hydrogels have the advantage of being biocompatible and biodegradable. They can be obtained at a relatively low cost, and often they present cell binding sites. For instance, collagen-based hydrogels have been used to repair nasal bone defects in rats (Lindsey *et al.*, 1996). Similarly, HA hydrogels were used to successfully deliver bone morphogenetic protein (BMP)-2, promoting high bone formation in the cranial defect site of the rats (Patterson *et al.*, 2010).

However, naturally derived hydrogels present poor mechanical properties and batch to batch variability (N. A. Peppas *et al.*, 2006; Slaughter *et al.*, 2009). Some of these limitations can be addressed by using purely synthetic materials. Among

the synthetic hydrogels, the most used building blocks are poly(acrylic acid) and its derivatives such as poly(2-hydroxyethyl methacrylate) (HEMA), used in many drug delivery applications (Gulsen and Chauhan, 2005). Poly(ethylene glycol) (PEG) hydrogels are also widely used in a variety of biomedical applications such as controlled released of biomolecules or as bare scaffold for TE (Lin and Anseth, 2009). Unlike naturally derived scaffolds, synthetic polymers hydrogels have excellent mechanical properties as the building block can be finely controlled to obtain tuneable mechanical properties and shapes. However, some of the chemicals used to produce these types of biomaterials and/or their cross-linking agents may have a toxic activity affecting the viability of cells. Moreover, as they are chemically synthesised hydrogels, they may not present suitable cell-binding motifs. However, they can be easily modified with ECM proteins (such as laminin, collagen, etc.) or decorated with biological components that could promote cell adhesion and proliferation (Drury and Mooney, 2003; Nicholas A. Peppas *et al.*, 2006). Advantages and disadvantages of natural and synthetic hydrogels are summarised in **Table 2**.

Table 2 Most common types of hydrogels and their relative advantages and disadvantages.

Type	Composition	Advantages	Disadvantages
Natural	Agarose, alginate, chitosan, collagen, gelatin, hyaluronic acid, silk (N. A. Peppas *et al.*, 2006; Slaughter *et al.*, 2009; Patterson *et al.*, 2010)	High bioactivity, structural resemblance to natural ECM	Low viscosity, not suitable for implantation, batch to batch variability, low mechanical properties
Synthetic	poly(2-hydroxyethyl methacrylate) (HEMA), poly(ethylene glycol) (PEG) (Gulsen and Chauhan, 2005; Lin and Anseth, 2009)	Tunability of mechanical properties, No batch-to-batch variability	Low bioactivity, may have toxic effects on cells, poor cell adhesion

1.6.2 Self-assembled peptide hydrogels

Proteins are a major component of human tissues and, for this reason, there is a wide interest in using polypeptides to create successful scaffolds for TE (Lee and Mooney, 2001). In fact, amino acids can be used as building blocks providing the primary structure of the hydrogels. Peptide hydrogels are based on short peptides of L-amino acids, naturally present in the human body. Peptide hydrogels are ideally suited for TE applications as they show low immunogenicity and high biocompatibility (Markey *et al.*, 2017). According to the characteristics of their side chains, individual amino acids are classified as hydrophobic, hydrophilic, charged, etc. (**Figure 6**). Hydrophobic amino acids can be divided into two subgroups, aliphatic (A, I, L, M, V), and aromatic (F, W, Y), which contain an aromatic ring structure. Aliphatic amino acid side chains have merely hydrophobic characteristics. Aromatic side chains are mainly hydrophobic but can also be involved in π–π stacking interactions, where their π-conjugated systems overlap (R. V Ulijn and Smith, 2008). Hydrophilic uncharged amino acids may be involved in hydrogen bonding interaction either via hydroxyl (S, T), amine (H) or amide (N, Q) groups. Alternatively, charged amino acids (D, E, K, R, protonated H) can be exploited to introduce charge-charge interactions that can stabilise (using opposite charge) or prevent (using same charge) the scaffold assembling mechanism. The remaining amino acids (G, P, S) have rather unique characteristics and can be used to confer chain flexibility (G), conformational

rigidity (P), or to provide specific sites for chemical modification in peptide chains (C).

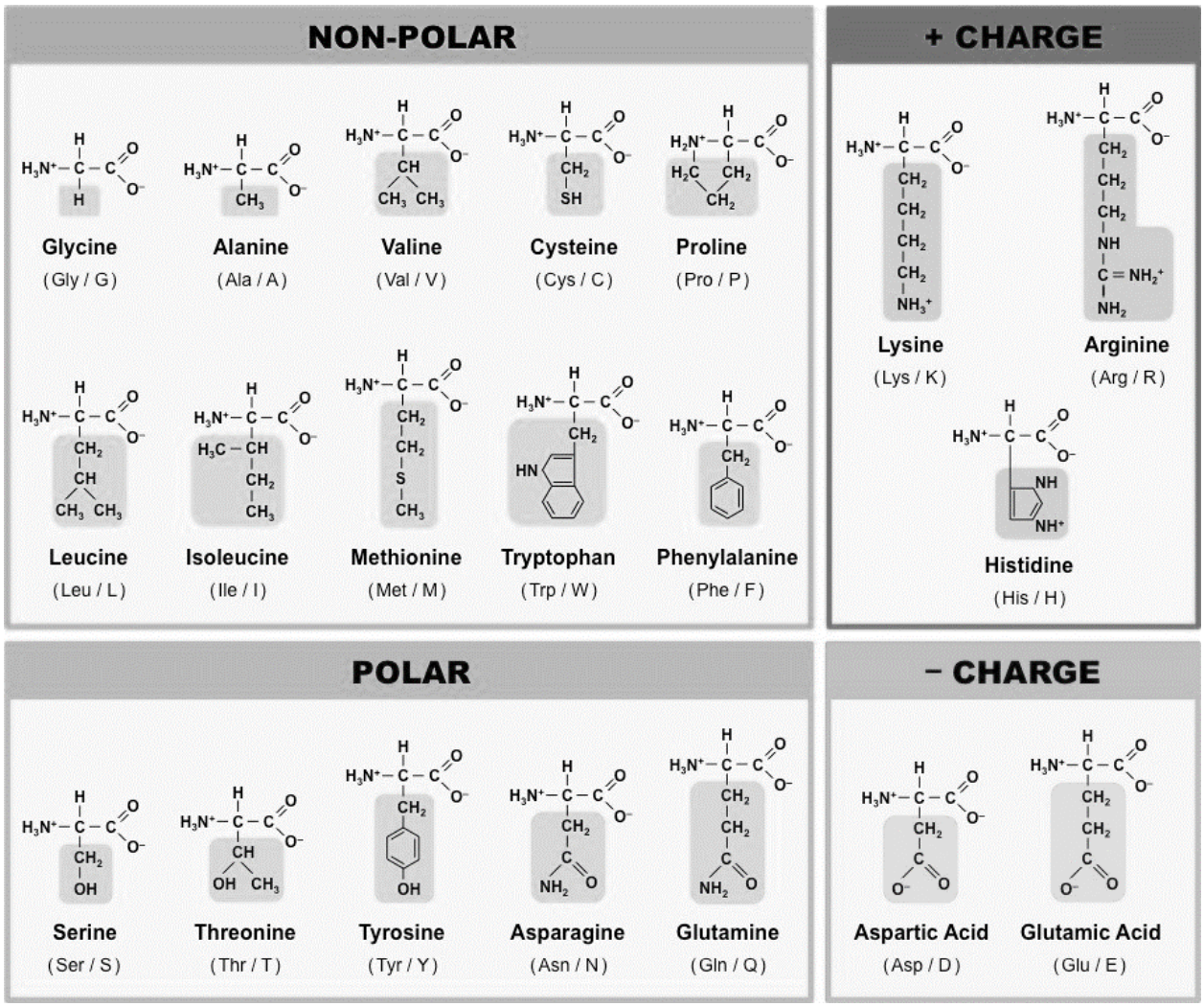

Figure 6 Amino acids commonly used as building blocks for the synthesis of peptide-based hydrogels. They are divided into different groups based on the chemical properties of their side chains. Adapted from BioNinja.com

In addition to their side chain characteristics, the –CO–NH– peptide groups on the main chain can form secondary structures through amide hydrogen bonding. Depending on the properties of their individual amino acids, peptides can adopt in solution different structures such as β-sheets, β-hairpins, α-helices and random

coils that spontaneously self-assemble into supramolecular scaffolds. The assembly can be triggered in response to a pH shift, ionic strength changes, increase in peptide concentration, light, or temperature effects (R. V Ulijn and Smith, 2008). For example, Stupp and co-workers have developed a class of self-assembled peptide-based hydrogels (SAPHs) that spontaneously form rod-like shaped scaffolds due to the combination of hydrophilic, hydrophobic and charge-charge interactions (Capito *et al.*, 2008). Similarly, Zhang and collaborators fabricated a β-sheets-based biomaterial that spontaneously self-assembled where, for the first time, a 'bottom-up' approach, in which materials are assembled molecule by molecule, was used. This. They demonstrated that different types of cells can be cultured in 3D within these hydrogels, providing a realistic platform to study cell adhesion and cell-cell interaction for TE studies (Kisiday *et al.*, 2002; Zhang, 2003; Davis *et al.*, 2005; Fatouros *et al.*, 2014). Based on Zhang's work, Saiani's group developed a class of β-sheet forming peptide-based hydrogels (Saiani *et al.*, 2009). These materials were based on short repetitive sequences (8 to 10 amino acids) such as alanine (A) and phenylalanine (F) with glutamic acid (E) and lysine (K), namely AEAEAKAK, AEAKAEAK, FEFEFKFK and FEFKFEFK. They showed that F-based octapeptides were able to form defined β-sheet fibres (~3 nm thick) and 3D fibrillary hydrogels regardless the position of E and K in the sequence. Octapeptide-based hydrogels were proved be highly

biocompatible, injectable and low immunogenic for a wide range of biomedical applications (Castillo, Guerrero and Acosta, 2017; Qi *et al.*, 2018).

1.6.3 Aromatic short peptide hydrogels

Amino acids with an aromatic ring in their side chains can be used to generate short peptide hydrogels where π–π stacking interactions maintain the structure of the scaffold. Reches and Gazit demonstrated for the first time that amyloid peptides have a core of di-phenylalanine (FF) units that can spontaneously self-assemble to form nanotubes (Gazit, 2009). They proposed that dipeptides containing the FF sequence are able to form stable peptide nanotubes by a combination of main-chain hydrogen-bonding and sidechain π-stacking interactions. It has also been shown that the chemical coupling of large aromatic groups such as 9-fluorenylmethoxycarbonyl (Fmoc) to the N-terminus of some peptides helps them to spontaneously assemble into self-supporting hydrogels (Yang *et al.*, 2004; V. Jayawarna *et al.*, 2006). These gels are easy to synthesize. They show ultrastructural resemblance to the ECM due to their peptide composition and nanofibrous morphology and have tuneable mechanical properties. Since then, numerous hydrogels have been synthesised based on the short building block di-phenylalanine coupled with an Fmoc group at the N-terminus (Fmoc-FF). It has been proposed that these peptides spontaneously form anti-parallel β-sheets where the Fmoc groups act like a zipper to interlock the

different sheets together (**Figure 7**). The rotational twist introduced by the β-sheets generates a cylindrical structure that is held together by π–π stacking of adjacent sheets (Zhao and Zhang, 2007; R. V. Ulijn and Smith, 2008).

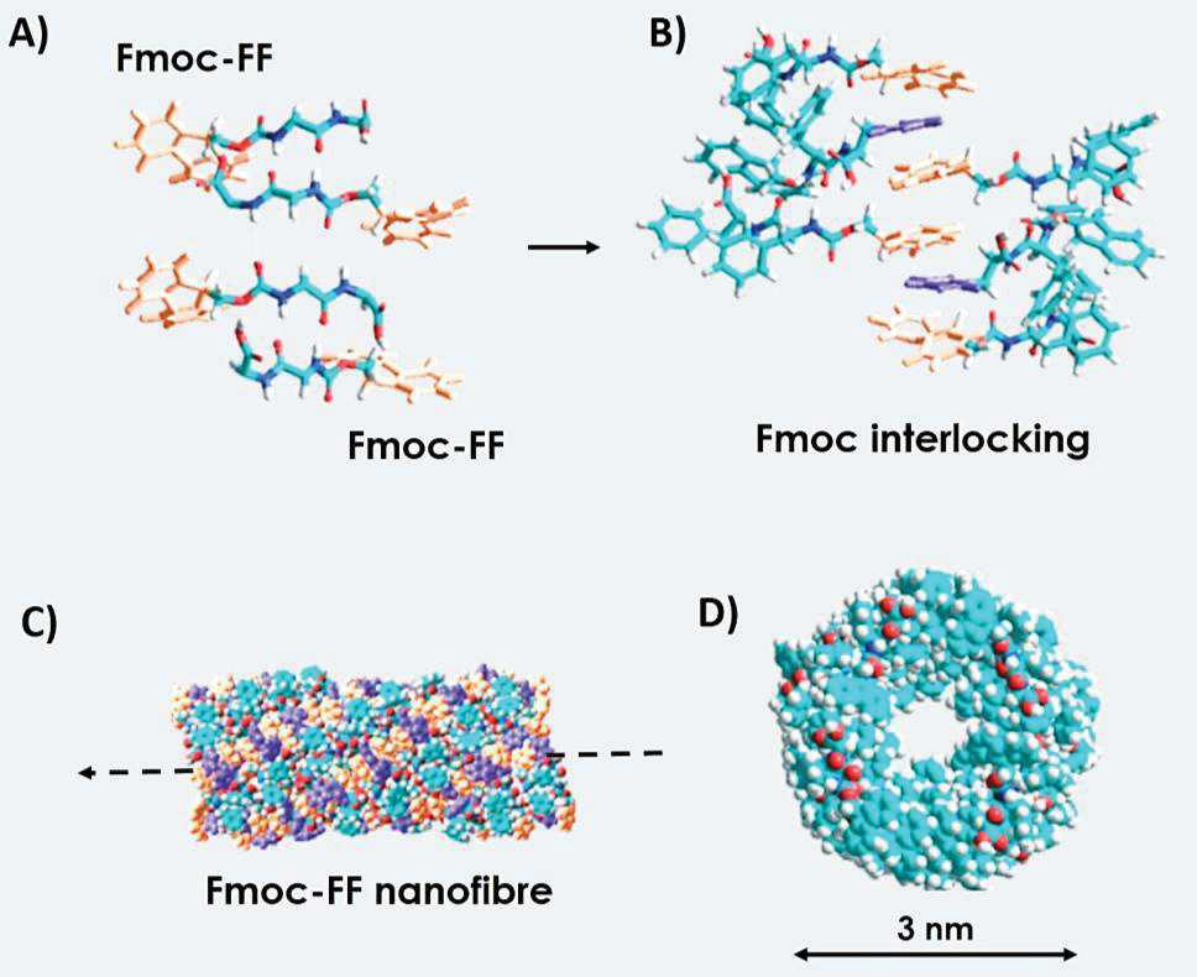

Figure 7 Formation of the Fmoc-FF peptide hydrogel structure. The peptide spontaneously organises into β-sheets with anti-parallel orientation (**A**). Due to π–π interactions between the Fmoc groups, these β-sheets then come together (**B**). The interlocking Fmoc groups act like a zipper to create a cylindrical structure (**C** and **D**). Adapted from (R. V Ulijn and Smith, 2008).

Short peptide hydrogels can be chemically and biologically engineered to enhance cell adhesion and cell proliferation, both in 2D and 3D culture (depending on cell types). For instance, Jayawarna *et al.* added different Fmoc-coupled amino acids such as Fmoc-serine (Fmoc-S), Fmoc-lysine (Fmoc-K) and

Fmoc-aspartic acid (Fmoc-D), to the well-established Fmoc-FF dipeptide in order to improve cell biocompatibility. Of all the tested scaffolds, Fmoc-FF/S showed enhanced cell adhesion and cell spreading compared to the bare Fmoc-FF (Jayawarna *et al.*, 2009). Another remarkable contribution was that of Zhou *et al.* who designed an enhanced ECM-mimicking scaffold composed of mixture of the Fmoc-FF dipeptide and the Fmoc-RGD tripeptide (Zhou *et al.*, 2009). The authors demonstrated that the RGD motif was well incorporated into the basic Fmoc-FF structure, providing a scaffold that was able to promote fibroblast viability and proliferation. This work has been progressed by incorporating other Fmoc-protected peptides with the integrin-binding collagen sequence GFOGER or the laminin sequences IKVAV or YIGSR, with the aim of creating a customised scaffold targeted at specific research goals.

These peptide-based scaffolds form self-supporting hydrogels through cooperative assembly of the single building blocks (Fmoc-FF, Fmoc-S and Fmoc-RGD).They are usually provided in lyophilised powder and, upon contact with water, they form a water-like solution referred as “Pre-gel”. The Pre-gel is then stabilised to form a self-supportive hydrogel whn exposed to a divalent-cation containing solution. This process is usually referred as “two-step process” (Mart *et al.*, 2006)

Moreover, by tailoring the amount of peptide used, the stiffness of these hydrogels can be tuned, closely mimicking different types of tissues (**Figure 8**).

Ultimately these formulations can be used to create a tailored scaffold, able to direct the differentiation of cells to a specific lineage or to enhance cell attachment or spreading.

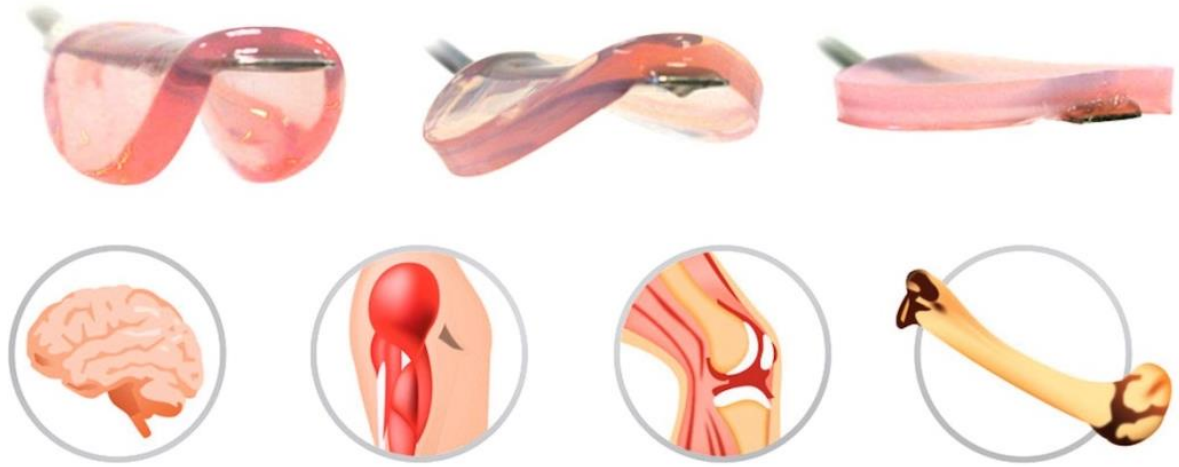

Figure 8 Fmoc-based peptide hydrogels with tuneable stiffness to mimic different human tissues for TE applications. Soft hydrogels (0.8-1.1 kPa, left) can be used to mimic very soft tissues such as brain; medium soft (3-4 kPa, middle) and stiff hydrogels (8-9.2 kPa, right) can be used for harder musculoskeletal tissues such as muscle, cartilage or bone. Adapted from Biogelx.

1.6.4 Hydrogel-based bone regeneration

As described in the section 1.5.2 current treatment for bone disease consists mostly of surgery, conservative treatments, or using of inhibitory/stimulatory drugs for the bone remodelling process. Additionally, bone grafts are widely used to enhance bone repair and bone regeneration. BTE could offer new strategies for tackling bone disease and bone physiopathology, providing hydrogels that can be used to promote bone repair and bone regeneration (Costa *et al.*, 2013; Zhang *et*

al., 2021). For instance, hydrogels can be injected at the bone injury site, and they can be used to carry cells at the site of transplantation. This can happen *via* a minimally invasive surgery, potentially with less complications for the patient. Additionally, hydrogels can be used as carriers of immunomodulatory agents that can be released to recruit cells at the defective site, thus promoting new bone tissue formation (Yue *et al.*, 2020). For example, alginate hydrogels have been used for this purpose (Singh and Peppas, 2014). Dosier *et al*. have demonstrated that stem cells encapsulated within bone morphogenetic protein-2 (BMP-2)-loaded hydrogels promoted high bone regeneration at the bone defective site (Dosier *et al.*, 2015). Similarly, chitosan hydrogels have been used to constantly deliver BMP-2 and transforming growth factor β (TGF-β) at the implant site over 30 days (Saravanan *et al.*, 2019). Alternatively, SAPHs could be used as scaffolds for bone regeneration. They present all the imperative features for a successful scaffold for BTE. An example of this approach is the peptide Acetyl-$(RADA)_4$-$CONH_2$ (also known as (RADA)4 or RADA16), widely used to encapsulate proteins and small molecules (Nagai *et al.*, 2006; Koutsopoulos *et al.*, 2009). Kaipatur and co-workers have demonstrated that a RADA16-based hydrogel can successfully incorporate the cytokine RANKL. This hydrogel can therefore be used to locally control the release of RANKL to induce osteoclastogenesis (Xing *et al.*, 2017). Likewise, SPG-178-hydrogel, a peptide-based SAPH with the 13-amino acid sequence RLDLRLALRLDLR, was used to culture rat skeletal

muscle cells into in a rat calvarias defect model. This scaffold was successful in promoting proliferation and osteogenic induction at the defective site (Tsukamoto *et al.*, 2017). Fmoc-FF has also been used in BTE due to its capacity to self-assemble into hydrogels without need of cross-linking agents (Ghosh *et al.*, 2019). The authors there described a blend of alginate/FmocFF hydrogel as a potential platform for bone regeneration. They demonstrated that pre-OBs successfully adhere to the scaffold inducing osteogenic differentiation and calcium mineralisation.

1.6.5 Limitations of SAPHs

As mentioned earlier, hydrogels form nanofibrous networks that can entrap a large amount of water forming a 3D scaffold. Due to their viscoelastic features combined with high porosity and high permeability, hydrogels are widely used for BTE applications, as they closely resemble the natural characteristics of the ECM. Hydrogels can be directly implanted into the bone defective site and can act as recruiters of bone cells or as carriers of cells, proteins and/or cytokines that can promote bone regeneration. These goals can be achieved with both natural and synthetic hydrogels, with different advantages and disadvantages (**Table 2**). SAPHs may be seen as intermediate between the natural and synthetic hydrogels as they closely mimic the ECM at the nanoscale level, they are biocompatible (due to their peptide composition), and they can support cell adhesion and cell growth both in 2D and in 3D culture.

However, despite their undeniable potential, SAPHs have some drawbacks. Firstly, the mechanical properties of the hydrogels are often not adequate for a scaffold that should mimic the bone tissue (Luo *et al.*, 2022). SAPHs such as RADA16 have shown good cell adhesion properties whilst achieving very low rheological properties (G' = ~100-200 Pa), nowhere near the actual stiffness of the bone. Due to their chemical synthesis, the stiffness can be increased by tailoring the amount of peptide used, as demonstrated by Wan *et al.* In fact by increasing the peptide concentration they obtained significantly stiffer hydrogels (˜G' 41.1 ± 8.6 kPa) (Wan *et al.*, 2016). However, changing the formulation of the hydrogels by increasing the peptide concentration or using a high crosslinking density may lead to a more dense hydrogels fibres that could hinder the migration of cells, cytokines and exchange of nutrients (Ulubayram *et al.*, 2002).

.

1.6.6 Hydrogel Nanocomposites

For the reasons outlined above, designing hydrogel composites has gained widespread popularity amongst the field of BTE. Nanocomposites are defined as hybrid hydrogels that incorporate nanoparticles or nanostructures (also called *nanofillers*) physically or covalently cross-linked with the main structure (Haraguchi and Takehisa, 2002). By using this approach a new class of biomaterials that combine the biocompatibility and plasticity of the hydrogels with the enhanced structural support and mechanical performance of the

nanofillers (e.g. increased mechanical strength, bioactive signals) is obtained (Gaharwar, Peppas and Khademhosseini, 2014).

Hydrogel nanocomposites present several advantages over “naked” hydrogels. Firstly, introducing nanofillers within the hydrogel’s mesh results in an increased mechanical toughness and strength. In fact, the nanofiller could strengthen the hydrogels nanofibers providing a better distribution of loads and stresses (Gaharwar, Peppas and Khademhosseini, 2014). Secondly, by creating a nanocomposite, the hybrid hydrogels act as a biomimetic scaffold. In fact, it has been shown that most nanofillers can induce local release of cytokines inducing cell growth, cell differentiation and guiding bone healing (Li *et al.*, 2013; Tozzi *et al.*, 2016). Nanofillers can also be loaded, in turn, with drugs or cytokines. Therefore, they act as nanocarriers for a local delivery in the surrounding microenvironment. At the same time, since the nanocarriers are encapsulated within the hydrogel, the half-life of these molecules may be extended by preventing their degradation and by a slow, controlled released *in situ* (Lau and Kiick, 2015).

Several classes of fillers have been studied. The most commonly used for BTE are bioceramics (hydroxyapatite, calcium phosphate, silica…), carbon-based nanotubes (graphene), polymeric nanoparticles, and metal/metal oxide nanoparticles (gold, silver, etc.). For an extensive description of all the different

classes of nanofillers, the reader is referred to a review by Tozzi *et al.* (Tozzi *et al.*, 2016).

1.6.6.1 Hydroxyapatite as hydrogel nanofiller for BTE

Hydroxyapatite (Hap), defined by the chemical formula $Ca_{10}(PO_4)_6(OH)_2$, constitutes the main inorganic component of the bone and contains 99% of the total calcium in the human body. Along with collagen, Hap contributes to bone hardness and elasticity (Feng, 2009). Hap is one of the most stable calcium phosphates under physiological conditions and it has gained widespread popularity among nanofillers due to its ability to induce mineralisation *in vitro* by providing additional nucleation sites (Zhou and Lee, 2011; Tozzi *et al.*, 2016). Incorporation of Hap into synthetic pHEMA gels, for instance, resulted in a biomaterial with a similar mineral composition to that found in mammalian bones. This allowed a successful implantation of the scaffolds in the defective bone sites of the rat, favouring the development of new bone matrix whilst leading to increased osteoblast differentiation and bone mineralization (Wahl and Czernuszka, 2006). Similarly, Hap-modified gellan gum hydrogels have shown to successfully differentiate OCs precursors towards mature bone cells (Maia *et al.*, 2018). Aside from the increased bioactivity, biocompatibility and osteoconductivity of Hap nanocomposites, incorporation of Hap has been associated with enhanced mechanical properties of the scaffolds. In fact, Hu *et al.* created a new Hap/agarose composite hydrogel that showed exceptional

mechanical properties (high compressive strength ~400 MPa) and a two-fold higher elastic modulus than bare agarose (~1100 MPa) (Hu *et al.*, 2016). Likewise, Ghosh and co-workers demonstrated a higher mechanical strength (storage modulus up to 29 kPa) of Hap-decorated, Fmoc-based hydrogels compared to naked hydrogels (Ghosh *et al.*, 2017a).

Furthermore, incorporation of Hap into hydrogels seems to provide additional anchoring points that allows differentiation of osteoprogenitor cells (Wahl and Czernuszka, 2006). In nature, bone tissue cells attach to mineralised surfaces during bone healing and repair. As such, cells that are undergoing differentiation are able to keep recruiting cells of the osteoblast lineage by secreting colony stimulating factors (CSFs), TFG-β and BMPs. Furthermore, the mineral matrix allows osteoblasts to deposit the extracellular collagen that will constitute the ECM. (Wu *et al.*, 2020). All in all, minerals can be directly incorporated into biomaterials to fabricate hybrid scaffolds with reinforced properties. Peptide amphiphiles like Fmoc-FF, are ideal templates for the incorporation of Hap, showing great similarity with the native bone matrix and providing the ideal template for the deposition of Hap crystals, as they can mimic the Gly-X-Y motifs of collagen (Rivas *et al.*, 2019).

1.7 Research question

Most BTE studies are focused on the development of new bone and the interaction of biomaterials with OBs (or stem cells-derived OBs), their bone deposition, and bone repair. On the other hand, OCs and their resorptive activity are often overlooked. However, as discussed in the previous sections, bone is a highly dynamic tissue that undergoes a continuous remodelling process involving both new bone deposition and bone breakdown. Therefore, an optimal biomaterial for bone replacement should take into account both processes.

Furthermore, OCs are abnormally activated in several pathologies that result in bone mass loss and increased risk of fractures (Helfrich, 2005). Thus, there is interest in the development of new therapeutic agents that inhibit OCs overactivation as a strategy to counteract excessive bone degradation. However, generating mature, bone-resorbing OCs is not trivial and different protocols have been developed throughout years that may be appropriate for some studies but unsuitable for others (Marino *et al.*, 2014). Moreover, new protocols are needed for OCs culture and differentiation that take into accounts the differences between tissue culture polystyrene (TCPS) and the actual bone microenvironment. The following section, presents a more in-depth discussion of the current challenges in OCs culture and the advantages and disadvantages of each culture protocol.

1.7.1 OCs culture

Culturing OCs precursors to obtain mature bone-resorbing cells has become an essential skill for any researcher wishing to study bone physiopathology, bone microenvironment, or any new bone-related therapeutic agent. In the past, mature OCs were isolated from neonatal animals by mechanically fragmenting their bones (Chambers *et al.*, 1984). Nowadays, there are two main sources of OCs: human peripheral blood mononuclear cells (PBMCs), or a murine cell line used as a bone-resorbing model (Raw 264.7 cells) (Marino *et al.*, 2014).

PBMCs can be obtained from peripheral/venous human blood via density centrifugation with Ficoll-Plaque reagent (Yeo *et al.*, 2009). Thus, freshly isolated PBMCs can be differentiated into mature, bone-resorbing OCs upon stimulation with M-CSF (human or mouse 25–50 ng/ml) and RANKL (human or mouse 50–100 ng/ml). Being isolated directly from human donors, these are the most reliable source of human OCs. However, due to the heterogeneity of the samples, the number of OCs can be highly variable (Riedhammer, Halbritter and Weissert, 2015).

Alternatively, mature murine OCs can be obtained by differentiation of Raw 264.7 cells (Teitelbaum, 2000a), which are a well-established murine macrophage pre-OC model widely used to study OC function. Established in 1978 from leukaemia-induced mice (ATCC, 2018), Raw 264.7 cells are semi-

adherent and can be easily cultured in flasks, glass and dentine discs depending on the experimental purpose. Generally, they can be maintained for long passage numbers even though the highest number of mature OCs is obtained between passages 4-18 (Marino *et al.*, 2014).

Raw 264.7 cells are RANKL-sensitive OC precursors, meaning that mature OCs can be obtained after 5-7 days of RANKL stimulation (human or mouse 50–100 ng/ml) (Collin-Osdoby and Osdoby, 2012). These cells do not need the addition of M-CSF as they have an endogenous expression of this cytokine and its receptor c-fms (Shadduck *et al.*, 1993; Marino *et al.*, 2014).

Despite these advantages, current methods of culturing OCs need improvement. In fact, although commercial cell lines are widely used, there are still some issues that need to be addressed. The advantages and disadvantages of the current OC culture methods are listed in **Table 3**. Firstly, even though 2D culture on TCPS is the traditional method of culturing cells, it is not the most representative system for the *in vivo* environment. In fact, due to the difference in stiffness, the mechanotransduction signalling induced by rigid TCPS dishes (Young's modulus in the gigapascal range), could influence the polarization state, function and differentiation of the OCs (Sridharan *et al.*, 2019). Secondly, because the i*n vitro* system is far simpler than the actual microenvironment where the cells live, cultured cells may act differently to an *in vivo* situation. This can affect both primary cells and commercial cells lines because the crosstalk between cell-cell

and cell-matrix that happens *in vivo* can be difficult to reproduce on an *in vitro* system.

Table 3 Advantages and disadvantages of the different sources of OCs (Raschke *et al.*, 1978; Shadduck *et al.*, 1993; Alge *et al.*, 2006; Pan *et al.*, 2009; Collin-Osdoby and Osdoby, 2012; Marino *et al.*, 2014)**.**

	Advantages	Disadvantages
PBMC's - derived OCs	a) More reliable culture system b) Human-derived primary cells c) Genetic and phenotypic markers are maintained d) Avoid ethical problems of using animals e) More physiologically significant results	a) Donor-to-donor variability b) Hard to propagate in culture c) Need licensing and permissions d) More cytokines needed (M-CSF and RANKL) e) Limited passage number f) Higher cost
Raw 264.7 - derived OCs	a) Easy access and culture system b) High mature osteoclasts yield c) Less growth factor needed (RANKL) d) Easy characterization e) High passage number f) Low Cost	a) Tumour-derived cells b) Simplistic cell model c) Passage-dependent somatic mutation d) Different response than natural microenvironment e) Genetic and phenotypic difference from their origin tissue

Moreover, although different sources of OCs can be used, there are still a wide range of differences when using primary cells or cell lines. For instance, using primary cells can raise issues with licensing and permission as well as higher costs due to the need for more nutrient, cytokines and growth factors. On the other hand, using cell lines benefits from easy access, low maintenance costs, less expertise needed in handling them etc. However, they may provide a different response to a physiological bone environment and may be considered not as representative as the primary cells due to their tumour origin (Alge *et al.*, 2006; Pan *et al.*, 2009).

Reasons such as those discussed above (**Table 3**) are why new methods of culturing and differentiating OCs are needed. Therefore, the overall objective of this study is to generate a new customised SAPH that can act as a platform for the culture and differentiation of OCs.

The **hypothesis** for this study is that by tailoring the stiffness of Fmoc-based hydrogels, a bone-mimicking hydrogel scaffold can be generated that will serve as a substrate for the culture and appropriate differentiation of OC. Stiffer hydrogels are potentially attractive substrates for the culture of OCs. Moreover, the addition of specific component (e.g. RGD, Hap, collagen…) that could possibly interact with cells, may help to create a superior bone mimicking biomaterial.

1.7.2 Global aims

The overall aims of this PhD project are defined below. Specific aims for each chapter will be outlined at the beginning of each chapter.

1. Assess cytocompatibility of Raw 264.7 on different Fmoc-based hydrogels formulations;
2. Develop a new customised Fmoc-hydrogel as a platform to culture and differentiate osteoclasts;
3. Incorporate collagen peptides designed to contain specific sequence motifs recognized by osteoclast precursors, into Fmoc-based hydrogels;
4. Assess differentiation of Raw 264.7 pre-OCs into mature OCs using newly developed hydrogels scaffolds.

Chapter 2 - Hydroxyapatite-decorated peptide hydrogels as substrates for Osteoclast Differentiation and Culture

Note: A version of the work presented in this chapter has been published as follows:

Mattia Vitale, Cosimo Ligorio, Bethan McAvan, Nigel W. Hodson, Chris Allan, Stephen M. Richardson, Judith A. Hoyland & Jordi Bella (2022) Hydroxyapatite-decorated Fmoc-hydrogel as a bone-mimicking substrate for osteoclast differentiation and culture. Acta Biomaterialia, 138, 144-154.

Available here: https://doi.org/10.1016/j.actbio.2021.11.011. The printed (PDF formatted) version is provided as **Appendix A**

2.1 Introduction

As discussed in Chapter 1 bone is a highly dynamic tissue that constantly undergoes a remodelling process through the action of two main cell types: OCs, cells that break down bone, and OBs, cells that lay down new bone matrix (Weiner and Traub, 1992; Sims and Martin, 2014; Nedeva *et al.*, 2021). Bone is also a very well organised tissue where living cells are embedded in a 3D structure of organic-inorganic nanocomposite that confers to the bone its typical high strength and resistance (Currey, 2003; Reznikov, Shahar and Weiner, 2014).

OCs are one of the main cell types involved in bone disease. In fact, a disruption in the equilibrium between bone resorption and bone formation can cause bone pain and bone damage, leading to an increased risk of bone fractures (Phan, Xu and Zheng, 2004; Raimondi *et al.*, 2015; Veis Novack and Mbalaviele, 2017; Nedeva *et al.*, 2021). The aim of BTE is to provide scaffolds that can be used to mimic the bone microenvironment and potentially to study the mechanisms involved in bone diseases. Hydrogels are a suitable choice of scaffold due to their viscoelastic properties, high water content and ECM-mimicking nanofibrous network features (Ahmed, 2015; Bai *et al.*, 2018).

A particular class of hydrogels that has gained much attention over the last decades are self-assembling peptide-based hydrogels (SAPHs). They are made of short peptide building blocks that self-assemble into gels due to a pH shift,

temperature change, change in media buffering, etc. (Hellmund and Koksch, 2019; Chiesa *et al.*, 2020; Imere *et al.*, 2021; Ligorio *et al.*, 2021). They can be also functionalised with biological motifs that control the final properties of the scaffold and mediate cell-cell/cell-material interactions (R. V Ulijn and Smith, 2008). Amongst the SAPHs, Fmoc-based peptide hydrogels are widely used in different TE applications. They form rigid, cylindrical-shape molecular structures through a combination of hydrogen-bonding and π-stacking interactions without the need for additional crosslinking agents (Reches and Gazit, 2003; Vineetha Jayawarna *et al.*, 2006; Diaferia, Morelli and Accardo, 2019). The Fmoc-FF dipeptide can be used to form stable hydrogels that can be further functionalised by changing the peptide amino acid sequence in order to enhance cell adhesion and cell proliferation (Jayawarna *et al.*, 2009; Zhou *et al.*, 2009). However, despite their good biological properties, these peptide hydrogels still lack sufficient mechanical strength to mimic tissues with higher stiffness such as bone. Recent studies have shown how hydrogels can be modified with the use of nanofillers, which not only add functionality to the composite hydrogels but also improve the resulting mechanical properties of the scaffolds (Drury and Mooney, 2003; Manias, 2007; Tozzi *et al.*, 2016). Additionally, it has been demonstrated that by changing the nanotopography and composition of the hydrogels, cell fate can be controlled promoting differentiation, increased cell numbers, etc. (Taylor *et al.*, no date; Chen *et al.*, 2019). Hap is one of the most used nanofillers for BTE

studies as it is the main component of the inorganic part of the bone (Boskey, 2013). It has been used as a scaffold reinforcement to improve mechanical strength of the hydrogels but also due to its cytocompatibility and bioactivity (Gkioni *et al.*, 2010; Ma *et al.*, 2016; Tozzi *et al.*, 2016; Suvarnapathaki *et al.*, 2020).

Having considered the overall properties of Fmoc-based SAPHs (cytocompatibility, tuneable stiffness, functionalisation…) they represent a suitable choice for BTE application. However, most studies to date have focused their attention on OBs and their bone deposition activity, whereas very little is known about the interaction of OCs and biomaterials. As mentioned earlier, a successful scaffold for bone regeneration should take into account the complexity of the bone turnover and provide biomaterials that can regulate OC activity accordingly (Detsch and Boccaccini, 2015).

Furthermore, as discussed in section 1.7.1, there are challenges associated with the current protocols of culture and differentiation of OCs. There are also dramatic differences between TCPS, a rigid and strictly 2D culture substrate, and the actual bone microenvironment.

For these reasons, the aim of the work reported in this Chapter was to use Hap nanopowder as nanofiller to develop a new, customised Fmoc-based hydrogel that could act as a bone-mimicking substrate to culture and differentiate OC

precursors into OCs. To achieve this goal an Fmoc-FF, Fmoc-serine (Fmoc-S) and Fmoc-arginyl-glycyl-aspartate (Fmoc-RGD) ternary peptide-hydrogel (Fmoc-FF/S/RGD) was used for Hap nanopowder incorporation. The ultrastructure of the newly developed, Hap-decorated Fmoc-FF/S/RGD hydrogel was characterized by Atomic Force Microscopy (AFM), and its mechanical properties were analysed by oscillatory rheometry. Finally, the murine pre-OC cell line Raw 264.7 was used to explore whether the Hap-decorated Fmoc-FF/S/RGD hydrogel could be used as substrate for osteoclast culture and differentiation. Cell morphology, viability and differentiation were investigated *via* F-actin, TRAP staining, intracellular viability assays (LIVE/DEAD™ cell imaging), and qPCR to quantify appropriate gene expression.

The specific aims of this Chapter were:

1- To develop a new Hap-decorated Fmoc-hydrogel nanocomposite.
2- To characterise the ultrastructure and mechanical strength of the Hap-decorated hydrogel nanocomposite *via* AFM and rheology.
3- To assess the potential of this Hap-decorated hydrogel nanocomposite as a platform to culture and differentiate OCs *in vitro*.

2.2 Materials and Methods

2.2.1 Materials

Peptide lyophilised powders for Fmoc-FF/S (F, Phenylalanine; S, Serine; batch Nº FFS052RM) in a molar ratio 1:1, and Fmoc-FF/S/RGD (R, Arginine; G, Glycine; D, Aspartic Acid; batch Nº FFSRGD027RM) in a 1:0.5:0.5 molar ratio, were provided by Biogelx Ltd, UK. The peptide purity (97% and 99%, respectively) was assessed in house by Biogelx *via* High Performance Liquid Chromatography (HPLC). Hydroxyapatite nanopowder ($Ca_{10}(PO_4)_6(OH)_2$, particle size <200 nm), was outsourced from Sigma-Aldrich (677418). All these reagents were stored at room temperature (RT) until use.

2.2.2 Preparation of Fmoc-FF/S, Fmoc-FF/S/RGD and Hap-decorated solution

Hydrogels of different concentrations (5-30 mM) were prepared following the manufacturer's protocol. Briefly, lyophilised Fmoc-peptide powders were rehydrated in 7 mL glass vials (Sigma-Aldrich) to the desired concentration using sterile, deionized H_2O (dH_2O), to form a viscous peptide solution referred to as "pre-gel". The water was pre-warmed to 37°C to help dissolving the peptide powders. In order to mix the solution and to remove any air bubbles, the pre-gels were further homogenised by a combination of low speed vortexing (PV-1, Grant Instruments (Cambridge) Ltd) and ultrasonic water bath sonication for 2 min at

RT (FB 15050 Sonicator, Fisherbrand, UK). To prepare the Hap-decorated hydrogels, 1 mg of Hap nanopowder was dispersed into 1 mL of dH_2O by sonication. This dispersion was then used to incorporate the Hap into the pre-gel solutions. **Table 4** provides the full list of the Fmoc-peptide masses, final concentrations, and volume of dH_2O used for each hydrogel formulation.

Table 4 Fmoc-hydrogels preparation ratios.

Concentration of **Fmoc-FF/S** peptide solution (mM)	Mass (mg)	Volume of dH_2O (mL)	Concentration of **Fmoc-FF/S/RGD** peptide solution (mM)	Mass (mg)	Volume of dH_2O (mL)
5	22	5	**5**	24	5
10	43	5	**10**	49	5
15	67	5	**15**	74	5
20	88	5	**20**	99	5
30	132	5	**30**	148	5

2.2.3 LIVE/DEAD staining

A Live/Dead assay kit (Invitrogen L3224) was used to assess the viability of Raw 264.7 cells cultured on the different Fmoc-hydrogel formulations with or without Hap. Following the manufacturer's protocol, 600 µL of the assay solution containing 4 µM ethidium homodimer-1 (EthD-1) and 2 µM Calcein AM were pipetted onto the cell-hydrogel constructs. After 30 min of incubation cells were washed 3 times in Dulbecco's Phosphate Buffer (PBS, Gibco UK) and imaged

using a Nikon Eclipse 50i fluorescence microscope (emission wavelengths: green channel for live cells 515 nm; red channel for dead cells 635 nm; excitation wavelength: 495 nm). Cell images were collected at 24 h, 48 h, 5 days, and 7 days post culture. Three images per time point were acquired.

2.2.4 Cell morphology: F-actin staining

Morphology and cytoskeleton arrangement of Raw 264.7 cells cultured on Fmoc-FF/S and Fmoc-FF/S/RGD hydrogels, with and without Hap, were investigated using Alexa Fluor 488 Phalloidin (Invitrogen, UK, A12379). After 7 days in culture, medium was removed from the hydrogels and cells were fixed in 4% (w/v) paraformaldehyde (PFA, Sigma-Aldrich) for 30 min and permeabilised in 0.5% (v/v) Triton X-100 solution (Sigma-Aldrich) in PBS for 5 min. The samples were then incubated with 1:200 Alexa Fluor 488 Phalloidin for 30 min. After 3× washes in PBS, nuclei were counterstained with 1:8000 Hoechst 33342 (Thermo Fisher Scientific) in PBS. Stained samples were imaged by using a Leica SP8 upright dipping lens confocal microscope, with excitation filters of 495 nm (green, Alexa Fluor) and 351 nm (blue, Hoechst). Cell analysis was performed with ImageJ v. 1.51 (https://imagej.nih.gov/ij). In order to produce three 8-bit greyscale images, individual channels were obtained from the composite fluorescence images in red, green and blue (RGB). Greyscale images were thresholded using Huang's approach (Huang and Wang, 1995) and touching cells were separated into individual objects by applying a watershed algorithm (Soille

and Vincent, 1990). Cell diameter and nuclei of at least 100 cells were measured by using the "analyse particle" plugin from ImageJ.

2.2.5 Fluorescent labelling of Hap nanoparticles

In order to visualise the Hap distribution within the hydrogels network, the nanopowder was prior labelled with Calcein AM to obtain a fluoro-Hap, following the method described by Hale *et al*. (Hale, Ma and Santerre, 2000). 5 mg of Hap nanopowder were dispersed in 1 mL of dH_2O by sonicating to create a stock solution (conc. 5 mg/mL). Then, 1 mL aliquot of 1 mg/ml Hap (working solution) was incubated with 1 µL of Calcein AM (4 µM, Invitrogen L3224) for 2 h at 4°C, under constant agitation. Following the incubation, the Hap/Calcein was washed 3 times with 1 mL dH_2O and the obtained fluoro-Hap was incorporated within the hydrogel following the procedure described in section 2.2.2. Hydrogels containing fluoro-Hap were imaged by using a Leica SP8 upright dipping lens confocal microscope, with excitation filters of 495 nm (green, Alexa Flour) and 351 nm (blue, Hoechst). Image analysis was performed by using Imaris cell analysis software (v.9.8). Cumulative release of Hap from the Fmoc-FF/S/RGD hydrogel was monitored over time using the same method described above to label the Hap nanoparticles.

2.2.6 Preparation of hydrogels for cell culture

When used for cell culture, the pre-gel solutions prepared as described in section 2.2.2 were warmed in an incubator at 37°C for 30 minutes. Additionally, solutions were sterilised under UV light for 20 min. Then, ~200 µL of pre-gel solution (with and without Hap) were pipetted into the inner well of a 35 mm glass bottom dish (VWR, UK, 734-2905), as illustrated in **Figure 9**. A smooth movement, without removing the tip from the solution was performed, in order to prevent formation of air bubbles. The peptide solution was then left to dry for 90 min at 37°C. After this step, in order to crosslink the hydrogels, 1 mL of pre-warmed high glucose Dulbecco's Modified Eagle's Medium (with 4.5 g/L glucose, L-Ala-L-Gln, sodium pyruvate and sodium bicarbonate) (DMEM, Sigma-Aldrich, FG0445), was added dropwise to the centre of the pre-gel solution to avoid gel disruption. Further 3 mL of DMEM were slowly added to each dish to a final volume of 4 mL/dish. Hydrogels were incubated overnight at 37°C and 5% CO_2 before cell seeding.

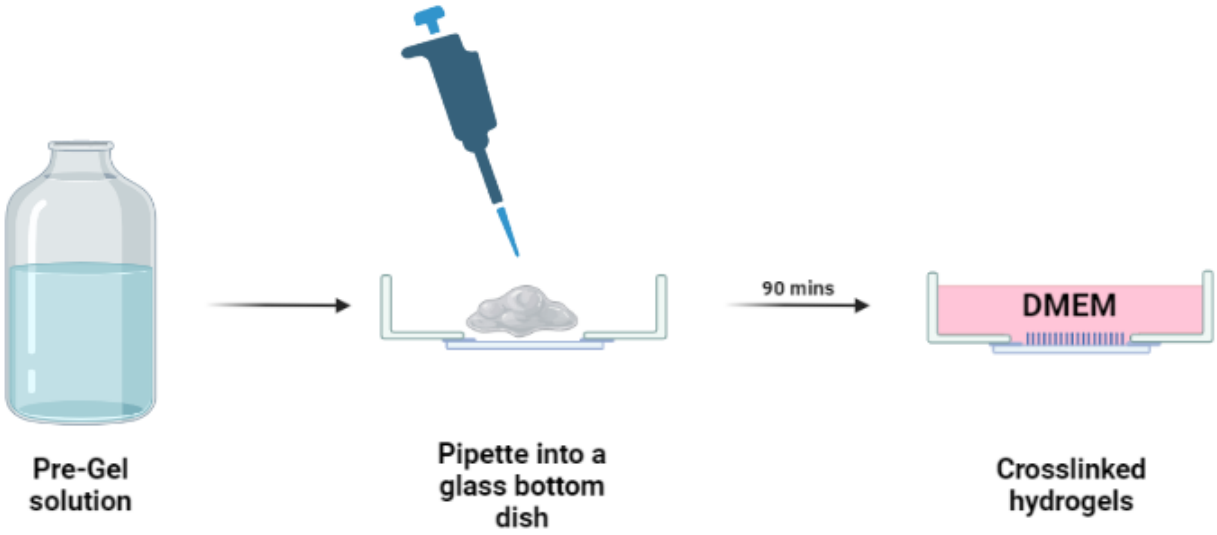

Figure 9 Schematic illustration of the protocol to prepare hydrogels for cell culture.

2.2.7 Hydrogel's ultrastructure: Atomic Force Microscopy (AFM)

Hydrogels with and without Hap were diluted up to 5 mM using pre-filtered double deionised water (ddH_2O). Samples for AFM analysis were prepared by depositing 100 µL aliquots of diluted hydrogel solutions onto freshly cleaved mica (Agar Scientific, UK) for 60 s at room temperature and allowing them to adhere. Excess liquid was then removed by capillary action using Whatman Nº 1 filter paper. Hydrogel-coated mica samples were finally washed for five times using 200 µL of ddH_2O and left to air-dry overnight before imaging. Imaging was performed using a Bruker Multimode 8 AFM with a NanoScope V controller and a "J" scanner, operating under the NanoScope Controller software (v 8.15) (Bruker, USA). Scanning was performed in air at room temperature in ScanAsyst™ (Peak Force Tapping) mode, using ScanAsyst-Air™ probes (Bruker AXS S.A.S, France) with nominal resonant frequency (f_0) and spring constant (k)

of 70 kHz and 0.4 Nm^{-1} respectively. AFM images (2 μm^2) were acquired with a 512 × 512 pixels resolution at a scan frequency of 1 Hz. Height data was first order flattened, and average fibre/nanopowder widths were determined and analysed using the NanoScope Analysis software (v 1.40) (Bruker, USA). *N*=200 fibres were analysed as a measure of homogeneity of the hydrogels structure. Hap nanoparticles were also imaged by AFM to check their size distribution range. Briefly, 100 µL aliquots of 1 mg/ml Hap were drop-casted into a polylysine–coated mica for 60 s at room temperature. Samples were then dried and imaged 24 h later following the same procedure described above.

2.2.8 Mechanical characterization of the hydrogels: Oscillatory Rheology

The mechanical properties of the hydrogels, with and without Hap, were measured on a Malvern Kinexus Pro rheometer using a 20 mm/diameter parallel-plate geometry with a 0.5 mm gap size. Samples were prepared by pipetting 300 µL of pre-gel solution into a 24-well plate containing 1 mL/well of DMEM cell culture medium to form a spheroid-shaped hydrogel. After incubation for 2 h, fully formed hydrogels were transferred to the rheometer plate. The elastic and viscous moduli of the hydrogels were recorded as a function of frequency between 0.1 and 100 Hz (shear strain of 0.1 %), at 25 °C.

2.2.9 Raw 264.7 hydrogel cell culture

Murine macrophage Raw 264.7 cells (TIB-71™) were purchased from ATCC™ and maintained in monolayer culture using DMEM containing 10% (v/v) foetal bovine serum (FBS) and 5% (v/v) Penicillin-Streptomycin-Amphotericin antibiotic mixture (PSA, 100 units/mL penicillin, 100 µg/mL streptomycin, 0.25 µg/mL amphotericin) (Sigma-Aldrich). Media was replaced every 48 h and upon reaching 70-80% confluency, cells were gently detached from the tissue culture flask by scraping and the cell suspension was pelleted by centrifugation (400 ×g for 5 min). Cells were then counted using an automated cell counter (Countess™ 3, Invitrogen™), and fresh culture medium was added to the pellet to obtain a cell density of 4×10^5 cells/mL. 2 mL of cell suspension were then added to each hydrogel's formulation (with and without Hap) and they were incubated at 37°C and 5% CO_2. Medium was changed every 24 h for the first two days, and then every other day for up to 7 days. **Figure 10** illustrates the typical Raw 264.7 morphology at low and high cell densities.

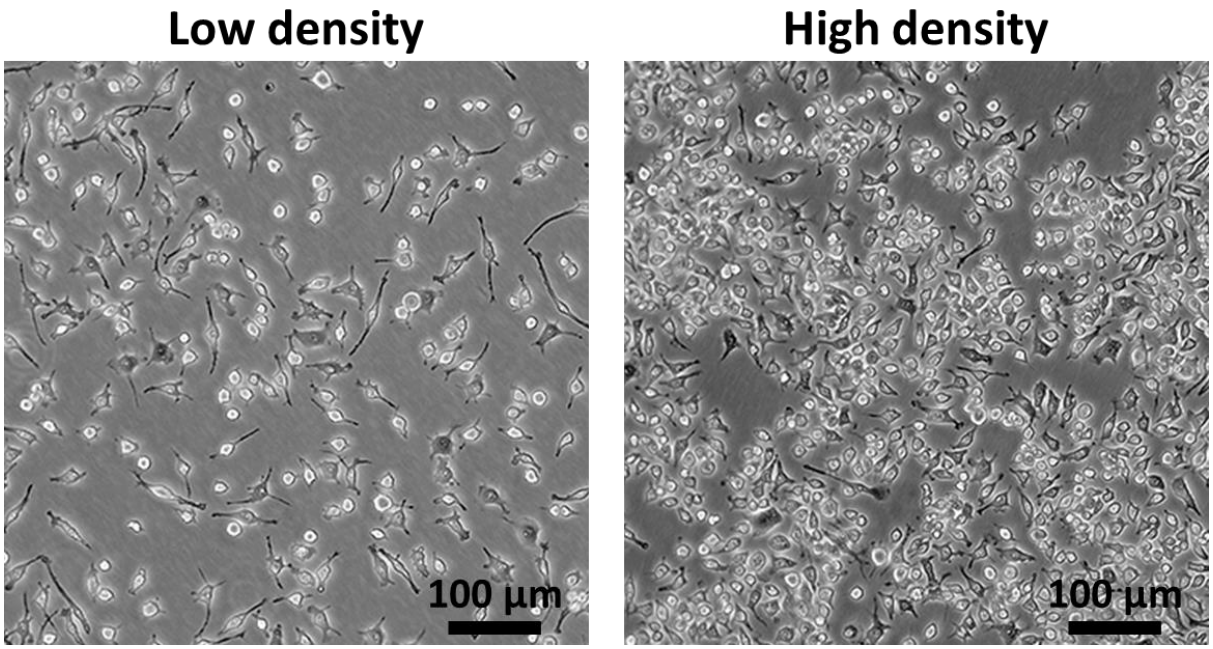

Figure 10 Photo image of Raw 264.7 morphology at low and high cell density. Figure adapted from ATCC (ATCC, 2018).

2.2.10 Scanning electron microscopy

Hydrogel morphology and cell-hydrogel interactions were evaluated by Scanning Electron Microscopy (SEM). Briefly, 100 µL of the pre-gel solutions with and without Hap were pipetted into ThinCert well inserts (0.4 µm pore size Greiner Bio-One Ltd, UK). The inserts were then placed into 24-well plates and incubated at 37°C with a total volume of 1.3 mL DMEM to fully crosslink the hydrogels. The following day, Raw 264.7 cells were seeded onto the hydrogels as described above. After 7 days, cells were washed in PBS and fixed in 2.5 % (w/v) glutaraldehyde (Sigma-Aldrich) and 4% (w/v) PFA (Sigma-Aldrich) in 0.1 M HEPES buffer (Sigma-Aldrich). After rinsing the samples in PBS, for cell observation all samples were dehydrated in a graded ethanol (EtOH) series (25,

50, 75, 95, and 100% v/v EtOH/water). Samples were maintained at 100% EtOH and dried in a K850 Critical Point Drier (CPD, Quorum Technologies, UK). After the CPD step, samples were transferred into metallic pins and coated with gold palladium alloy using an SC7620 Mini Sputter Coater (Quorum). Samples were then imaged on a Quanta 250 FEG SEM (Thermo Fisher Scientific) at 20 kV.

2.2.11 Viability assessment

A Quant-iT™ PicoGreen™ dsDNA Assay Kit (Invitrogen P11496) was used to assess the viability of Raw 264.7 cells cultured on the Hap-decorated Fmoc-FF/S/RGD hydrogels. Cells were cultured into ThinCert well inserts as described in section 2.2.10. At each time point (24 h, 48 h, 5 days and 7 days), medium was removed from the inserts and the cell-cultured hydrogels were transferred into 1.5 mL Eppendorf tubes by gently peeling off the membrane of the ThinCert inserts. Then, 200 µL of 10 mg/mL Pronase in ddH_2O (a commercial mixture of proteases from *Streptomyces griseus,* Roche, UK) were added to each Eppendorf tube and the mixtures vortexed for 20 s following an incubation of 5 min in a water bath at 37°C. An equal volume of 2× TE buffer (20 µM Tris-HCl, 2 mM EDTA, 0.4% Triton X-100, pH 7.5; Sigma-Aldrich) was added to each sample in order to extract the dsDNA. 100 µL of the dsDNA were then pipetted into a 96-well plate where an equal volume of PicoGreen Reagent (200-fold dilution in 1× TE buffer) was added. After 5 min of incubation at room temperature the fluorescence intensity was measured by using a BioTek™ FLx800™ microplate fluorescence

reader (excitation wavelengths: 480-512 nm; emission wavelength: 520 nm). The fluorescence intensity measured was normalised using day 1 of culture as a baseline control. All measurements were performed at least 3 times for each time point to ensure reproducibility.

2.2.12 TRAP immunofluorescence staining

Differentiation of Raw 264.7 cells into mature osteoclasts was determined by using a TRAP monoclonal antibody (mAb). After 7 days in culture on hydrogels, cells were stained following the procedure described in section 2.6 using 1:200 anti-TRAP mAb conjugated Alexa Fluor 594 (Santa Cruz Biotechnology, UK, sc-376875) in PBS-Bovine Serum Albumin (BSA, Sigma-Aldrich) for 90 min. After the incubation time, cells were washed three times for 5 min with PBS and imaged immediately using a Nikon Eclipse 50i fluorescence microscope (excitation wavelength 495 nm). Fluorescence intensity ratio was measured from 100 cells and normalised to the background by using ImageJ v. 1.51.

2.2.13 TRAP gene expression

Raw 264.7 cells were cultured in Hap-decorated Fmoc-FF/S/RGD hydrogels using ThinCert well inserts, as described in section 2.2.10. After 3 and 7 days in culture the hydrogels were removed from the inserts and transferred to 1.5 mL Eppendorf tubes. Then, 1 mL of TRIzol™ Reagent (Invitrogen, 15596026) was added to each hydrogel and RNA was extracted following the manufacturer's

protocol. Quality and quantity were determined using a Nanodrop ND-1000 Spectrophotometer (Nanodrop Technologies). Following the RNA extraction, RNA samples were reverse transcribed into cDNA using a High Capacity Reverse Transcription Kit (Applied Biosystems, UK). Obtained cDNA was further diluted to 5 ng/µL according to the Nanodrop reading and qPCR was performed in triplicate using a StepOne™ Real-Time PCR System (Applied Biosystems, UK) using TaqMan probes with the universal PCR Master Mix (Life Technologies, 4304437) in a total volume of 10 µL. The TaqMan probe for Trap was used (Mm00475698_m1) and data was analysed using the $2^{-\Delta Ct}$ method and normalised to the endogenous house-keeping gene GAPDH (Mm99999915_g1).

2.2.14 Statistical analysis

All quantitative values are presented as mean ± standard deviation. All experiments were performed using at least three replicates. Data were plotted using Origin 2019b and compared using an unpaired *t* test, unless stated otherwise. Two levels of significance were used: 0.005 (**) and 0.001 (***).

2.3 Results and Discussion

2.3.1 Fmoc-based hydrogels as substrates for Raw 264.7 culture: Raw 264.7 adhesion and morphology on different formulations of Fmoc-hydrogels

Fmoc-based SAPHs were used to culture pre-OCs to ascertain their suitability as a platform for OC culture and differentiation. Their nanofibrous structure combined with a high water content make them a suitable option for TE studies (Diaferia, Morelli and Accardo, 2019). Furthermore, as described in a previous section, they can be further functionalised with organic and inorganic molecules that could improve cell adhesion and direct cell fate such as trigger polarization, differentiation etc. (Gaharwar, Peppas and Khademhosseini, 2014). Two different Fmoc-based formulations were tested in order to optimise a protocol for culturing OCs: Fmoc-FF/S and Fmoc-FF/S/RGD. Different peptide concentrations were used to assess how Raw 264.7 cells react to different stiffness in order to select the most suitable hydrogel substrate. **Figure 11** shows F-actin staining of Raw 264.7 cells cultured up to 96 h on a 2D plastic monolayer (TCPS) and on different concentrations of the two hydrogel formulations. After 96 h post culture, Raw 264.7 cells on hydrogels maintained the same polyhedral shape as on the TCPS control. In fact, cells were well spread in all the different formulations tested. They were 10-15 μm in diameter and formed characteristic cluster arrangements,

with round nuclei and several actin pseudopodia protruding towards the exterior. All the formulations tested provided cell adhesion but the 15-20 mM concentrations of both Fmoc-FF/S and Fmoc-FF/S/RGD showed homogeneous cell distribution throughout the hydrogels.

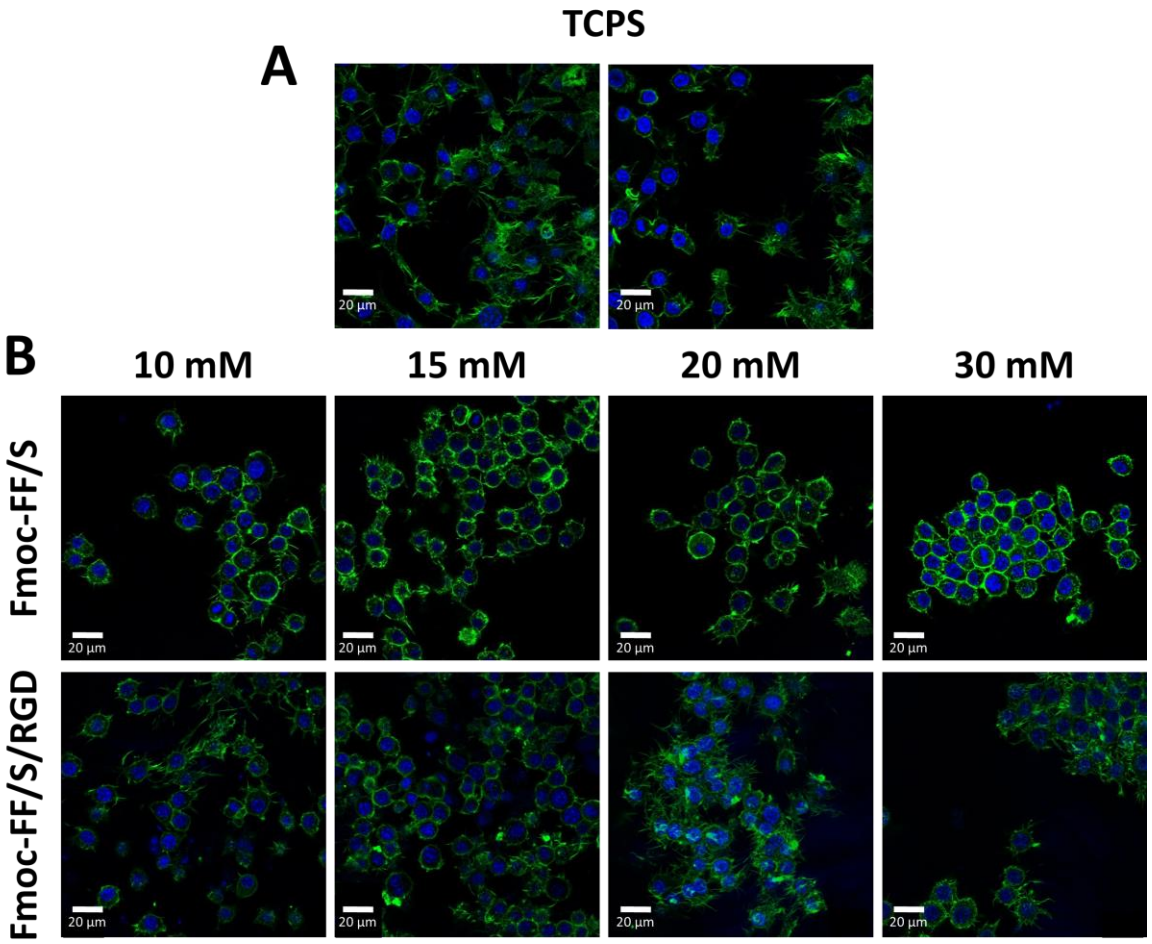

Figure 11 F-actin staining of Raw 264.7 cells cultured on a TCPS surface (**A**) and Fmoc-based hydrogels (**B**). Raw 264.7 cells cultured on hydrogels maintain the same physiological shape, diameter and spreading as those on TCPS (N=2), up to 96 h post culture. The cells are clearly visible and spread on each of the hydrogel formulations tested. Elongated pseudopodia are clearly observable in green (Alexa Fluor 488 phalloidin). Nuclei are stained with Hoechst 33342 (blue). Scale bars on each panel indicate 20 µm.

Next, we tested whether these hydrogel formulations were able to maintain cell viability of Raw 264.7 cells. The LIVE/DEAD™ assay was used as a surrogate of cell viability and each Fmoc-based formulation was tested every 24 hrs for up to three days. Although Fmoc-FF/S hydrogels do not present any specific cell-binding motif, cells cultured on them were viable up to 72 hrs, (**Figure 12)**. In fact, mainly live cells were observed, showing their characteristic cluster morphology.

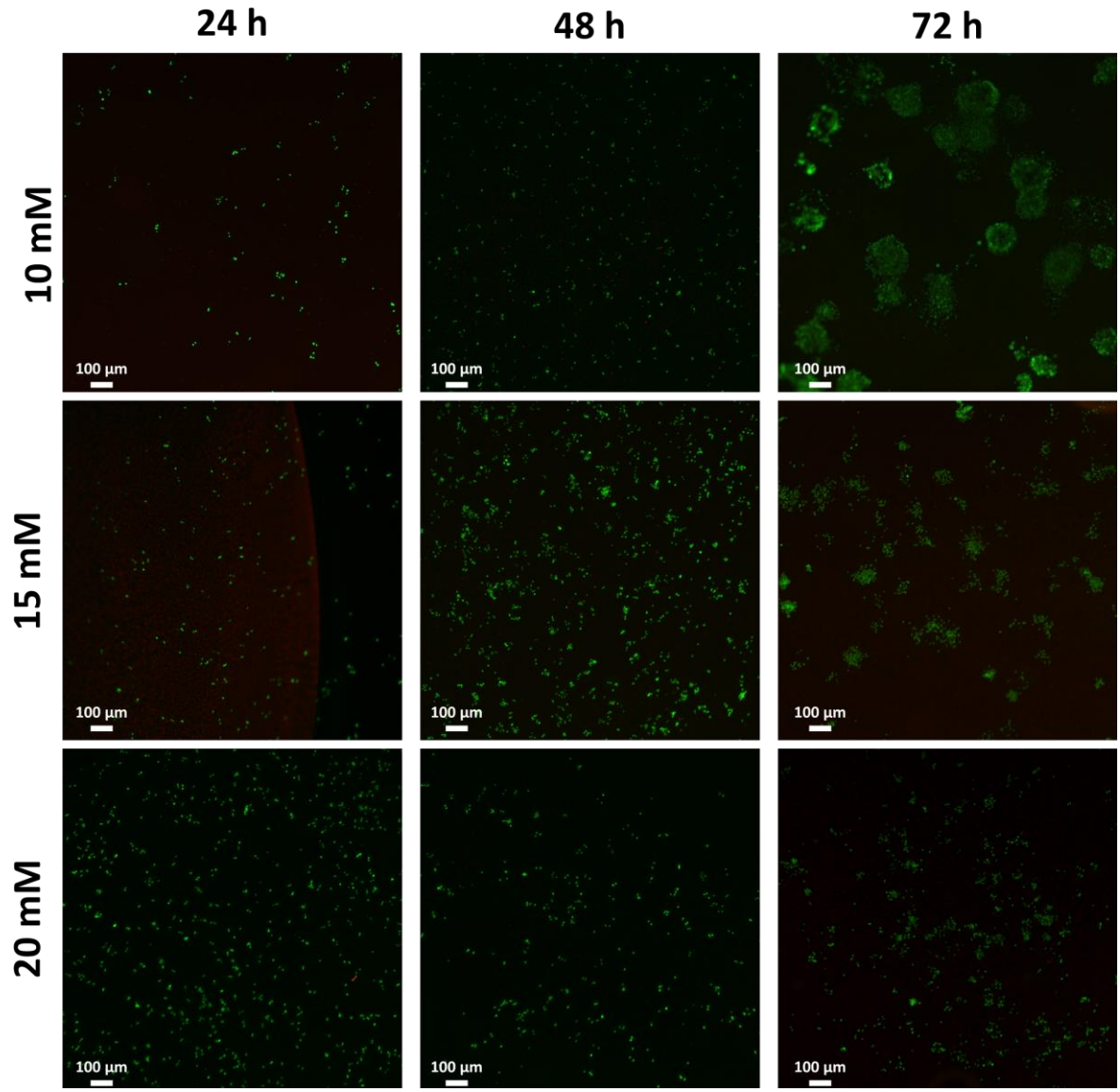

Figure 12 Live/Dead assay of Raw 264.7 cells cultured on Fmoc-FF/S hydrogel at different time points. Calcein AM (green) and Ethidium homodimer-1 (red) were used to assess viable and dead cells respectively. Scale bars on each panel indicate 100 µm.

Similarly, to Fmoc-FF/S, cells cultured on Fmoc-FF/S/RGD hydrogel were mostly viable. Indeed, as seen in **Figure 13**, the presence of the RGD binding motif in the peptide hydrogel structure caused cells to adhere to the hydrogels, facilitated their proliferation, and maintained cell viability over time.

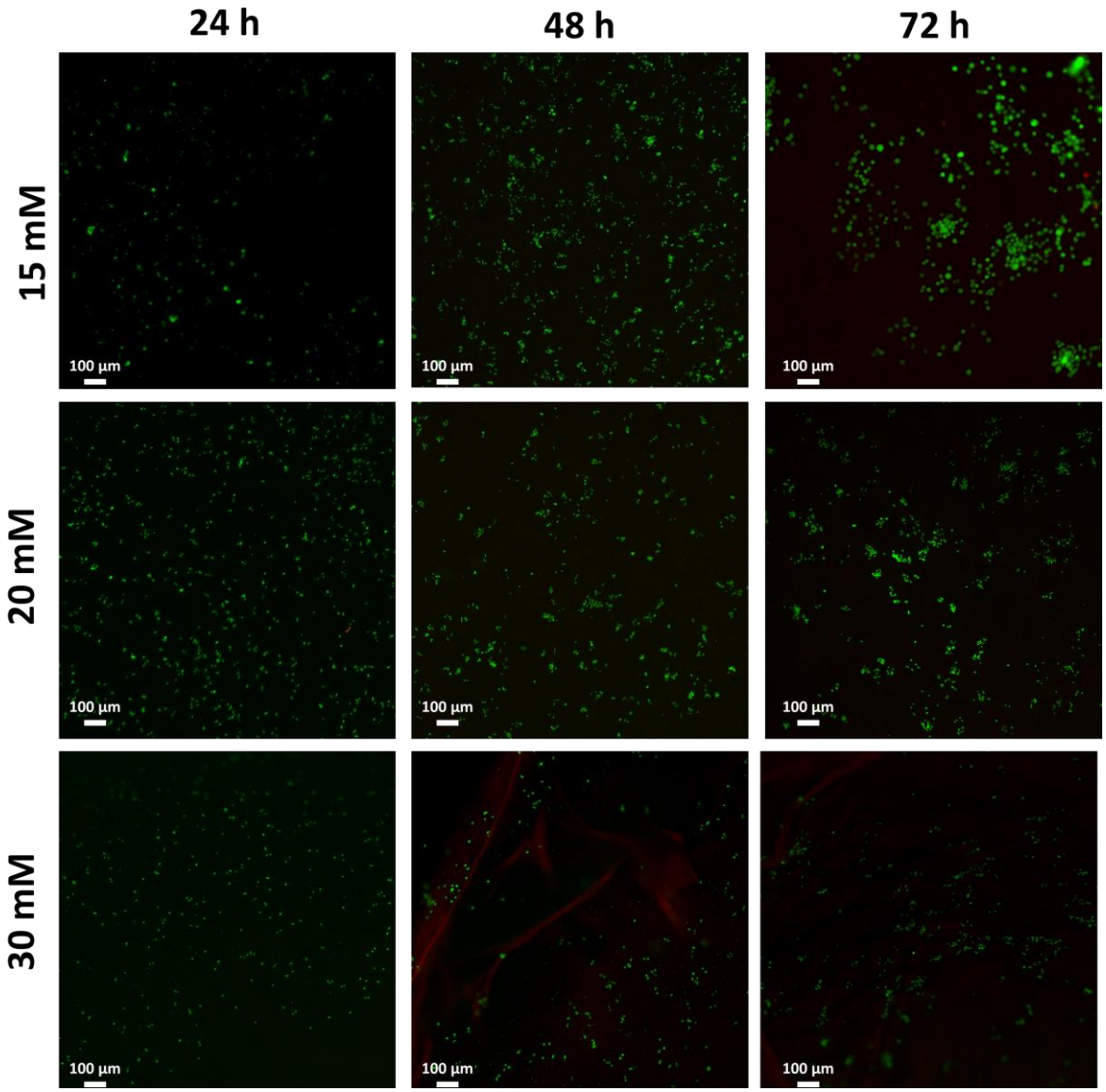

Figure 13 Live/Dead assay of Raw 264.7 cells cultured on Fmoc-FF/S/RGD hydrogels at different time points. Staining and scale bars as in **Figure 12**.

2.3.2 Hydroxyapatite-decorated nanocomposite self-assembled peptide hydrogels: formulation and characterization

After successfully demonstrating adhesion of Raw 264.7 cells to both hydrogels Fmoc-FF/S and Fmoc-FF/S/RGD, we decided to develop a multicomponent hydrogel to use as scaffold for OC culture and differentiation.. Raw 264.7 cells

were viable when cultured on both formulations. Fmoc-FF/S/RGD contains the RGD cell binding motif which is the main integrin-binding site for OC when adhering to the bone (Teitelbaum and Ross, 2003; Phan, Xu and Zheng, 2004). As explained before, these peptide-based scaffolds form self-supporting hydrogels through cooperative assembly of the single monomers (hydrogelator or building blocks) Fmoc-FF, Fmoc-S and Fmoc-RGD when exposed to a divalent-cation containing solution. (**Figure 14**).

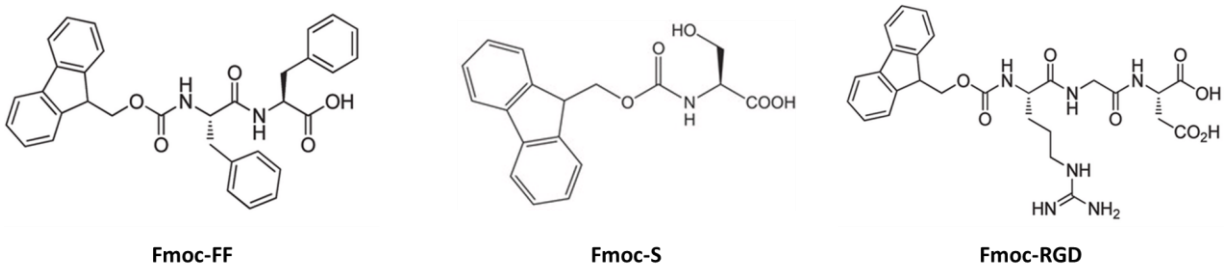

Figure 14 Molecular structure of the three building blocks Fmoc-FF, Fmoc-S, Fmoc-RGD. The Fmoc-FF/S is made from Fmoc-FF and Fmoc-S in a 1:1 ratio. The Fmoc-FF/S/RGD hydrogel is made from these two peptides plus Fmoc-RGD in a 1:0.5:0.5 ratio.

Both hydrogel/s were modified by incorporation of Hap nanopowder, used here as "nanofiller". Hap is the main component of the inorganic part of the bone and it is widely used as extra scaffold component for bone regeneration due to its similarity in chemical composition, structure and density (Boskey, 2013; Kattimani, Kondaka and Lingamaneni, 2016). Furthermore, it has been shown that mineralisation of hydrogels through addition of Hap can increase the mechanical properties of the scaffold as well as its biocompatibility and

bioactivity (Hu *et al.*, 2017). For the reasons mentioned above, we developed and optimised a protocol of incorporation of Hap nanoparticles within Fmoc-based hydrogels (**Figure 15A**).

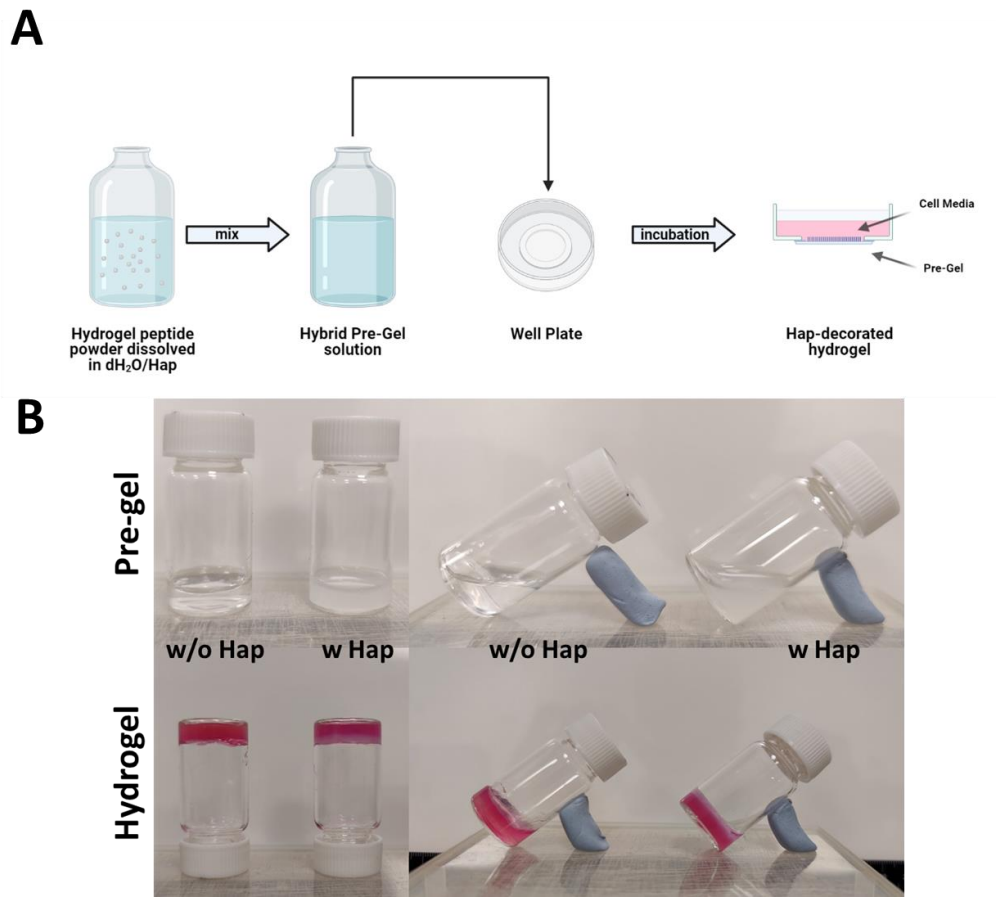

Figure 15 (**A**) Schematic representation of the optimised protocol used to incorporate the Hap nanopowder within hydrogels. (**B**) Pre-gel and hydrogel vials images with or without addition of Hap.

As can be seen from **Figure15B**, both naked and Hap-decorated hydrogels formed a stable, self-supporting structure, as shown by the glass vial flip test. Compared to the unmodified gels, showing a clear and transparent pre-gel

solution, hydrogels incorporating Hap were cloudy, confirming the Hap presence in the gel network.

The effect of Hap nanoparticle addition on the storage moduli of the modified hydrogels was investigated (**Figure 16**). Four different concentrations of Hap nanoparticles were tested: 0.5, 1, 2, 3 mg/mL. Addition of Hap up to 3 mg/ml to Fmoc-FF/S showed a detrimental effect on G' (~3.94-fold decrease compared to the undecorated hydrogel, $p<0.001$). A similar behaviour was observed for Fmoc-FF/S/RGD when adding up to 3 mg/ml of Hap (~ 2.34-fold decrease compared to the naked hydrogel, $p<0.001$). Only Fmoc-FF/S/RGD decorated with up to 1 mg/ml Hap showed a significantly increased storage modulus among the Hap concentrations tested ($p<0.001$). For this reason, 1 mg/ml Hap was used for both hydrogel formulations (Fmoc-FF/S and Fmoc-FF/S/RGD) as final concentration for this study.

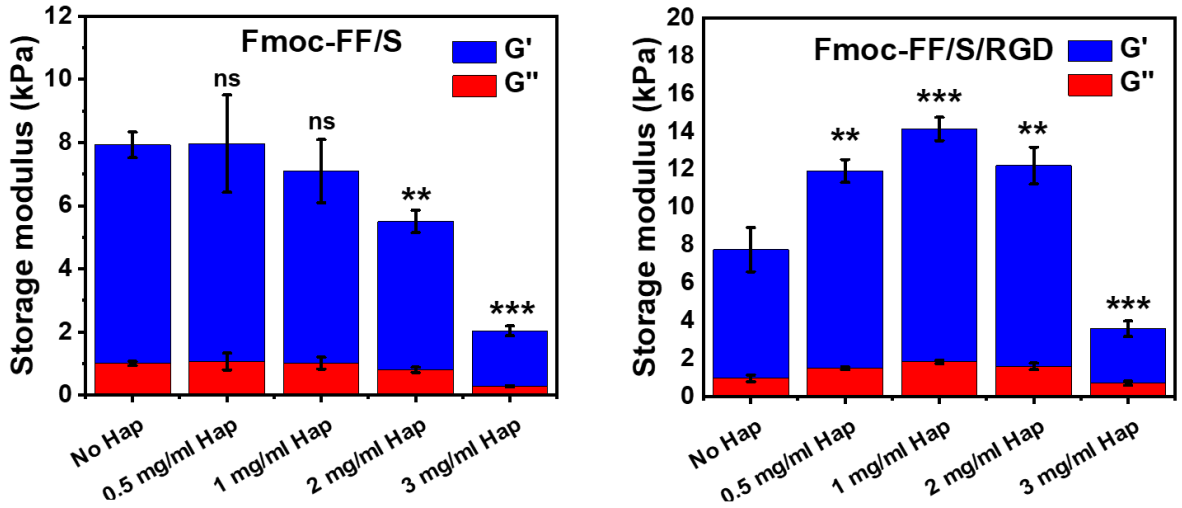

Figure 16 Effect of Hap nanoparticle concentration on the storage moduli (1 Hz frequency, 0.1% shear strain) of Fmoc-FF/S and Fmoc-FF/S/RGD decorated hydrogels. . (Data are shown as mean ± SD; ∗∗∗p -value < 0.001; ∗∗p -value < 0.05).

Additionally, the Hap distribution within the hydrogel network was analysed through confocal microscopy, as described in section 2.2.5.

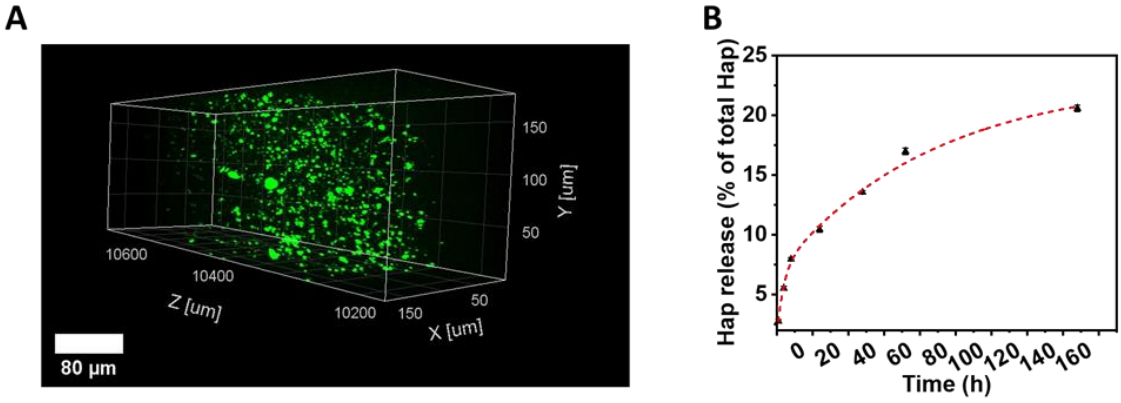

Figure 17 Homogeneous distribution of Hap nanoparticles within the hydrogel network. (**A**) Image stack of Fmoc-FF/S/RGD hydrogel showing calcein-stained Hap (conc. 1mg/ml) homogenously distributed within the gel network. (**B**) Cumulative release fit of Hap from Fmoc-FF/S/RGD hydrogel over time. Data were obtained using the same method described above to label the Hap nanoparticles.

As it can be seen from **Figure 17A**, a 500 µm z-stack showed that the Hap nanoparticles are homogeneously distributed within the hydrogel network. Similarly, the amount of Hap that leeched from the hydrogels was quantified (**Figure 17B)**. An initial burst release of Hap (within the first hours of the self-assembling process) was firstly observed. This release seemed to reach a plateau after 48 h and overall, the amount of Hap that leached from the gel network after 7 days (168 h) was calculated to be ~20%.

2.3.3 Hydroxyapatite-decorated hydrogels nanotopography: Atomic Force Microscopy

The hydrogels microstructure was analysed using AFM (**Figure 18**). All the formulations were tested with and without the addition of 1 mg/mL of Hap.

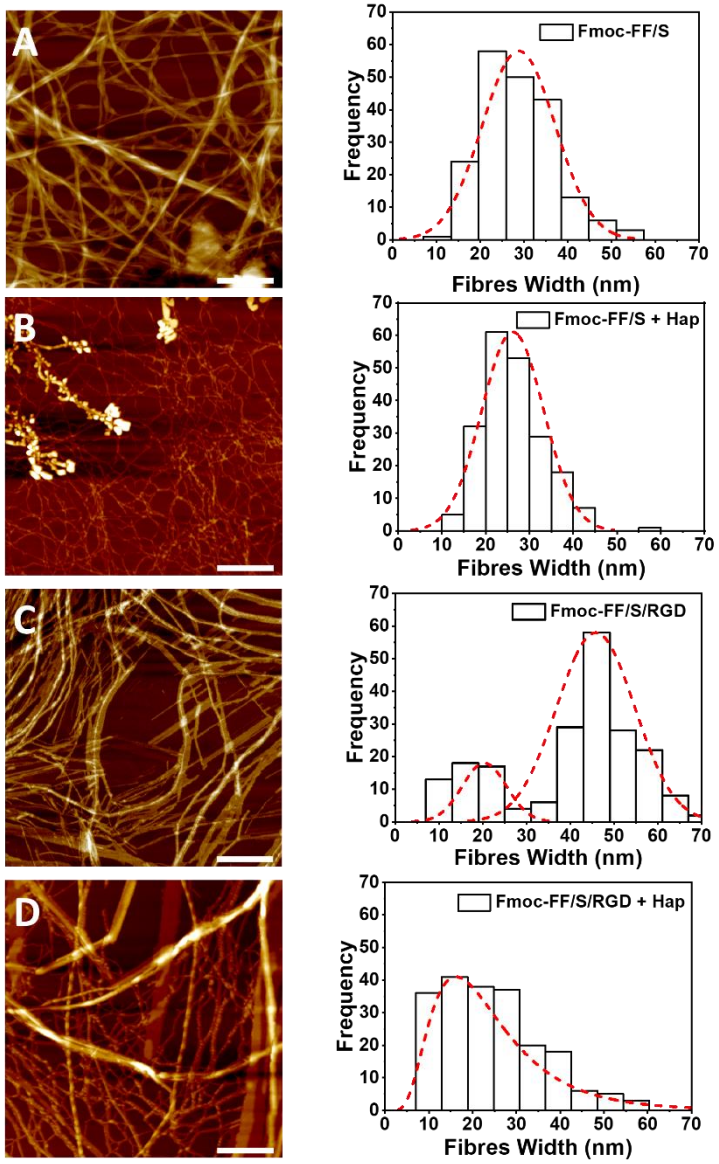

Figure 18 Analysis of hydrogel microstructure by AFM and distributions of fibre widths as measured on the AFM images (**A-D**). Hydrogel nanotopography of Fmoc-FF/S (**A**) and Fmoc-

FF/S/RGD (**C**) without added Hap, and Fmoc-FF/S (**B**) and Fmoc-FF/S/RGD (**D**) after incorporation of Hap (Scan size 2 μm^2 , Scale bar 400 nm).

All formulations showed the nanofibrous morphology typical of hydrogels (**Figure 18**), with long bundles and extensive fibre entanglement, irrespective of the addition of Hap. This suggests that the incorporation of Hap nanoparticles does not disrupt the hydrogel self-assembling mechanism nor causes fibre precipitation (**Figure 18**). Fibre width distribution was also analysed for all the hydrogel formulations, with and without Hap. Fmoc-FF/S hydrogels showed a unimodal fibre distribution irrespective of Hap addition. Average fibre widths were 26 (±7) nm (with Hap) and 29 (±9) nm (without Hap), suggesting little or no difference between these two formulations. However, Fmoc-FF/S/RGD without Hap showed a bimodal fibre width distribution, with a first peak centred at 19 nm and a second, more populated distribution, centred at 44 nm (**Figure 18C**). In contrast, after Hap incorporation, Fmoc-FF/S/RGD showed a broad unimodal distribution with a predominance of thinner fibres (~10 nm in diameter), positive skewness, with a peak around 15 nm. The similarity in fibre width distributions of Fmoc-FF/S hydrogels with or without added Hap is probably due to the lack of interaction between Hap and neither of the two monomers Fmoc-FF and Fmoc-S (**Figure 14**) (Tavafoghi Jahromi, G. Yao and Cerruti, 2013; Ghosh *et al.*, 2017b). The introduction of a third monomer, Fmoc-RGD causes a bimodal distribution in the fibre widths of the Fmoc-FF/S/RGD hydrogel, with thinner and thicker fibres. In fact, as demonstrated in a similar

peptide-based hydrogel system, the occurrence of thicker and thinner fibres can be caused by addition of a third peptide that, probably due to steric interference by the longer RGD chains, may hinder the formation of fibre-fibre lateral interactions (Green *et al.*, 2018). In the presence of Hap, the distribution changes to unimodal and is dominated by thinner fibres. A direct interaction between the Hap nanoparticles and the peptide fibres could be at the root of this observation. Addition of Hap may induce the peptide fibres to form thinner structures to help "accommodating" such particles within the hydrogel structure. The reasons presented here are in line with the model described by Zhou *et al.* where Fmoc-FF and Fmoc-RGD self-assemble into a cylinder-like structure with the RGD motif repeating itself on the fibre surfaces (Zhou *et al.*, 2009). It has also been demonstrated that nanoparticles decorating fibre surfaces can decrease the mobility of the monomers, causing a relaxation of the fibres (Kwon and Sung, 2018). For this reason, during the hydrogel self-assembling mechanism, the presence of Hap in the system "forces" the formation of thinner fibres, due to steric interaction.

2.3.4 Hydroxyapatite particle size and periodicity on the Fmoc-FF/S/RGD fibres

Having found that there was an interaction between the Hap particles and the fibres within the Fmoc-FF/S/RGD hydrogels, the Hap distribution was also analysed *via* AFM. Size distribution of the Hap nanoparticles alone ranges

between ~5 and 25 nm and, when sitting on the hydrogels fibres, a tighter distribution of nanoparticles can be observed (**Figure 19**).

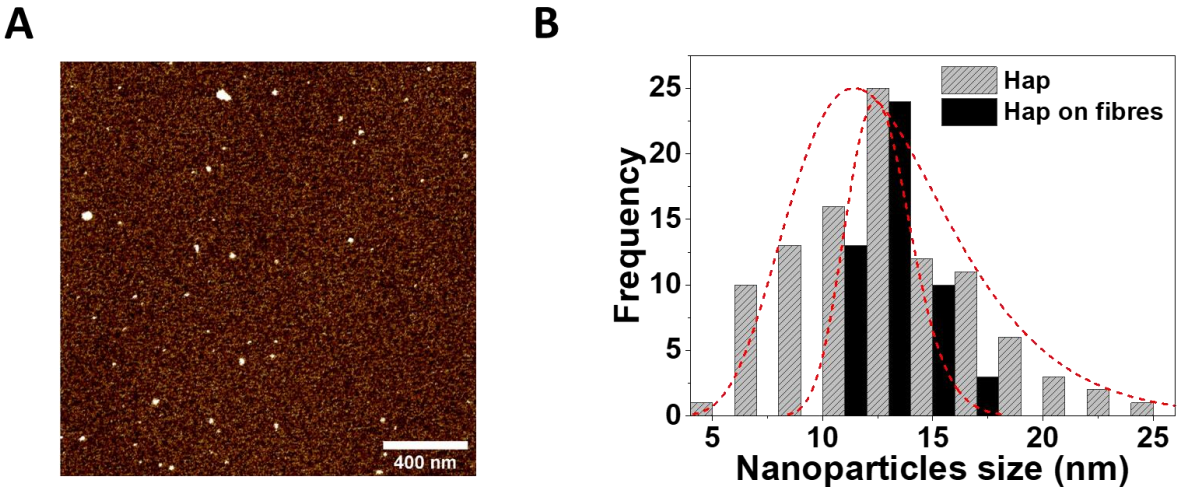

Figure 19 Size distribution of Hap nanoparticles. (A) AFM image of Hap nanoparticles (concentration 1 µg/ml) on a 2 μm^2 scan size region of polylysine–coated mica. (B) Size distribution of Hap nanoparticles when alone (grey bars), and on the Fmoc-FF/S/RGD hydrogel fibres (black bars).

Interestingly, it was observed that, when incorporated into the Fmoc-FF/S/RGD hydrogels, Hap nanoparticles seemed to be arranged in a specific pattern. As can be seen from **Figure 20**, the Hap is repeating itself along the fibre's axis with a periodicity of ~ 34 nm.

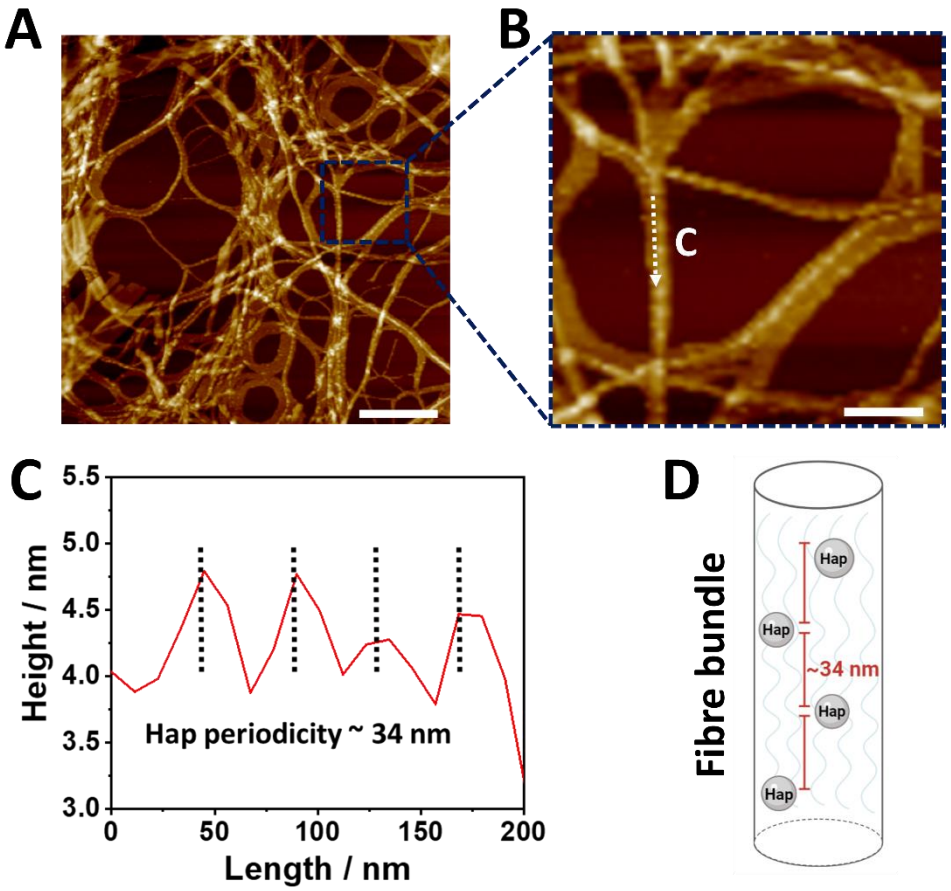

Figure 20 Topography of Hap-decorated Fmoc-FF/S/RGD hydrogels. (**A**) 2 μm^2 AFM images of Fmoc-FF/S/RGD incorporating Hap in a repeating pattern. (**B**) Enlarged AFM image of the area outlined in **A** showing Hap nanoparticles decorating the Fmoc-FF/S/RGD fibres. (**C**) Corresponding height profile of the linear scan indicated by the white dotted arrow in B. (**D**) Schematic model of a hydrogel fibre incorporating Hap nanoparticles. Scale bar for A is 400 nm. Scale Bar for B is 200 nm.

Ghosh and co-workers demonstrated that Hap nanoparticles can strongly interact with polar and positively charged amino acids (such as Arginine, present in the RGD sequence) (Tavafoghi Jahromi, G Yao and Cerruti, 2013; Ghosh *et al.*, 2017b). The scaffold used for this experiment contains Fmoc-RGD as one of the monomers hydrogelators and for this reason, it was hypothesised that Hap

nanoparticles can interact with the positively charged Arg side chains from the Fmoc-RGD peptide. This hypothesis can explain the more homogeneous distribution of Hap nanoparticles in the Fmoc-FF/S/RGD hydrogel compared to that in the Fmoc-FF/S one, which does not contain the RGD motif (**Figure 18**). Large-range electrostatic interactions may be involved when incorporating the Hap nanoparticles (negatively charged) into Arginine-containing hydrogels (positively charged at formulation). As previously demonstrated by Cerruti *et* al., it is reasonable to believe that the RGD motif present in the hydrogel formulation exposes the side chains of the Arginine and the Aspartic Acid (positively and negatively charged, respectively) and that these may be involved in large-range electrostatic interactions (Tavafoghi Jahromi, G Yao and Cerruti, 2013; Rivas *et al.*, 2019).

2.3.5 Hydrogel mechanical properties, rheological characterization

As described in the previous sections, one of the advantages of using Hap as nanofiller is to obtain a nanocomposite hydrogel with enhanced mechanical properties (Manias, 2007). For this reason, the effect of the Hap incorporation on the hydrogels was evaluated by rheology. Fmoc-FF/S and Fmoc-FF/S/RGD were analysed with and without the addition of 1 mg/mL of Hap. Both hydrogel formulations were subjected to a frequency sweep experiment (frequency range 0.1 to 100 Hz, strain 0.1 %). Regardless of the addition of Hap, all the hydrogels were able to form a self-supporting spheroid-like scaffold as demonstrated by the

storage modulus (G') being constantly higher than the viscous modulus (G''), throughout the entire experiment (**Figure 21**) (Yan and Pochan, 2010).

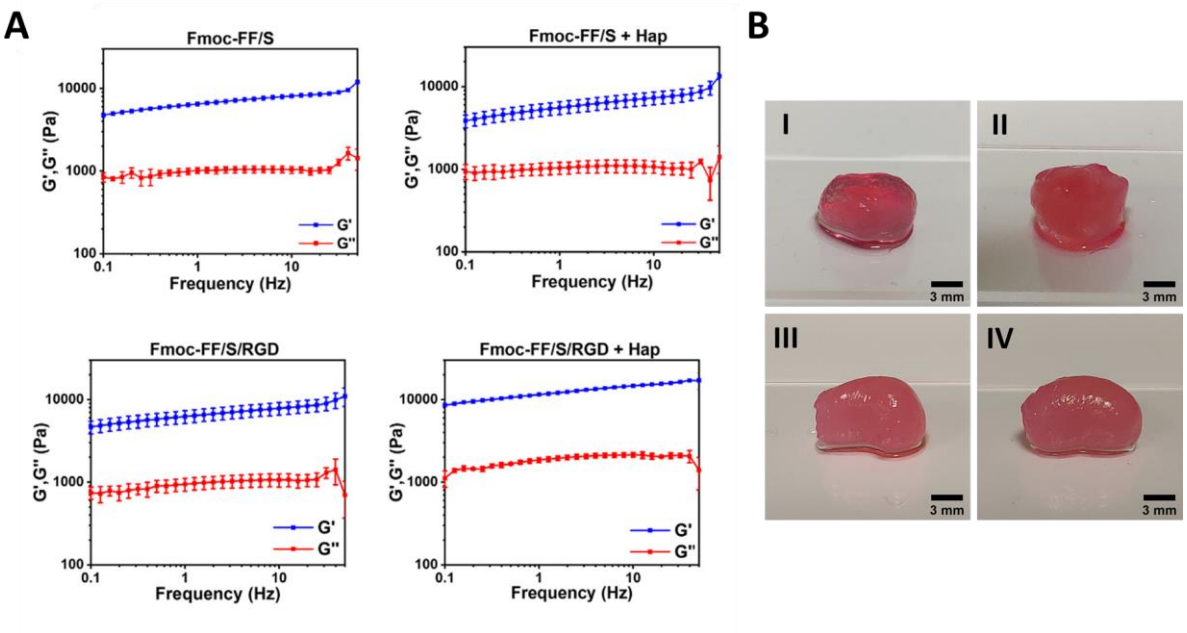

Figure 21 (A) Frequency sweep rheology measurements (0.1-100 Hz 0.1 % strain) of Fmoc-FF/S and Fmoc-FF/S/RGD hydrogels, with and without Hap incorporation. (B) Photographs of the spheroids of Fmoc-FF/S (I), Fmoc-FF/S + Hap (II), Fmoc-FF/S/RGD (III) and Fmoc-FF/S/RGD + Hap (IV) used for the rheology experiments, evidencing dimensional stability for all the formulations. All measurements were performed at least 3 times at 25 °C.

The values of the storage modulus G' and the loss modulus G" were recorded for all formulations at a fixed frequency of 1 Hz, 0.1% strain in order to assess the resulting stiffness of the scaffolds (**Figure 22**).

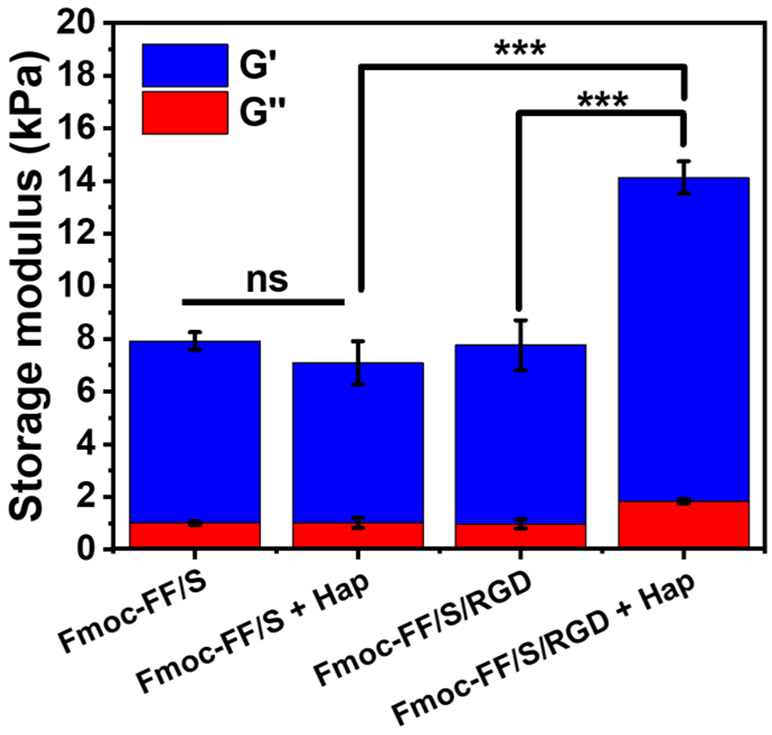

Figure 22 Comparison of the storage and loss moduli of each hydrogel formulation at 1 Hz, 0.1% strain. (Data are shown as mean ± SD; ∗∗∗p -value < 0.001; ∗∗p -value < 0.05).

Hydrogels without incorporated Hap showed similar G' values (6.9 ± 0.3 kPa for Fmoc-FF/S *vs* 6.8 ± 1.0 kPa for Fmoc-FF/S/RGD) suggesting no differences between these two hydrogel formulations. Hap incorporation to Fmoc-FF/S did not change significantly (*p* value = 0.8958) the resulting stiffness of the hydrogel (6.9 ± 0.33 *vs* 6.1 ± 0.8 kPa). However, incorporation of Hap to Fmoc-FF/S/RGD caused a significant increase in G' compared to both the undecorated Fmoc-FF/S/RGD hydrogels (12.3 ± 0.6 *vs* 6.8 ± 0.3 kPa, $p < 0.005$) and the Hap-decorated Fmoc-FF/S hydrogels (12.3 ± 0.61 *vs* 6.1 ± 0.8 kPa, $p < 0.001$). Again, these findings are in line with those of Ghosh and colleagues (Ghosh *et al.*, 2017b) and demonstrate that incorporation of Hap nanoparticles within Arginine-

containing, Fmoc-based scaffolds results in stiffer hydrogels. Similarly, to what is observed in the AFM analysis, Hap interaction with Fmoc-FF/S/RGD is stronger mainly due to the presence of Arg side chains in the peptide-hydrogel structure. For this reason, the increase in stiffness is greater in RGD-presenting hydrogels than what is observed for the Fmoc-FF/S hydrogels. It is possible that the high concentration of Hap nanoparticles, interacting with the RGD motif, induces a higher number of fibre entanglements and fibre-fibre associations, resulting in a more tighter fibre mesh and therefore a stiffer scaffold (Tavafoghi *et al.*, 2016).

2.3.6 Hydroxyapatite-decorated hydrogels: a new platform for OC culture and differentiation

One of the major goal of this chapter was to develop an optimised scaffold to culture OCs which, , are involved in many diseases affecting the bone (Teitelbaum, 2000a). The aim was to create a bone-mimicking substrate that resembles the typical bone features and could potentially act as scaffold to culture and differentiate OCs cells. For this reason, the Hap-decorated hydrogels were considered a suitable option to achieve this goal. In fact, their nanofibrous network, combined with a higher degree of mineralisation, due to the presence of Hap, makes them attractive biomaterials for BTE studies.

Raw 264.7 cells were used as pre-osteoclast model. They are a murine-derived cell line widely used to assess OC differentiation and bone resorbing ability (Marino *et al.*, 2014). These cells are able to form mature bone-resorbing OC

after 5-7 days stimulation with the cytokine RANKL (Collin-Osdoby and Osdoby, 2012). They undergo a dramatic change in morphology and typical morphology features are usually observed when mature OC are formed such as the presence/absence of an acting ring surrounding the cells cytoplasm and more than three nuclei per cell. Similar parameters were used when Raw 264.7 were cultured on the Hap-decorated hydrogels. **Figure 23** shows the analysis of Raw 264.7 cell culture and differentiation on 15 mM Fmoc-FF/S and Fmoc-FF/S/RGD hydrogels with and without Hap.

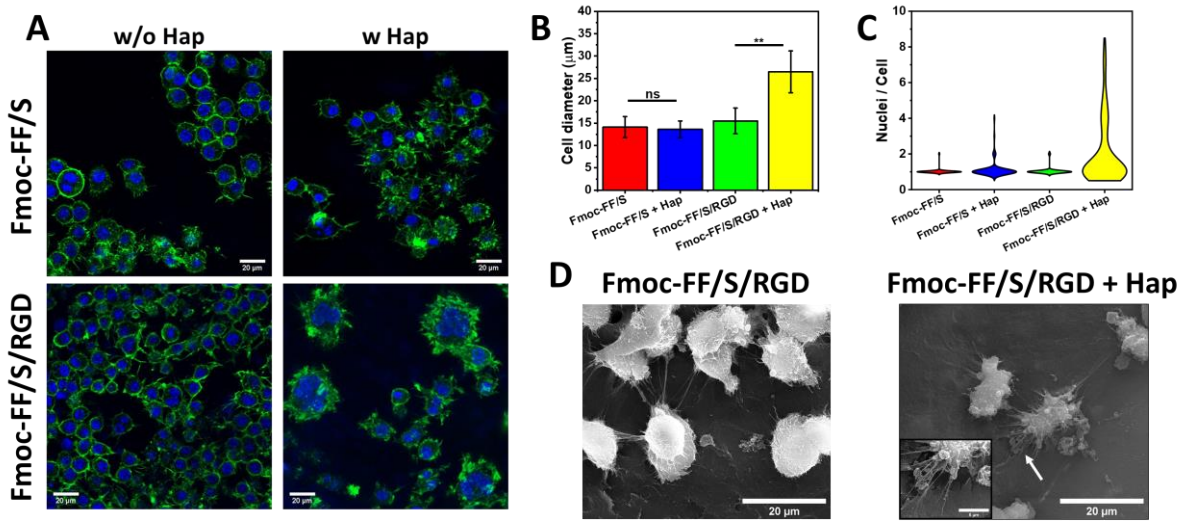

Figure 23 Analysis of Raw 264.7 cell culture and differentiation on 15 mM Fmoc-FF/S and Fmoc-FF/S/RGD hydrogels with and without Hap. (**A**) F-actin staining of Raw 264.7 cells after seven days culture on the different hydrogels (green: F-actin, Alexa Fluor 488 phalloidin; blue: Nuclei, Hoechst 33342; scale bars 20 µm). (**B**) Measurements of cell diameter (data shown as mean ± SD, N = 43, ∗∗p < 0.05). (b) Analysis of multinucleation by a violin distribution plot (data shown as number of nuclei per cell, N = 100). (**D**) SEM images of Raw 264.7 cells cultured on Fmoc-FF/S/RGD with or without incorporated Hap. White arrow shows elongated pseudopodia of Raw 264.7-derived OC. (Data are shown as mean ± SD; ∗∗∗p -value < 0.001; ∗∗p -value < 0.05).

As can be seen from **Figure 23A**, Raw 264.7 cells showed the presence of an acting ring surrounding all the cells in all the formulation tested, regardless the presence of Hap. However, cell morphology changed dramatically when they were cultured on Fmoc-FF/S/RGD with Hap. In fact, they showed cell spreading and an increased cell diameter. **Figure 23B** represents the mean cell diameter of Raw 264.7 cultured on all the different formulations. Cells cultured on Fmoc-FF/S/RGD with Hap were larger (26.5 ± 4.7 μm) than their counterparts cultured on either the undecorated hydrogels (15.5 ± 2.9 μm) or Fmoc-FF/S with (13.6 ± 1.9 μm) and without Hap (14.1 ± 2.3 μm). Secondly, the number of nuclei per cells was analysed. For this purpose, a violin plot was used as it represents one of the best options to compare the distribution of quantitative data across different formulations. Again, cells cultured on Hap-decorated Fmoc-FF/S/RGD hydrogels up to 9 nuclei/cell with a higher number of cells with 4-8 nuclei. This distribution was significantly different from that seen for cells cultured on the other hydrogels ($p < 0.0001$, non- parametric ANOVA).

The morphology of Raw 264.7 cultured on Fmoc-FF/S/RGD with and without Hap was also analysed by SEM (**Figure 23D**). Cells cultured on the undecorated hydrogels displayed rounded morphology, smaller diameter and long pseudopodia interconnecting each other's. On the other hand, Raw 264.7 cultured on the Hap-decorated RGD hydrogels showed spread morphology, larger diameter and prominent pseudopodia that connect them to the scaffold. It is also

reasonable to hypothesize that they are embedded into a so called “resorptive” pit, as can be seen from the higher magnification micrograph (**Figure 23D**). This is usually described as “focal” adhesion as cells tightly interact with the hydrogels surface through the interaction of these pseudopodia.

Based on these results, Fmoc-FF/S/RGD represents the best scaffold to culture and differentiate of Raw 264.7 cells to mature OCs. Two crucial factors need to be considerate in this case. Firstly, the presence of RGD motif. In fact, as explained in the first chapter OCs connect to the bone predominantly by the use of αvβ3 integrin that is located on the cell membrane and strongly interact with the RGD motif present on the bone (as part of ECM proteins) (Teitelbaum and Ross, 2003; Phan, Xu and Zheng, 2004). In fact, it has been demonstrated that blocking the αvβ3-RGD interaction (and consequent signalling), causes an impairment of OC differentiation and function. We assessed the extent of αvβ3-RGD interaction on the Fmoc-FF/S/RGD hydrogels by blocking the αvβ3 integrin by pre-incubating the Raw 264.7 with an anti-αvβ3 antibody.

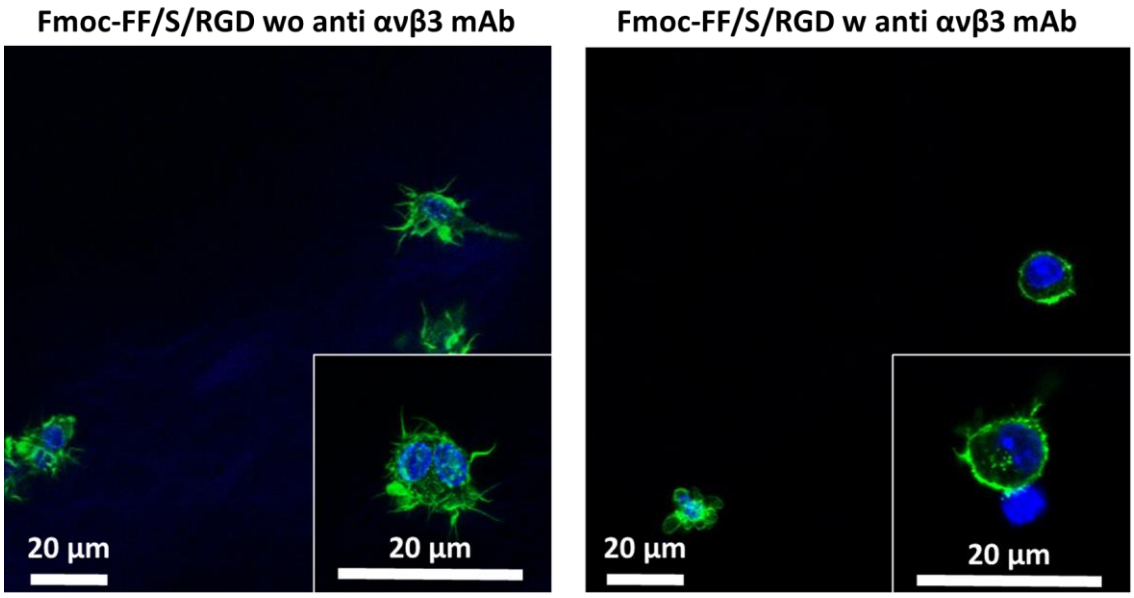

Figure 24 F-actin staining of Raw 264.7 cultured on Fmoc-FF/S/RGD with Hap in presence/absence of $\alpha v\beta_3$. Cells treated with the antibody (right panel) showed rounded morphology with minimal or no focal adhesion. Untreated cells are spread with prominent pseudopodia interacting with the gel matrix.

As illustrated in **Figure 24**, after 24 h post culture, cells pre-treated with anti αvβ3 mAb appeared to be rounded with minimal or no spreading when cultured on Fmoc-FF/S/RGD. On the other hand, when no antibody was used cells showed spread appearance. Hence, the presence of RGD motifs allows Raw 264.7 cells to better adhere to the Fmoc-FF/S/RGD hydrogel. However, RGD-motif alone was not enough to guarantee differentiation of Raw 264.7 as this occurred only in presence of Hap nanoparticles. For this reason, Hap is the second most important factor for OCs-differentiation. In fact, it has been demonstrated that Hap is widely used as nanofiller for different type of scaffolds due to its bioactive and biocompatibility properties (Tozzi *et al.*, 2016; Bai *et al.*, 2018). Moreover, Hap presence in scaffolds has been linked to OC multinucleation, pronounced

actin ring and cell spreading (Botelho *et al.*, 2006; Detsch, Mayr and Ziegler, 2008; Ciapetti *et al.*, 2017). All of these features have been observed and described in this newly developed Fmoc-based system.

2.3.7 Hydroxyapatite-decorated hydrogels as a substrate for osteoclast culture and differentiation

Of all the combinations tested, Hap-decorated Fmoc-FF/S/RGD hydrogel demonstrated potential to be used as platform scaffold for OC culture and differentiation. For this reason, additional assays to assess cell viability and effective OCs-differentiation were performed. First, viability was analysed by means of LIVE/DEAD™ and PicoGreen Assay (**Figure 25**).

Viability of Raw 264.7 cultured on Hap-decorated Fmoc-FF/S/RGD hydrogels was assessed for up to 7days. As can be seen in **Figure 25A** cells were mainly live throughout the whole time points and, interestingly, from 48 h onward, cells started to form clusters (displayed in the higher magnification picture) to eventually form cells with larger diameter after 7 days post culture, with little or no cluster present. Similarly, PicoGreen assay showed almost a 70% increase in cell proliferation over time with a significant ($p < 0.005$) rise in dsDNA concentration. (Figure 25b).

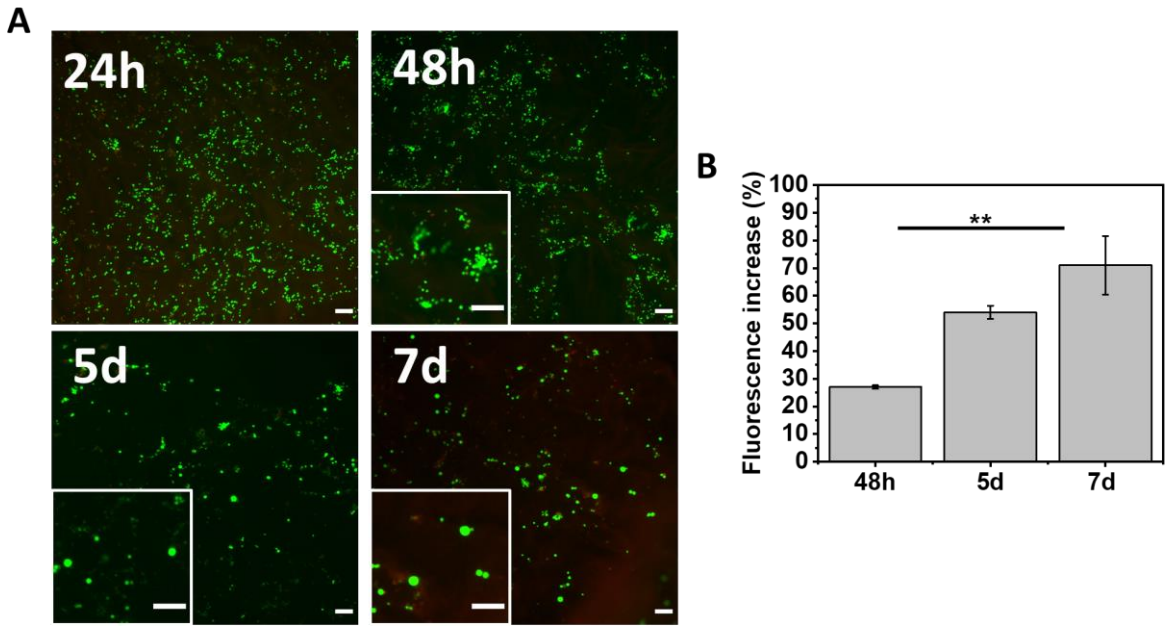

Figure 25 (**A**) Analysis of viability of Raw 264.7 cells cultured on Fmoc-FF/S/RGD + Hap at different time points using a LIVE/DEAD assay (green: viable cells, calcein AM; red: dead cells, ethidium homodimer-1; scale bar 100 μm). (**B**) PicoGreen fluorescence quantification of dsDNA of Raw 264.7 cells cultured on Fmoc-FF/S/RGD + Hap at different time points (Data are plotted based on the fluorescence increase compared to 24 h values used as baseline control).

By the analysis of these two sets of combined data, it is reasonable to postulate that Raw 264.7 cells begin their OC-commitment within 3 days post seeding and at day 7 they eventually form OCs, as widely described in literature (Marino *et al.*, 2014). Thus, the increase in dsDNA observed in **Figure 25B** can be linked not to an increase in cell number but it could be due to the presence of multinucleated cells and therefore a higher quantity of DNA per cell.

Finally, in order to confirm that Raw 264.7cells do form OCs when seeded onto the Hap-decorated Fmoc-FF/S/RGD hydrogels, one of the common OCs marker was assessed: Tartrate-Resistant Acid Phosphatase (TRAP) (Ballanti *et al.*, 1997;

Hayman, 2008). TRAP is one of the most important OC OC marker and it is a protein phosphatase that it is used to soften the bone matrix by pumping ion H^+ within the sealing zone of the bone. Its expression is localised within the cell membrane area, lysosomes and Golgi cisternae (Ljusberg *et al.*, 2005). For this reason, by using a monoclonal antibody against TRAP, its expression was assessed on Raw 264.7 cells cultured on Hap-decorated Fmoc-FF/S/RGD hydrogels compared with the undecorated counterpart. Thus, as illustrated in **Figure 26A**, Raw 264.7 cells cultured on the decorated hydrogel had a positive, bright expression localised within the cell membrane. Furthermore, the intensity of this expression was significantly higher than the naked hydrogels ($p < 0.005$).

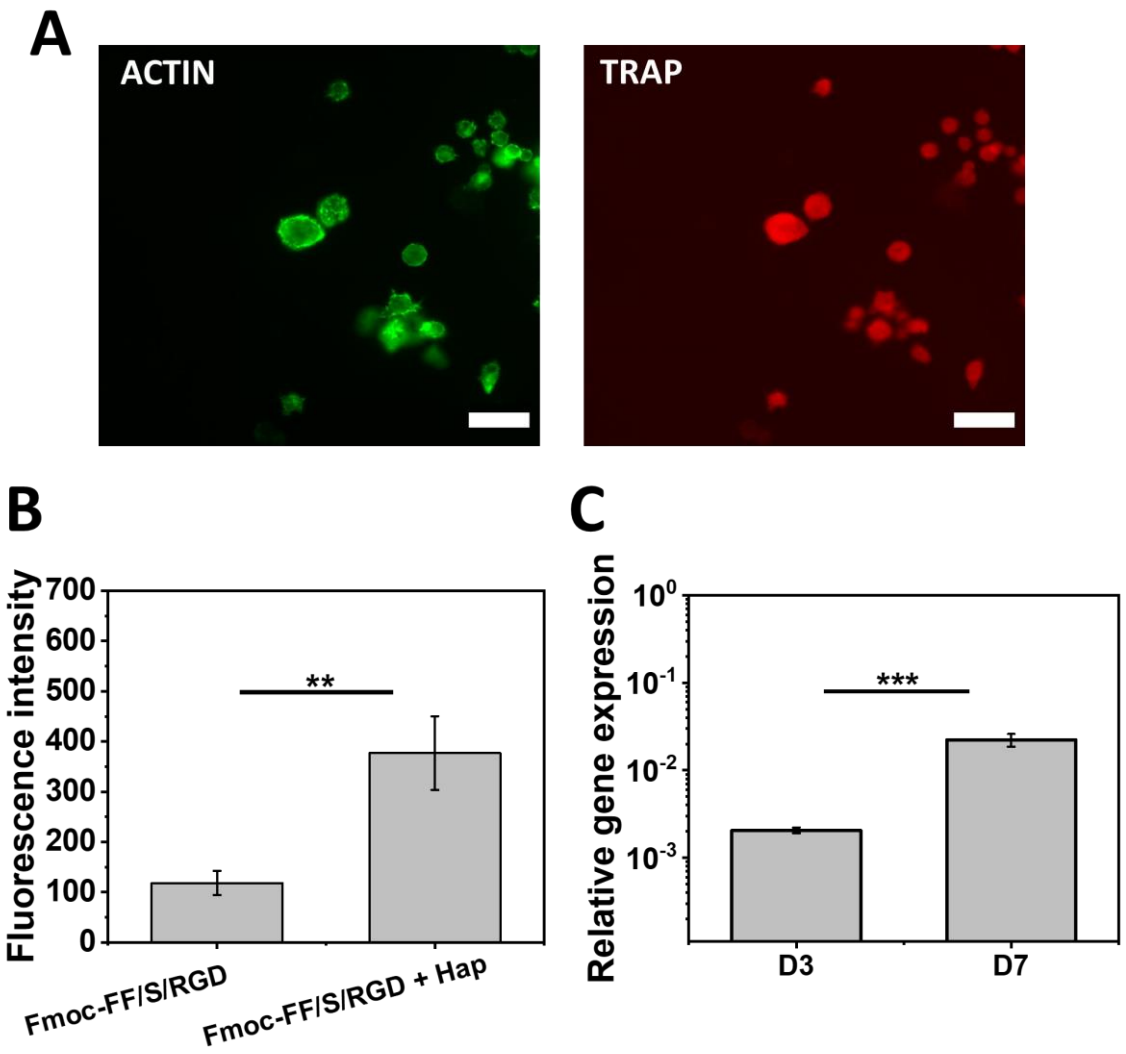

Figure 26 (**A**) Immunofluorescence staining of TRAP (green: F-actin, Alexa Fluor 488 phalloidin; red: TRAP, anti-TRAP mAb conjugated Alexa Fluor 594). (**B**) Relative TRAP immunofluorescence intensity of cells cultured on Hap-decorated Fmoc-FF/S/RGD hydrogels compared to the naked Fmoc-FF/S/RGD (fluorescence intensity was measured from at least N = 100 cells and corrected against the background). (**C**) Gene expression of TRAP relative to GAPDH by Raw 264.7 cells (n = 3) after three (D3) and seven (D7) days culture on Hap-decorated Fmoc-FF/S/RGD hydrogel. (Data shown as mean ± SD; ∗∗∗$p < 0.001$; ∗∗$p < 0.05$).

TRAP expression was also analysed by qRT-PCR. Having considered that the OC-commitment started at day 3 post culture (as observed from the viability data, **Figure 25A**), the level of this marker was compared with the one obtained at the

end point of cell culture (day 7). **Figure 26C** shows the gene expression of TRAP relative to the house-keeping gene GAPDH. Again, the level of expression was significantly higher at day 7 confirming the differentiation of Raw 264.7 to mature OCs.

All these results taken together, the change in morphology of Raw 264.7 when cultured in presence of RGD and Hap, the presence of multinuclei, increase expression of TRAP as typical OCs marker suggest that this newly developed Hap-decorated hydrogels system successfully support viability of pre-OCs cells and the osteoclastogenesis *in vitro*.

2.4 Conclusions

The aims of this chapter were to test different formulations of Fmoc-based hydrogels in order to find a suitable scaffold to be used as a platform to culture and study OC differentiation and function. Indeed, two different Fmoc-based hydrogels were tested: Fmoc-FF/S and Fmoc-FF/S/RGD. Both formulations showed good cell viability and Fmoc-FF/S/RGD was chosen due to the presence of RGD as specific integrin-binding site for OCs. Furthermore, to improve the quality of the resulting scaffold, Hap was used as nanofiller to be combined within the hydrogels due to its biocompatibility and bioactive properties. Thus, a Hap-decorated Fmoc-based peptide hydrogel that could be used as a bone-mimicking scaffold for 2D culture and differentiation of OC cells was successfully formulated.

Here are presented the major finding of this chapter:

- Hap nanoparticles were successfully incorporated within the hydrogels structure without affecting the self-assembling mechanism of the resulting scaffolds.
- AFM results showed that Hap nanoparticles can decorate the peptide hydrogels fibres, possibly through a physiochemical interaction between the Fmoc-RGD-functionalised peptide nanofibers and the Hap surface, in a repeated pattern.

- This could also explain the increased mechanical properties (raise of G') observed *via* rheology for Fmoc-FF/S/RGD incorporating Hap compared to the undecorated hydrogels or not containing the RGD peptide.
- Our newly developed Hap-decorated hydrogel containing the RGD binding motif showed potential as scaffold to culture and differentiate pre-OCs to mature OCs. In fact, typical OC-like features were observed such as multinucleation, presence of actin ring, and change in morphology (e.g. cell spreading, higher cell diameter).
- Similarly a significant change in TRAP expression (a typical OCs-marker) was noted both through immunofluorescence and qRT-PCR suggesting the effective differentiation to OCs (Hayman, 2008).
- Interestingly, compared to other different hydrogel systems for culturing OCs (such as gellan gum, alginate or hyaluronic acid hydrogels (Zehnder, Boccaccini and Detsch, 2017; Maia *et al.*, 2018; Hulley, Papadimitriou-Olivgeri and Knowles, 2020)), this system closely resembles the typical OC-bone interface. In fact, OCs interact with a biomineralized peptide surface in an active way through OC-typical RGD-integrin binding (integrin $\alpha_v\beta_3$);
- Importantly, this functionalised hydrogel supports osteoclastogenesis *in vitro* and does not require the presence of inducing factors such as RANKL (Collin-Osdoby and Osdoby, 2012) to generate mature OCs. Although,

RANKL/RANK is considered to be an essential pathway for the differentiation of osteoclasts (Boyce and Xing, 2007), there are also evidence that topography of the surface can trigger the self-production of RANKL by OCs precursors (Narducci and Nicolin, 2009). In fact, Narducci *et* al have demonstrated that hydroxyapatite substrate might be able to induce a self-production of RANKL cytokine that directly stimulates a different behaviour in terms of phenotype expression from monocyte/macrophage lineage to mature and functional osteoclasts without the addition of exogenous factors.

Altogether, these results suggest that the Hap-decorated hydrogels developed here, despite its limitations (e.g., 2D platform, lack of collagen component, mechanical properties not as stiff as native tissue), could provide a material platform to design more complex and translatable biomaterials for OC culture and differentiation. Moreover, such hydrogels may help to investigate and develop novel *in vitro* models for bone regeneration/resorption studies. For example, this system could be loaded with drugs that inhibit OC differentiation (Tang *et al.*, 2016; Aderibigbe, 2017) to develop more efficient pharmacological treatments to tackle excessive bone degradation, as it occurs in osteoporosis, osteoarthritis, and cancers.

Chapter 3 Incorporation of collagen proteins within self-assembling peptide hydrogels

Note: A version of the work presented in this chapter has been published as follows:

Mattia Vitale, Cosimo Ligorio, Ian P. Smith, Stephen M. Richardson, Judith A. Hoyland, Jordi Bella (2022) Incorporation of natural and recombinant collagen proteins within Fmoc-based self-assembling peptide hydrogels. Gels 8, 254, https://doi.org/10.3390/gels8050254. The printed version is available in **Appendix B**

3.1 Introduction

Simplicity is one of the key factors when developing new synthetic hydrogels-based biomaterials. The ability to mimic the native ECM whilst maintaining an equilibrium into the system by keeping the scaffold biocompatible and able to control the cellular behaviour with little or no chemical modification is paramount (Zhang, 2003). The use of peptide-based hydrogel system represents a valid approach and the advantages of this system have been described in Chapter 1. However, the simple monomers that these hydrogels are made of may not be sufficiently bioactive and provide low cell adhesion. For this reason, chemical modification of these peptides by addition of biologically active compounds could improve the resulting biological properties of the hydrogels. In fact, as they are exposed on the surface of the scaffold, they are available for interaction with cells (Guler *et al.*, 2006; Storrie *et al.*, 2007). For instance, chemical modification of hydrogels with amines and phosphate groups has been shown to control stem cell fate towards bone and adipose cells (Benoit *et al.*, 2008). Similarly, peptide hydrogels have been modified with laminin/integrin-binding motifs, such as IKVAV, YIGSR or RGD peptides to improve cell adhesion and viability (Salinas and Anseth, 2008; Zhou *et al.*, 2009; Jain and Roy, 2020). Furthermore, as described in Chapter 2, Fmoc-based hydrogels represent a suitable option to be modified with inorganic nanofillers such as Hap to form peptide-nanocomposite

hydrogels with enhanced mechanical properties and improved cell differentiation activity.

Another common approach is to modify hydrogels with collagen. Collagen is the most abundant protein in the body, providing strength and structural stability to tissues as well as cell-binding motifs (Brinckmann, 2005; Gordon and Hahn, 2010) and its incorporation within hydrogel has gained widespread popularity in tissue engineering applications. Additionally, its plasticity, availability in nature and its presence in the ECM makes it an ideal candidate for hydrogel modifications. The addition of collagen into hydrogels has shown enhanced cell-adhesion properties and control of stem cell differentiation (Wojtowicz *et al.*, 2010; Chiu *et al.*, 2011). Typically, collagen is sourced from animal skin and bones as a by-product of the food industry. The material obtained from these sources, while fit for most purposes, has a degree of heterogeneity and batch-to-batch variability. Furthermore, there are increasing concerns about the possibility of transmission of diseases such as encephalopathies (e.g. the "mad cow disease") (Ghosh *et al.*, 2012b; Khan and Khan, 2013) Extraction of collagen from animal connective tissues is also hampered by the large proportion of material that is crosslinked and insoluble (Terzi *et al.*, 2020). Thus, animal-derived collagens often require use of enzymes such as pepsin, which may digest the collagen proteins and decrease the mechanical properties of the final biomaterial, to some extent. Thus, there is renewed interest in the development

of recombinant methodologies for the production of collagen-like proteins (Toman *et al.*, 2000; Brodsky and Kaplan, 2013). This represents a valuable, cost-effective and most importantly safe alternative for collagen production. In fact, recombinant collagens have some advantages over natural derived collagen. Firstly, there is no risk of disease transmission as this type of collagen can be produced under controlled conditions in a laboratory; secondly, as the exact sequence is pre-designed, there is the possibility to produce any collagen protein chain; thirdly, recombinant techniques are helpful since they can be easily modified in order to obtain diverse structures (Ruggiero and Koch, 2008).

Genes which encode proteins with the same characteristic collagen sequence have been discovered in bacteria and phages as early as 2002 (Xu *et al.*, 2002). Over the last decade, numerous such proteins have been discovered in viral and bacterial genomes, some of which have characteristics associated with metazoan collagen, such as: forming trimers and Col domains adopting characteristic triple helical structure. However, several such proteins have higher melting temperatures.

These collagen-like proteins have been named EHEC Prophage collagen-like Proteins (EPclPs). They have many of the key collagen characteristics, such as: a key Gly – X – Y structure and they contain non-collagenous domains (Xu *et al.*, 2002; Boydston *et al.*, 2005; Yu *et al.*, 2014; Bella, 2016). These EPclPs can be used as "frame" structure to designed new protein like-collagens that presents

higher melting temperature (~ 42°C) and can be used for biomedical applications (Ghosh *et al.*, 2012a). These constructs were designed for expression in *E. coli*. H1 and H2 are examples of these first-generation constructs where a sequence from human type II collagen replaced the bacterial Col domain (**Figure 27**).However, their low melting temperatures represented a potential problem, as these collagens would not be stable at internal body temperatures, making them unsuitable for biomedical applications (Holster *et al.*, 2007). This is due to lack of hydroxylation of the proline residues of the collagen proteins, a modification that does not occur in *E. coli* as the enzyme prolyl-4-hydroxylase (P4H) is not present (Shoulders and Raines, 2009). Hydroxylation of the proline residues significantly improves stability of human collagen triple helical constructs (Berg and Prockop, 1973; Brodsky and Cronin, 2006) . In the second-generation of collagen constructs, several *de novo* sequences were designed with the amino acid composition of the bacterial Col domains, flanking an integrin binding sequence GFPGER (the bacterial collagen sequences did not contain integrin binding sites). Bacterial collagen sequences are intrinsically stable and do not require hydroxylation for stability purposes. The sequences could still support cell spreading assays, as the flanking motif can be recognized by integrins. One of the proteins used in this chapter, DCol1, is an example of this second-generation of recombinant collagens (**Figure 27**).

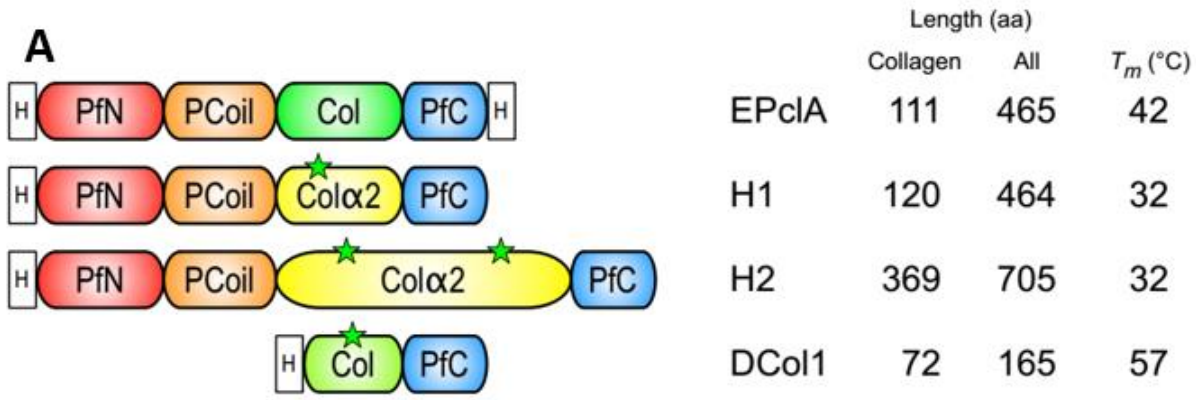

Figure 27 Domain architectures, sequence lengths and thermal stability of recombinant collagen constructs. The darker-hue green Col domain in EPclA represents a bacterial triple helical collagen domain, whereas the yellow Colα2 domains represent varying lengths of human type 2 collagen sequence. The light green Col domain in DCol1 is a shorter collagen sequence made up of two 30 amino-acid blocks flanking the GFPGER integrin binding site. DCol1 sequence design was guided by the amino acid preferences of EPclA. The Tm values show the denaturation temperatures of the respective collagen domains. PfN (red) – phage fibre N terminal capping domain; PfC (blue) – phage fibre C terminal capping domain; PCoil (orange) – coiled-coil domain forming a trimeric helix (Ghosh et al., 2012); H – terminal 6xHis tags, which can be N or C terminal. The green stars show GFPGER integrin binding sites.

For the reasons mentioned above, the aim of this chapter was to develop a quick, yet effective protocol to incorporate natural and recombinant collagen proteins within Fmoc-based SAPHs via diffusion. The protocol of incorporation was optimised combining the previous knowledge acquired by modifying peptide hydrogels with inorganic component with the previous expertise of Bella lab to express and purify recombinant collagen-like protein *via* E.Coli.

Protein incorporation was assessed via SDS-PAGE to demonstrate effective incorporation of collagen as well as protein retention over time. Secondly, the resulting hydrogel stiffness was analysed by rheology in order to confirm no

disruption of the self-assembling mechanism. Finally, biological characterisation was assessed though cytocompatibility studies.

The aims of this chapter were to:

1- Develop and optimise a protocol to modify self-assembling peptide hydrogels with natural, synthetic or recombinant peptides/proteins of a wide range of molecular weights and sizes, without need for any chemical modification.
2- Characterise the collagen-modified hydrogel's stiffness and ultrastructure through rheology and SEM, respectively.
3- Assess the biological/ biocompatible properties of the collagen-modified hydrogel by using HT1080 fibrosarcoma cells.

3.2 Materials and methods

3.2.1 Proteins, peptide, and peptide hydrogels

Table 5 summarises the different peptides and proteins used in this work for hydrogel preparation and modification. Fmoc-FF/S (a mixture of Fmoc-diphenylalanine and Fmoc-serine peptides, 1:1 ratio) was obtained from Biogelx Ltd, UK (batch number FFS052RM). Peptide quality (97% purity) was assessed at Biogelx via High Performance Liquid Chromatography (HPLC). Rat Tail Collagen (RTC, Sigma-Aldrich, C3867) was obtained as an aqueous solution in 20 mM acetic acid, at a stock concentration of 3 mg/ml and 95% purity. The 42-amino acid integrin-binding GFOGER peptide (Knight *et al.*, 2000) (**Table 5**) was obtained from Cambcol Laboratories Ltd, UK as lyophilized powder and dissolved to a final concentration of 1 mg/ml in Dulbecco's Phosphate Buffered Saline (PBS, Sigma-Aldrich). For simplicity, the GFOGER peptide will be included in the general category of "proteins" used here for hydrogel modification. Recombinant eGFP (**Table 5**) was already available in purified form, previously produced from an in house pET15b-eGFP expression vector (Timothy John Eyes, 2014).

3.2.2 Recombinant collagen design and purification

A 165-amino acid recombinant collagen was designed in house by fusing a short collagen sequence (72 amino acids) with a trimerization domain from a collagen-like protein from *E. coli* (Ghosh *et al.*, 2012a). The amino acid sequence of designed collagen DCol1 is shown in **Table 5**. Gene synthesis, subcloning and

expression tests with different *E. coli* strains was carried out by ProteoGenix, France (*ProteoGenix*, no date). Best expression conditions were obtained with the protein expression vector pET28b using T7 Express cells. Bacterial pellets containing expressed DCol1 were re-suspended in 20 ml lysis buffer (PBS, lysozyme, 5 mM Imidazole, pH 7.5) with a protease inhibitor tablet (cOmplete Mini EDTA-free protease inhibitor, Roche). Cells were homogenized using a French cell press (Thermo IEC, USA, FA-078A) with a miniature pressure cell (FA-003) working at 20,000 psi. Disrupted cells were collected on ice before centrifugation for 2 hours at 12,500 rpm and 4°C. The pellets of cell debris were discarded, and the supernatant containing soluble protein was mixed with 2 ml of Nickel-nitrilotriacetic resin (HisPur™ Ni-NTA Thermo Scientific) previously equilibrated with 10 ml binding buffer (PBS, 5 mM Imidazole, pH 7.5). The resin-protein suspension was incubated on a roller unit overnight at 4°C, with continuous mixing to maximise binding. The following day gravity columns were prepared with the resin-protein suspension. The unbound fraction was collected. The columns were then washed twice with 20 ml of washing buffer (PBS, 60 mM Imidazole, pH 7.5) to remove contaminants. The columns were further washed with 250 mM Imidazole in PBS and the protein finally was eluted using 1 M Imidazole in PBS. All fractions were analysed by SDS-PAGE to determine which of them contained the purified protein. Dialysis tubing (Biodesign™ D100, 8000

MWCO) was used to remove the unwanted imidazole from the desired fractions by dialysing them against fresh PBS.

3.2.3 SDS-PAGE

Pre-cast NuPAGE™ 4-12% Bis-Tris mini protein gels (ThermoFisher Scientific), 1.0 mm gel thickness and 10 wells, were used with Invitrogen™ mini gel tanks. Samples were prepared by diluting 15 µl of analyte in 10 µl NuPAGE™ 4X LDS loading buffer (ThermoFisher Scientific) before heating at 95°C for 5 min on a heating block (HB120-S, Scilogex). Hydrogels samples were mixed with loading buffer up to a final volume of 100 µl to help dissolving the gel. After heating, 10 µl of each sample was loaded alongside 5 µl of prestained protein ladder, 10 to 250 kDa (PageRuler™ Plus, ThermoFisher Scientific)**.** All gels were run for 1 h at a constant voltage (120 V) using NuPAGE™ MES SDS running buffer (ThermoFisher Scientific). Gels were stained overnight at 4°C using Coomassie blue (InstantBlue™, Expedeon**)** and imaged using a compact scanner (CanoScan LiDE 220, Canon).

3.2.4 Circular dichroism spectroscopy

Secondary structures of the RTC and DCol1 proteins and the GFOGER peptide were analysed by circular dichroism (CD) spectroscopy using a Jasco® J-810 spectropolarimeter equipped with a Peltier temperature controller. Samples were diluted to a concentration of ~0.5 mg/ml in CD phosphate buffer (10 mM K_2HPO_4, 10 mM KH_2PO_4, 150 mM KF, pH 7.4) (Norma J. Greenfield, 2007).

CD spectra were measured between 190 nm and 260 nm at 4°C using a 1 mm pathlength CD-matched quartz cuvette (Starna Scientific). Data were collected every 0.2 nm with a 1 nm bandwidth. Spectral baselines were corrected by subtracting the spectrum of CD phosphate buffer (blank) collected under the same conditions.

3.2.5 Hydrogel modification protocol

13 mg of Fmoc-FF/S peptide powder were dissolved in 1 mL of sterile deionized H_2O to a concentration of 15 mM, hereafter referred as pre-gel solution. Collagen proteins were incorporated within the hydrogels by diffusion. In order to follow the incorporation of GFOGER, the peptide was prior labelled with 10 µM NHS-Fluorescein (Sigma-Aldrich) for 30 min at room temperature. Briefly, the proteins of interest were diluted up to the desired concentration in PBS; 1.5 mL of this solution was then placed into a 24-well plate (Corning, UK). A 1.5 mL solution of PBS was used as a protein-free control well. Approximately 300 µl of pre-gel solution were pipetted into the same well forming a spheroid-shape hydrogel which encapsulated the protein as the crosslinking process took place. After 24 h the resulting spheroids were scooped out of the well and protein incorporation/retention was analysed by cutting a slice of each hydrogel and by loading them into an SDS-PAGE as described in section 2.3.

3.2.6 Fluorescence spectroscopy

Fluorescence spectroscopy measurements were performed on RTC, eGFP and DCol1 on PBS (100 μg/ml, pH 7.4), on Fmoc-FF/S pre-gel solutions (15 mM, 13.2 mg/ml) and on 1:1 V/V mixtures of each protein in PBS and Fmoc-FF/S pre-gel solutions. Measures were carried out at room temperature using a FluoroMax-4 spectrofluorometer (HORIBA, UK). Samples were loaded into 0.2 cm path length quartz cuvettes. Fluorescence spectra were acquired using a 280 nm excitation wavelength and emission recorded in the 300-450 nm range.

3.2.7 Scanning electron microscopy (SEM)

The morphologies of Fmoc-FF/S hydrogels with and without incorporated collagens were analysed by Scanning Electron Microscopy (SEM). Briefly, hydrogels were prepared by pipetting ~300 μL of the pre-gel solutions into Thin-Cert well inserts (0.4 μm pore size Greiner Bio-One Ltd, UK). The inserts were then placed into 24-well plates and incubated at 37 °C with a total volume of 1.3 mL PBS containing the protein of interest to fully crosslink the hydrogels. After 24 h, hydrogels were fixed in 2.5% (w/v) glutaraldehyde (Sigma-Aldrich, UK) and 4% (w/v) paraformaldehyde (Sigma-Aldrich, UK) in 0.1 M HEPES buffer (Sigma-Aldrich, UK). After rinsing the samples in PBS, all samples were dehydrated in a graded ethanol (EtOH) series (25, 50, 75, 95, and 100% v/v EtOH/water). Samples were maintained at 100% EtOH and dried in a K850 Critical Point Drier (CPD, Quorum Technologies, UK). After the CPD step,

samples were transferred into metallic pins and coated with gold palladium alloy using an SC7620 Mini Sputter Coater (Quorum). Samples were then imaged on a Quanta 250 FEG SEM (Thermo Fisher Scientific) at 20 kV.

3.2.8 Mechanical properties of the hydrogels

The rheological properties of Fmoc-FF/S hydrogels with and without incorporated proteins (RTC, GFOGER, DCol1 or eGFP) were analysed via a rheological amplitude sweep test on a Discovery HR-2 rheometer (TA instruments, US). Each hydrogel sample was tested in the 0-100% shear strain range with a frequency of 1 Hz, gap size of 500 μm, temperature of 37 °C, and rheometer's plate diameter of 20 mm. The rheometer's upper head was lowered to the desired gap size and a soak time of 180 sec was used for equilibration. A solvent trap was employed to minimise sample evaporation. Once the rheological spectra were collected, representative storage and loss moduli at 0.02% and frequency of 1 Hz were selected for the summary rheology plots.

3.2.9 Hydrogel cell adhesion and spreading

Human Fibrosarcoma HT1080 cells (ATCC CCL-121) were maintained in TCPS using DMEM, Gibco containing 10% (v/v) foetal bovine serum (FBS) and 5% (v/v) Penicillin-Streptomycin-Amphotericin antibiotic mixture (PSA, 100 units/mL penicillin, 100 μg/mL streptomycin, 0.25 μg/mL amphotericin) (Sigma-Aldrich). When reaching confluency, cells were gently detached from the tissue culture flask by adding 4 mL of Trypsin-EDTA (Sigma-Aldrich) and pelleted by

centrifugation (400 ×*g* for 5 min). After cell counting, fresh culture medium was added to obtain the desired cell density. Collagen-modified hydrogels were prepared 24 h in advance as described in section 2.2.5. However, when used for cell culture, ~250 µl of pre-gel solution was pipetted into the inner well of a 35 mm glass bottom dish for confocal microscopy (VWR, UK, 734-2905), followed by the addition of 2 mL of the protein of interest in PBS to allow crosslinking and collagen incorporation. Cell adhesion and cell spreading analysis were evaluated as described by Humphries *et al.* (Humphries, 1998). Briefly, non-specific bindings were blocked by adding 1 mL of heat-denatured high grade BSA (BSA, Sigma-Aldrich), at 10 mg/ml concentration for 1 h. Then, 2 mL of cell suspension (4×10^5 cell/ml) was pipetted onto each hydrogel and incubated for 24 h at 37 °C and 5% CO_2. The following day, the cells were fixed in 4% (w/v) paraformaldehyde (Sigma-Aldrich) for 30 min and permeabilised in 0.5% (v/v) Triton X-100 solution (Sigma-Aldrich) in PBS for 15 min. Cell morphology and cytoskeleton arrangement was assessed using Alexa Fluor™ 488 Phalloidin (Invitrogen™, A12379) as previously described (Vitale *et al.*, 2022). RGB images were split in their channels and green channel images were used for morphological analysis by using ImageJ, version 1.51 (Schindelin *et al.*, 2012). Images were threshold using the Huang's algorithm and touching cells were separated through a watershed algorithm. Cell adhesion and spreading were

evaluated in terms of number of spread cells (%) and aspect ratio (major cell axis/minor cell axis).

3.2.10 Integrin-dependent cell adhesion assay

Cell adhesion on different modified hydrogels was also assessed in the presence of 10 μg/ml of the function-blocking monoclonal antibody mAb13 (Sigma-Aldrich, MABT821) which inhibits the interaction between collagen and the β1-integrin subunit. Following the procedure described by Tuckwell (Tuckwell, Smith and Korda, 2000), the antibody was diluted 10-fold in warm serum-free DMEM and the cells were incubated for 30 minutes in the presence of antibody, before seeding. The effect of the inhibition on the cell spreading assay was evaluated as described in section 2.9.

3.2.11 Statistical analysis

All quantitative values are presented as mean ± standard deviation. All experiments were performed using at least three replicates. Data were plotted using Origin® 2019b (OriginLab - Origin and OriginPro - Data Analysis and Graphing Software, no date) and compared using an unpaired t test, unless stated otherwise. One level of significance was used: $p < 0.05$ (∗ or #, where appropriate).

Table 5 Proteins and peptides used for hydrogel formation and modification. Sequences are shown with standard single amino acid symbols, plus O for 4-hydroxyproline. Capping groups: Fmoc, fluorenylmethoxycarbonyl protecting group; Ac, N-terminal acetylation; NH2, C-terminal amidation.

Molecule	**Sequence /Access IDs** (integrin binding sites in bold type)	**Amino acids (aa)**	M_w **(kDa)**	**Isoelectric point (pI)**
Fmoc-FF/S hydrogel Fmoc-FF peptide Fmoc-S peptide	 Fmoc-FF Fmoc-S	 2 1	 0.53 0.33	 7.81 7.81
Rat tail collagen [1] α_1 (I) chain α_2 (I) chain	 P02454, NP_445756 P02466, NP_445808	 1056 [3] 1040 [3]	 300 [2]	 9.52
GFOGER peptide	Ac-GPCGPPGPPGPPGPPGPPGPP**GFOGER**GPPGPPGPPGPPGPPGPPGPC-NH_2	42	11.2 [2]	6.96
DCol1 recombinant protein	MGSHHHHHHSGLVPRGSGPPGPPGPQGPAGPRGEPGPAGPKGEPGPAGPP**GFPGER**GPPGPQGPAGPIG PKGEPGPIGPQGPKGDPGETQIRFRLGPASIIETNSHGWFPGTDGALITGLTFLAPKDATRVQVFFQHLQV RFGDGPWQDVKGLDEVGSDTGRTGE	165	50.0 [2]	6.97
eGFP recombinant protein	MGSSHHHHHHSSGLVPRGSHMVSKGEELFTGVVPILVELDGDVNGHKFSVSGEGEGDATYGKLTLKFIC TTGKLPVPWPTLVTTLTYGVQCFSRYPDHMKQHDFFKSAMPEGYVQERTIFFKDDGNYKTRAEVKFEG DTLVNRIELKGIDFKEDGNILGHKLEYNYNSHNVYIMADKQKNGIKVNFKIRHNIEDGSVQLADHYQQN TPIGDGPVLLPDNHYLSTQSALSKDPNEKRDHMVLLEFVTAAGITLGMDELYK	259	29.1	6.61

[1] Rat tail collagen is predominantly type I collagen, a heterotrimer made of two α_1(I) chains and one α_2(I) chain.

[2] Molecular weights of the trimeric collagen molecules. [3] The amino acid number counts correspond to the processed, mature chains, of type I collagen.

3.3 Results and Discussion

3.3.1 Protein characterization

In order to develop a suitable protocol of protein incorporation within Fmoc-based hydrogels, three collagen molecules with different size were chosen. Rat Tail Collagen (RTC) is widely used as laboratory collagen-based substrate for mammalian cell culture and therefore was chosen as the largest protein to be incorporated within the hydrogels. Indeed, with an approximate molecular weight of 300 kDa this protein has widely been used as positive control to study cell-matrix interaction within 3D hydrogels (Elsdale and Bard, 1972; Rajan *et al.*, 2007). At the other end, the 42-amino acid synthetic collagen peptide GFOGER peptide was the shortest version of collagen (~11.24 kDa) used for hydrogel modification (O stands for 4-hydroxyproline; complete sequence given in **Table 5**). This peptide contains a GFOGER integrin-binding motif that binds integrins $\alpha_1\beta_1$ and $\alpha_2\beta_1$ (Knight *et al.*, 1998). The third collagen substrate used for hydrogel modification is DCol1 a recombinant collagen-like mini protein designed and produced in-house using a bacterial expression system. It contains a non-hydroxylated GFPGER motif (notice here that P stands for proline), which is also able to bind $\alpha_1\beta_1$ and $\alpha_2\beta_1$ integrins. Additionally, recombinant enhanced green fluorescent protein (eGFP) was used as a visible fluorescent reporter to visualise

protein incorporation to and leaking from the hydrogel during optimization of the modification protocol (Remington, 2011).

RTC and GFOGER were obtained from commercial sources. Their biochemical purity was deemed satisfactory for the purposes of the experiments reported here. Purification of recombinant DCol1 was monitored by SDS-PAGE (**Figure 28A**). The triple helical conformation of the collagen proteins was confirmed by circular dichroism (CD) spectroscopy (**Figure 28B**).

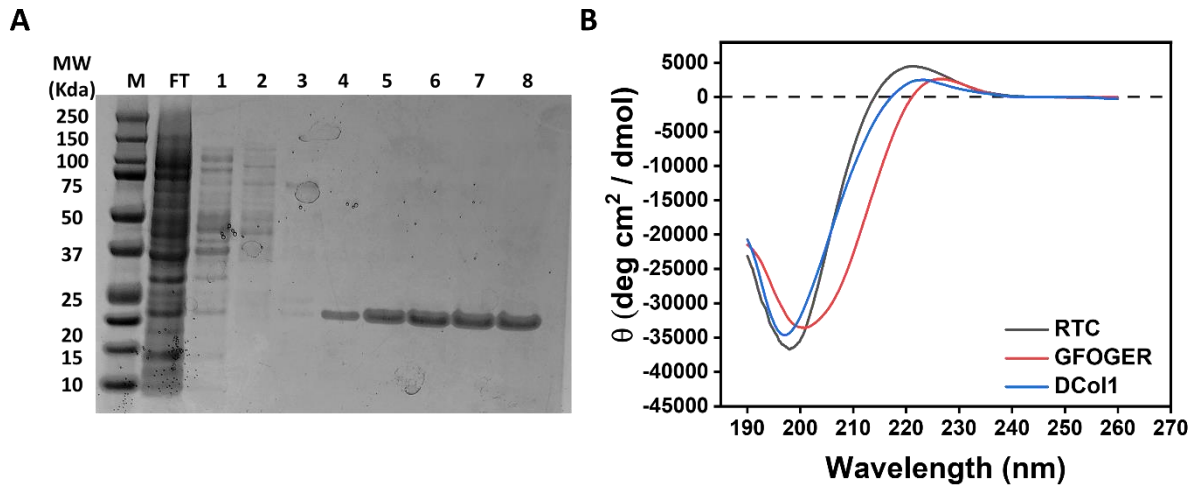

Figure 28 Collagen protein characterisation. (A) SDS-PAGE analysis of the purification of DCol1. Lane compositions: M, molecular weight markers; FT, flow through; 1–2, wash fractions with 60 mM imidazole; 3–4, elution fractions with 250 mM imidazole; 5–8 elution fractions with 1 M imidazole. (B) CD spectra at 4°C of RTC (grey), DCol1 (blue) and GFOGER (red). The vertical axis measures the mean residue ellipticity θ in degrees cm^2 $dmol^{-1}$. CD data were collected between 190 and 260 nm.

SDS-PAGE was first used to assess the yield and purity of DCol1 purification *via* nickel-affinity chromatography. **Figure 28A** show that DCol1 was successfully purified with high yield. Fractions eluted with 1 M imidazole show a single 20 kDa band that corresponds to the DCol1 monomer chain. The calculated

molecular weight of DCol1 based on its amino acid sequence is 16.6 kDa, but it is well known that proteins containing Col domains migrate on SDS-PAGE with an apparent, higher than expected molecular weight.

The secondary structure of the collagen proteins was analysed *via* CD between 190 and 260 nm (**Figure 28B**). All three spectra show the characteristic features of a collagen triple helix: a band of positive ellipticity (around +3000 to +5000 deg cm^2 $dmol^{-1}$) with a maximum at around 220 nm; and a deep band of negative ellipticity (around –35000 deg cm^2 $dmol^{-1}$) with a minimum around 198 nm (Kelly and Price, 2005; Norma J Greenfield, 2007; Drzewiecki *et al.*, 2016). These well-studied CD spectral features are associated with the polyproline II conformation from the individual chains in the collagen triple helical conformation (Sreerama and Woody, 1994).

3.3.2 Incorporation of proteins within self-assembly peptide hydrogels

The initial aim of this chapter was to develop and optimize a protocol for the incorporation of collagen proteins with different molecular weights into Fmoc-based self-assembling hydrogels, without any prior chemical modification and /or crosslinking. **Figure 29** schematically illustrates how the protocol was developed and adapted to successfully incorporate collagen protein into Fmoc-FF/S hydrogels.

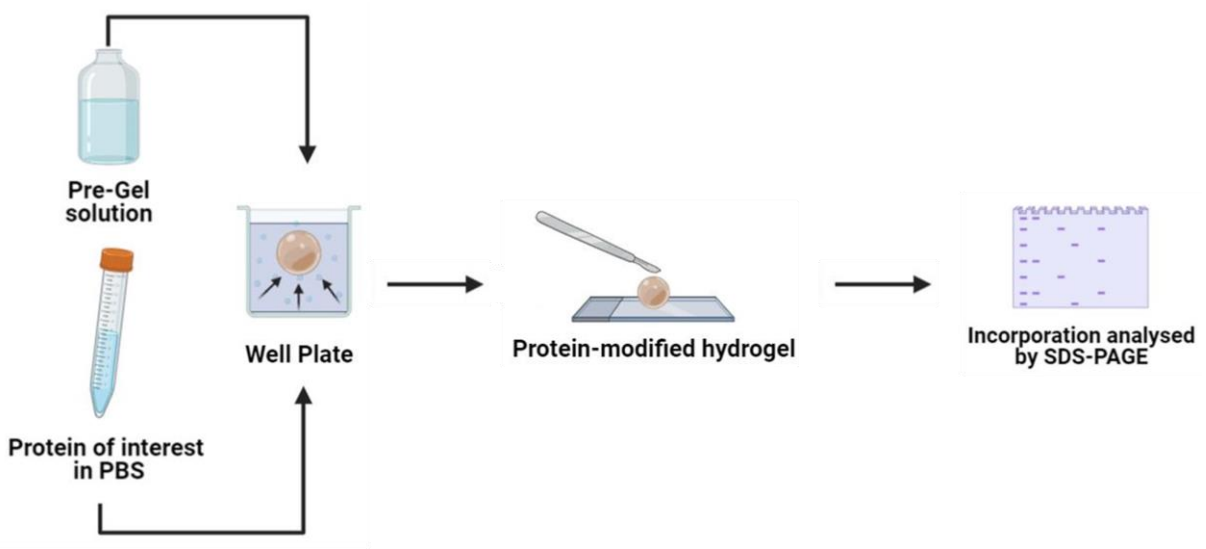

Figure 29 Schematic representation of the optimised protocol used to incorporate proteins within hydrogels. Protein of interest were diluted up to the desired concentration in the well plate. Fmoc-FF/S pre-gel solution was then pipetted into the protein containing solution to form a spheroid like to allow protein incorporation.

The incorporation of collagen proteins did not interfere with the self-assembling mechanism of the hydrogels. In fact, as shown in **Figure 30,** the resulting spheroids-like hydrogels were stable and formed a self-supporting hydrogel structure.

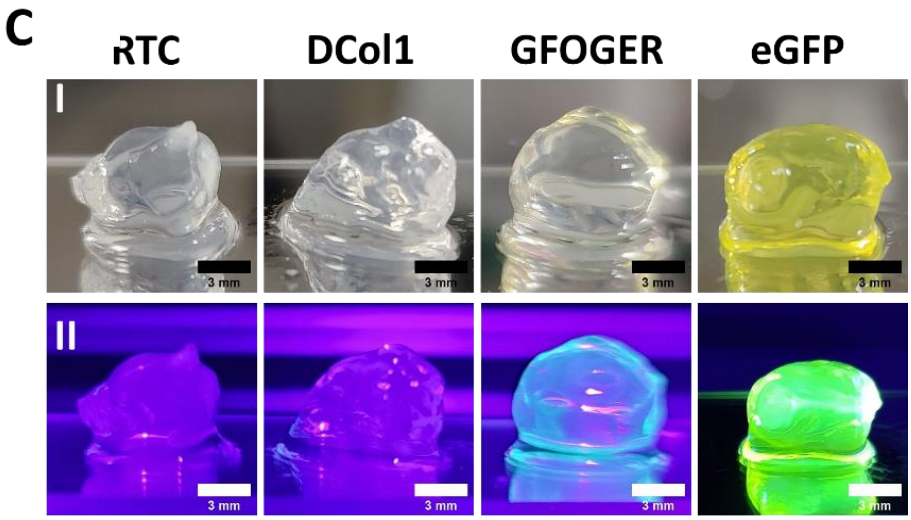

Figure 30 Analysis of spheroid-shaped hydrogels under visible (I) and UV (II) light. All spheroids show dimensional stability indicating a self-supporting structure consistent with a successful hydrogel self-assembling mechanism. Spheroids of hydrogels modified with eGFP and GFOGER show fluorescence under UV light, indicating successful protein and peptide incorporation (see main text).

As explained above, eGFP was used as protein reporter to follow protein incorporation into gels. Hydrogels modified with eGFP showed a high intensity of green fluorescence throughout their entire spheroids (**Figure 30**), indicating that the eGFP protein had been successfully incorporated by diffusion without affecting its native structure or the fluorescence of its chromophore.

The GFOGER peptide was too small for conventional SDS-PAGE analysis and therefore was labelled with NHS-Fluorescein prior to incorporation into the hydrogels so it could be detected on gels by fluorescence. **Figure 31** illustrates the successful labelling of GFOGER peptide with NHS-Fluorescein and its detection after SDS-PAGE under UV light.

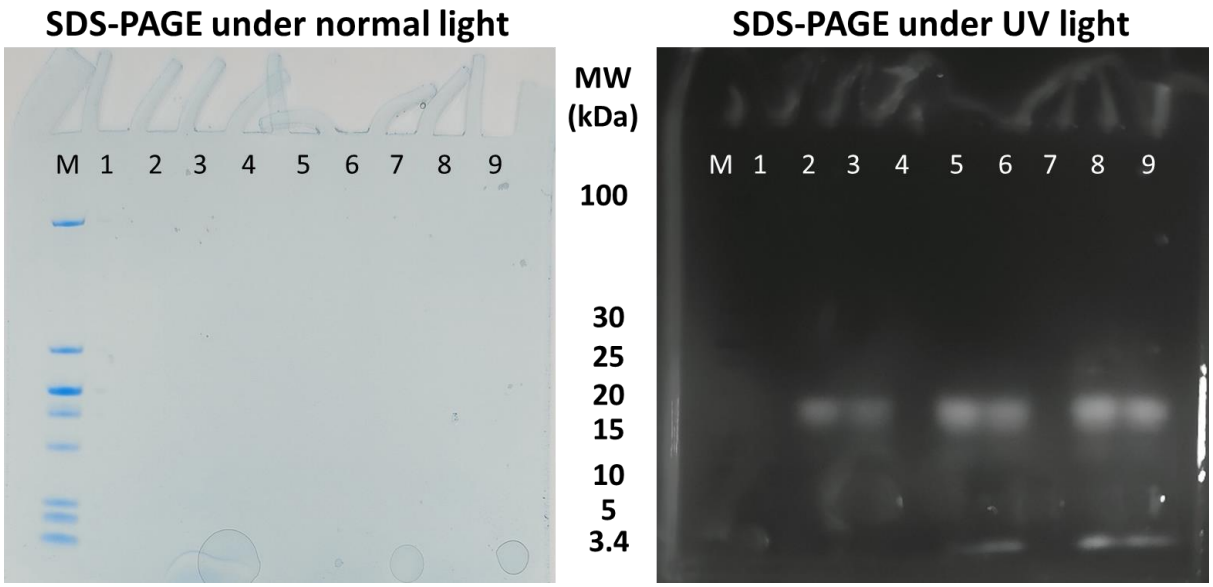

Figure 31 SDS-PAGE of GFOGER peptide labelled with NHS-Fluorescein under normal and UV light. Lane composition is: M, molecular weight; 2-3, 5-6, 8-9, NHS-Fluorescein labelled-GFOGER.

Thus, hydrogels incorporating eGFP and fluorescently labelled GFOGER showed a bright, green color when exposed to UV light (**Figure 30**) indicating that the proteins diffused throughout the whole scaffold without affecting their chromophore fluorescence.

Protein incorporation into the hydrogels was also assessed through SDS-PAGE (**Figure 32**). Bands corresponding to proteins incorporated into the hydrogel spheroids (**Figure 32A**, lane **2**) showed a slightly stronger intensity that the control bands from the protein stock solutions (lane **1**), indicating that the proteins were being concentrated within the constrained space of the spheroid due to a volume shrinkage. A similar phenomenon has been observed by Kim and co-

workers as they demonstrated that the fluorescence intensity of graphene oxide was much greater in a limited space as the cell pellet (Yoon *et al.*, 2014). Significantly, the intensity of the band protein remaining within the well, after "fishing out" the hydrogels, was much lighter than the control and the hydrogels, suggesting a clear protein uptake. Finally, protein retention over time was analyzed. Hydrogel spheroids were washed every 24 h with PBS and a hydrogel sample was taken each time point and analyzed *via* SDS-PAGE. As shown in **Figure 32B**, SDS-PAGE showed bands of the same intensity for all of the tested constructs, suggesting that all the proteins were successfully retained for at least the first 72 h.

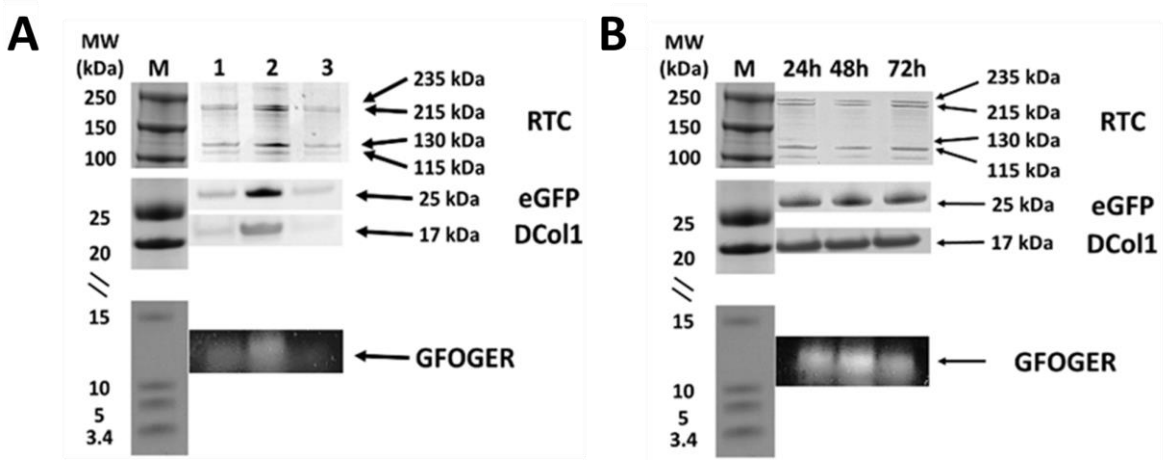

Figure 32 SDS-PAGE analysis of (**A**) protein incorporation into the hydrogel spheroids, and (**B**) retention inside the hydrogels over time. The GFOGER bands are obtained from fluorescence after UV exposure of the gels. Panel (**A**) Lanes: M, molecular weight markers; 1, protein stock solution; 2, protein incorporated into the hydrogel spheroid; 3, remaining protein into the well solution. Panel (**B**) Lanes: **M**, molecular weight markers; **24**, **48**, **72 h**, protein retention over time. Arrows indicate the different protein bands and their corresponding molecular weights.

Numerous co-assembled peptide hydrogel systems have been explored using alternative mechanisms (Storrie *et al.*, 2007; Capito *et al.*, 2008). For instance, Stupp et al. described a similar phenomenon when self-assembling peptide amphiphiles are mixed with high molecular weight polysaccharide hyaluronic acid, where a mix of both osmotic pressure of ions and strong electrostatic interactions is involved in the incorporation (Capito *et al.*, 2008). In the present case all proteins are expected to have the same sign of electric charge the Fmoc-FF/S peptide hydrogels (see **Table 4** for the predicted values of pI), and thus electrostatic interactions may not play a role in the incorporation of the proteins into the hydrogels. Instead, protein incorporation into the Fmoc-FF/S hydrogels may be driven simply by diffusion into the hydrogel mesh, with the two components (*i.e.*, Fmoc-FF/S and proteins) co-assembling upon contact. Additionally, hydrophobic interactions may also be involved during the co-assembly process. This has been investigated by using fluorescence spectroscopy analysis. As shown by the fluorescence spectra in **Figure 33**, each protein showed a peak of fluorescence emission between the 320-380 nm region (red line), due to the presence of tyrosine and tryptophan residues in their sequences (the GFOGER peptide was not used for these experiments as it lacks aromatic residues and will not produce any signal). When the proteins were mixed with Fmoc-FF/S (1:1 v/v ratio), a prompt and dramatic quenching of the fluorescence emission peak was observed (blue line), suggesting a strong interaction between the

fluorescent groups in the proteins proteins and the Fmoc-FF/S pre-gel solution. It is reasonable to postulate that as the self-assembly mechanism occurs, the hydrogels act as a "sink", where the proteins passively diffuse through the hydrogel mesh until an equilibrium is reached after 24 h (**Figure 32B**) as previously shown by Sassi *et al* (Sassi, Blanch and Prausnitz, 1996).

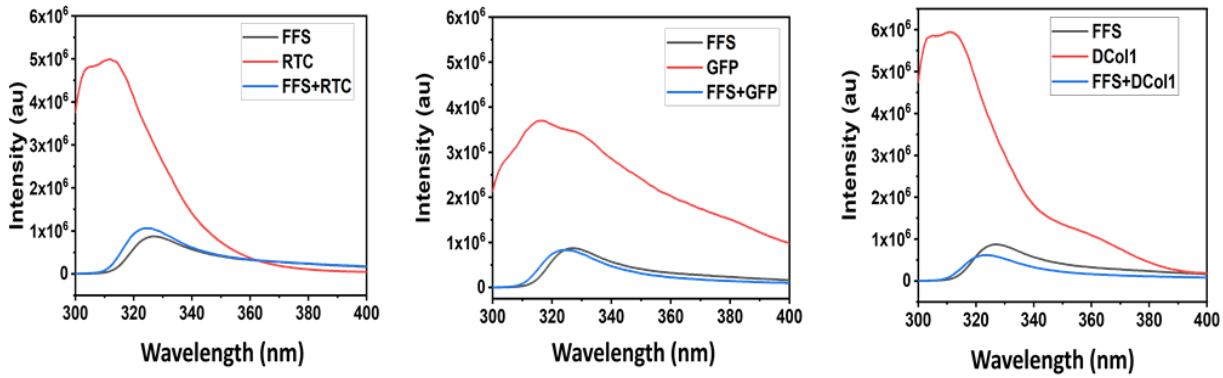

Figure 33 Fluorescence spectroscopy spectra of Fmoc-FF/S peptide (grey), collagen (red) and Fmoc- FF/S-collagen solutions (blue) prepared in PBS (pH = 7.4). Excitation wavelength 280 nm; emission wavelength recorded within the 300–400 nm range.

3.3.3 Hydrogels microstructure

The morphology of the hydrogels after collagen incorporation was studied by SEM. Both outer and inner faces of the unmodified and collagen-modified hydrogels were imaged to ensure that the hydrogels retained their structure (**Figure 34**). The unmodified control hydrogel Fmoc-FF/S showed the characteristic fibrous network structure with fibre entanglements and bundles of supramolecular stacks (Vineetha Jayawarna *et al.*, 2006). Similarly to what was observed by Mata *et* al., for a system where diffusion is involved, the hydrogel's inner surface displayed the distinctive nanofibrous multilayered architecture

(Inostroza-Brito *et al.*, 2015). Interestingly, the hydrogel surface features and morphology changed based on the protein size. Incorporation of RTC, the largest protein tested here, changed the morphology of the inner face of the hydrogel, which appeared to be much more disorganised than the rest of the hydrogels. On the other hand, no differences with the control Fmoc-FF/S were noticed on the outer surface of the hydrogels. As the collagen proteins reduced in size, the final structure of the hydrogels was more compact and less disorganized. For this reason, it is likely that the size and shape of the proteins that were incorporated into the hydrogels did influence their final structure.

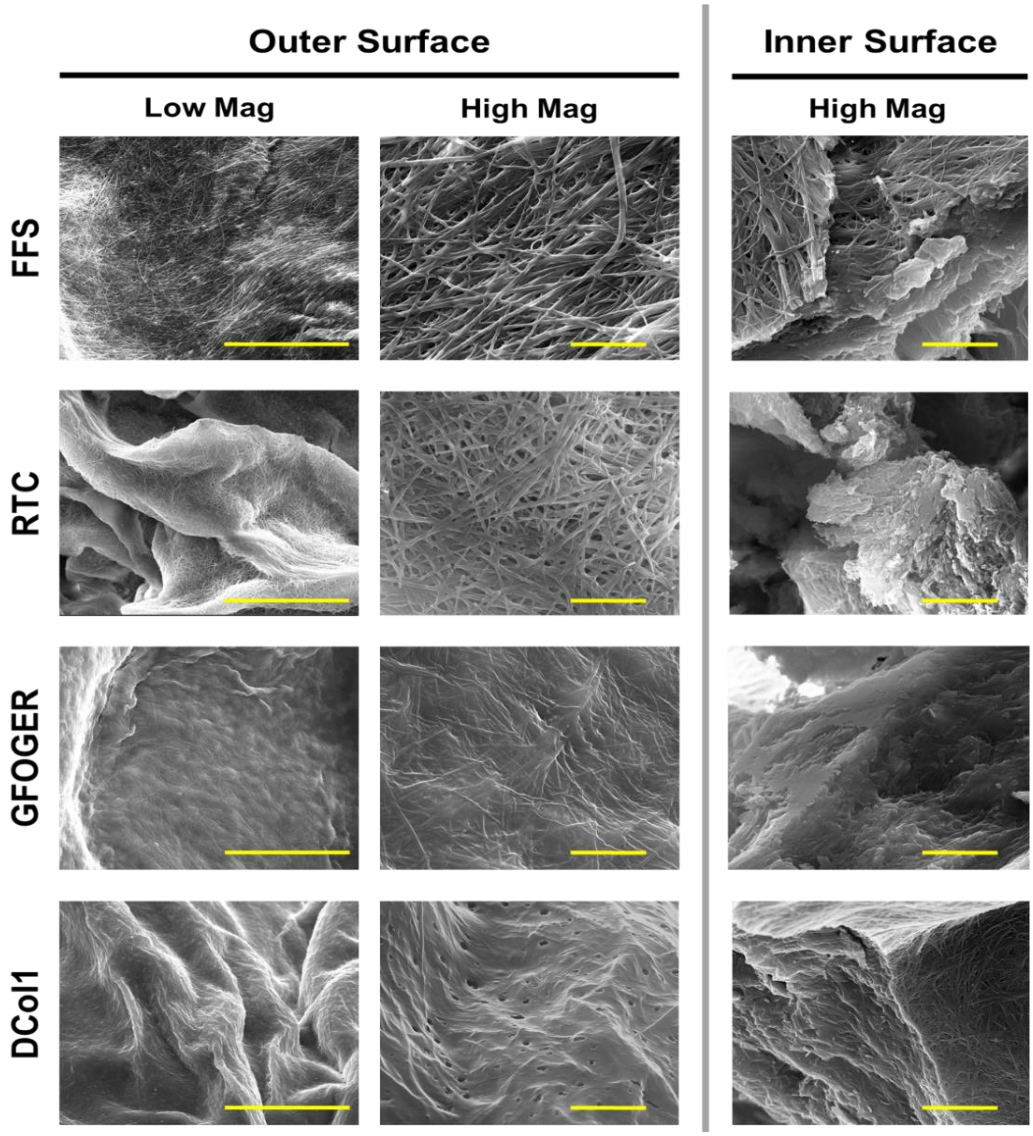

Figure 34 Scanning electron microscopy images showing the outer (left) surface morphology of Fmoc-FF/S and the collagen-modified hydrogels at lower and higher magnification and a cross section showing the inner (right) surface morphology at higher magnification. Low magnification scale bar is 50 µm; high magnification scale bar is 5 µm.

3.3.4 Mechanical characterization of the hydrogel

The effect on the hydrogel stiffness of the incorporation of the different proteins was evaluated by measuring the mechanical properties of the modified scaffold versus the control Fmoc-FF/S hydrogel. All proteins, including eGFP, were tested using three different concentrations: 1, 50 and 100 µg/ml. Resulting hydrogels

were subjected to an amplitude sweep experiment (strain range 0 to 100%, frequency 1 Hz, gap size 500 μm) at 37°C. As shown in **Figure 35**, the elastic modulus G' was consistently higher than the loss modulus (G'') for all the formulations tested. This suggests that all the proteins were successfully incorporated within Fmoc-FF/S without impairing its self-assembling mechanism and its ability to form self-supporting hydrogels.

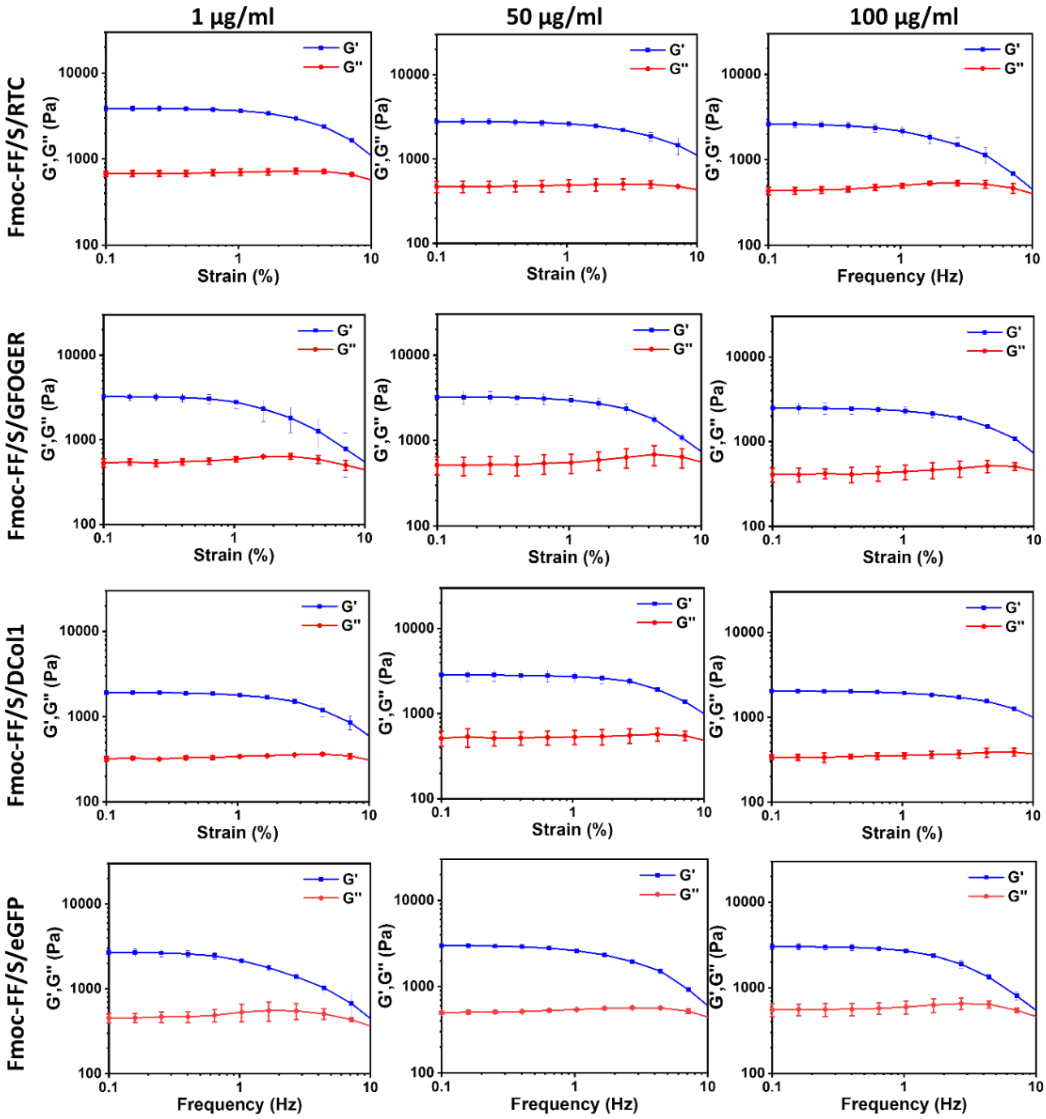

Figure 35 Rheological amplitude sweep test (shear strain range of 0 – 100 % 1 Hz) of Fmoc-FF/S hydrogels after protein incorporation. Measurements were repeated for each modified hydrogel at three different protein concentrations (1, 50, 100 µg/ml). Blue line represents the storage modulus (G') whereas the red line illustrates the loss modulus (G").

Next, in order to assess the stiffness of the Fmoc-FF/S hydrogels after protein incorporation the value of G' was recorded at a fixed frequency (**Figure 36**). No significant differences in G' were observed for any of the formulations compared to the unmodified control. These results were considered as positive as the

incorporation of the protein did not affect the "bulk" properties of the final protein-modified system in comparison to the unmodified control.

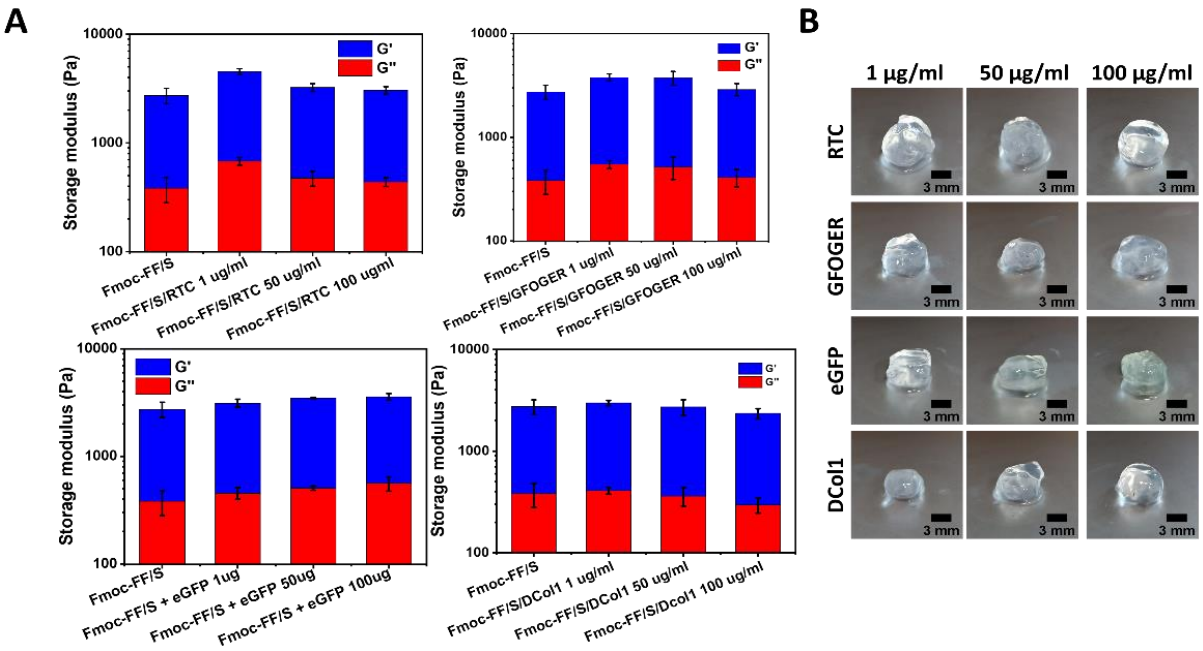

Figure 36 Analysis of the mechanical properties of the Fmoc-FF/S hydrogels after incorporation of proteins at different concentrations. (**A**) Storage and loss moduli (0.02% strain, 1 Hz) of Fmoc-FF/S hydrogels with and without collagen or eGFP at different concentrations (1, 50, 100 µg/mL). (**B**) Photographs of spheroids of Fmoc-FF/S modified with different collagen of eGFP proteins.

3.3.5 HT1080 cell culture on collagen-modified hydrogels

HT1080 cells were cultured on the collagen-modified hydrogels to assess their biological activity. This human fibrosarcoma cell line has been widely used as a model to test cell adhesion and cell spreading on collagen substrates, due to its high expression of $\alpha_2\beta_1$ integrin, a major collagen receptor (Tuckwell *et al.*, 1995, 1996). All the previously described collagen-modified hydrogels were tested at one fixed protein concentration (100 µg/ml); eGFP was excluded from this

analysis as it does not contain any cell binding site (Shimomura, Johnson and Saiga, 1962). To assess the biological activity of the collagen-modified hydrogels, two major parameters were evaluated: the ability of HT1080 cells to adhere to the modified hydrogels (as percentage of adhered cells), and the amount of cell spreading, compared to the unmodified Fmoc-FF/S hydrogel. **Figure 37** shows HT1080 cell adhesion and spreading for all the formulations tested. The RTC-modified hydrogel provided the highest levels of cell adhesion amongst all the hydrogels tested (51 ± 1% *vs* 14 ± 7% for the unmodified hydrogel, $p < 0.05$). This was already expected as RTC is used as positive control of cell adhesion studies in most cell biology laboratories. Likewise, incorporation of GFOGER peptide within Fmoc-FF/S resulted in a higher adhesion than the control (47 ± 4%, $p < 0.05$). DCol1 incorporation into Fmoc-FF/S provided the lowest level of cell adhesion (36 ± 6%) but it was still significantly higher than that of the unmodified Fmoc-FF/S hydrogel (14 ± 7%, $p < 0.05$).

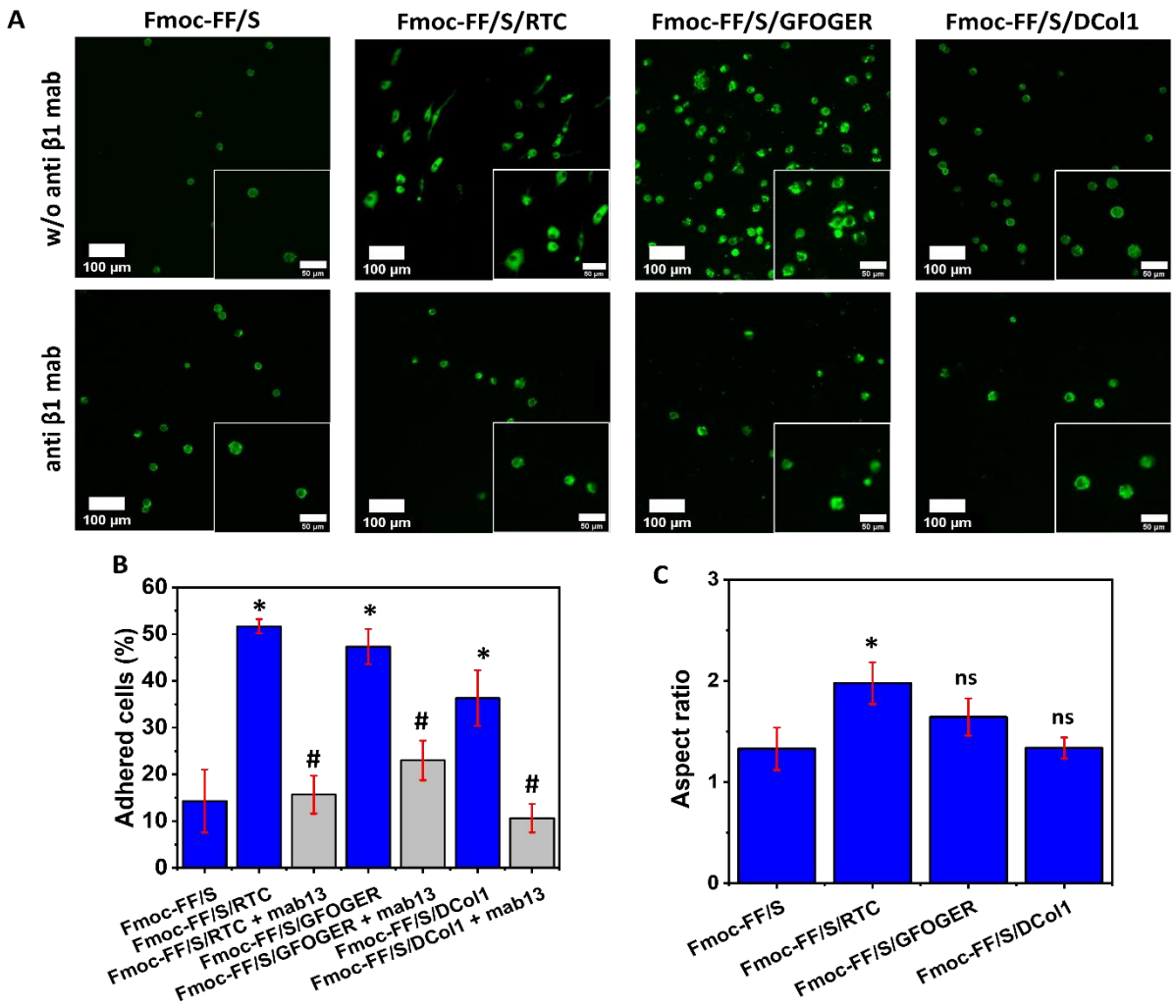

Figure 37 Adhesion and spreading of HT1080 cells on hydrogels, with and without collagen modification. (**A**) F-actin staining of HT1080 cells after 24 h culture on Fmoc-FF/S and the different collagen-modified hydrogels (green: F-actin, Alexa Fluor 488 phalloidin; scale bars 100 µm, inset 50 µm), with and without pre-incubation with mAb13 (anti β1) antibody. (**B**) Quantification of cell adhesion on the different hydrogels before (blue bars) and after (grey bars) pre-incubation with mAb13 antibody. (**C**) Mean aspect ratio of HT1080 cells cultured on different hydrogels. An aspect ratio of 1 is indicative of a round-shaped cell, while spread cells with elongated shapes have aspect ratio values above 1. Data shown as mean ± SD, n = 43, */# $p < 0.05$; ns, not significant. Adherence and spreading on each modified hydrogel are compared with the unmodified Fmoc-FF/S hydrogel (*). Adherence to modified hydrogels after mAb13 incubation (grey) is compared to that on the respective hydrogels before mAb13 incubation (blue, #).

Two main factors could be influencing the lower HT1080 cell adhesion to the DCol1-modified hydrogels. First, adhesion was evaluated after 24 h post-culture; seeding of cells into a new microenvironment could affect their adherence. In fact, it has been demonstrated that cells do need time for a physiological adaptation when seeded onto a new substrate with different mechanical properties (Ghosh *et al.*, 2007). A second factor could be related to the size of the protein and the availability of binding sites. DCol1 is small and the easy access to integrin binding sites could be hindered within the hydrogel mesh.

Spreading of HT1080 cells on the modified hydrogels was assessed. Cells were considered spread when the cytoplasm was visible around the entire circumference of the nucleus. **Figure 37C** shows the average aspect ratio of HT1080 cells seeded onto the different hydrogels. As expected, RTC and GFOGER-modified hydrogels supported cell spreading as HT1080 cells appeared to elongate creating focal adhesions. On the other hand, cells seeded on hydrogels functionalized with DCol1 did not spread, similarly to what was observed with cells seeded on unmodified Fmoc-FF/S hydrogels. Cells appeared rounded, with little or no cytoplasm visible. Poor HT1080 cell spreading on DCol1 has already been observed as a function of DCol1 concentration in previous 2D culture experiments in the laboratory (unpublished data). While the reasons for this poor spreading are still under investigation, they could be possibly linked to the DCol1 expression and purification process. For instance, DCol1 may

be carrying some intrinsic toxic component of bacterial origin whose effect becomes more pronounced when the protein is more concentrated.

HT1080 cells are well known to express a high quantity of $\alpha_2\beta_1$ integrin (Tuckwell *et al.*, 1995). For this reason, a β_1-integrin blocking antibody (mAb13) was used to test whether collagen binding was through the β_1 subunit. Optimal antibody concentration was first assessed in TCPS (data not shown) and then HT1080 cells were pre-incubated with 10 μg/mL of antibody before seeding onto the collagen-modified hydrogels. After treatment with mAb13, HT1080 cells seeded on the collagen-modified hydrogels showed a round morphology (**Figure 37A**), comparable to that seen when they were seeded on the Fmoc-FF/S hydrogel, which does not provide any integrin-binding sites. Similarly, the percentage of cell adhesion was significantly lower than that from the untreated HT1080 cells (**Figure 37B**) and did not show any significant difference with the adhesion to unmodified Fmoc-FF/S peptide hydrogels, suggesting that the β_1-integrin subunit is pivotal when binding to collagen. The data shows a significant reduction of HT1080 cell adhesion on all collagen-modified hydrogels after mAb13 incubation: RTC 15 ± 4% (*vs* 51 ± 1% before incubation, $p < 0.05$); GFOGER 23 ± 4% (*vs* 47 ± 4%, $p < 0.05$); DCol1 10 ± 3% (*vs* 36 ± 6%, $p < 0.05$). These results also confirm that the β_1-integrin subunit is clearly involved in HT1080 cell binding to the collagens incorporated within Fmoc-FF/S, consistent

with the integrin $\alpha_2\beta_1$ being one of the major receptors for collagens (Tuckwell, Smith and Korda, 2000; Farndale, 2014).

3.4 Conclusions

The aims of this Chapter were to develop a new protocol for the incorporation of natural, synthetic and recombinant collagen proteins and peptides within self-assembling Fmoc-based peptide hydrogels. Three different collagen proteins were used to modify the Fmoc-FF/S hydrogel: rat tail collagen (RTC); a synthetic 42-amino acid collagen-like peptide (GFOGER); and a bacterially expressed, 165-amino acid collagen-like protein (DCo1l) produced using a recombinant collagen technology previously developed in our laboratory.

Here are summarized the major findings of this Chapter:

- A simple, quick and cost-effective protocol was developed to incorporate the different collagen proteins into Fmoc-FF/S hydrogels, without cross-linking or any chemical modification to the collagen proteins or to the hydrogel-forming peptides.
- The same protocol was equally successful for the hydrogel incorporation of a globular protein, enhanced Green Fluorescent Protein (eGFP), used as a reporter during method development.
- In this protocol proteins are incorporated simply by the passive diffusion that occurs when they are combined with the pre-gel peptide solution. As the hydrogels form upon exposure to divalent cations, the proteins become entrapped in the hydrogel mesh in a hydrogels-incorporation simultaneous

co-assembly mechanism. The proteins are then retained over time without being washed away.

- Hydrophobic interactions between the peptides forming the hydrogel and the incorporated proteins seem to play a role, stabilizing the overall hydrogel network and allowing the incorporated collagens or proteins to be retained over time. These hydrophobic interactions could explain the rapid fluorescence quenching observed when Fmoc-FF/S was modified with collagens or eGFP.
- The protocol was equally successful for the hydrogel incorporation of proteins of different sizes and shapes, from the largest and longest RTC (300 kDa, over 1000 amino acids per chain in triple helical conformation) to the smallest and shortest GFOGER peptide (11.2 kDa, 42 amino acids per chain). Nevertheless, a size-dependent effect on the hydrogel nanostructure was observed through Scanning Electron Microscopy. The largest RTC caused a more disorganized co-assembled system than the smaller DCol1 recombinant collagen or synthetic GFOGER peptide.
- Rheological measurement showed no significant differences in stiffness between the unmodified and collagen-modified or eGFP-modified Fmoc-FF/S hydrogels. This is indeed a positive result as alteration of the mechanical stiffness of the resulting hydrogels could affect the

mechanotransduction signals involved in cell adhesion and spreading during cell culture (Ingber, 2006; Caliari and Burdick, 2016).

- Collagen-modified Fmoc-FF/S hydrogels provide enhanced cell culture scaffolds with improved cell adhesion properties. A greater number of HT1080 cells adhered to each of the three collagen-modified hydrogels when compared to the unmodified Fmoc-FF/S hydrogels. The collagen proteins become incorporated into the hydrogel networks without interfering with the self-assembly mechanism, and remain biologically active providing sites for cell binding.
- The specific nature of the interaction between HT1080 cells and the collagens incorporated into the hydrogels was demonstrated by blocking the β_1-integrin subunit. HT1080 cells pre-treated with a blocking antibody severely reduced their capability of binding the collagen proteins incorporated within the hydrogels.

Numerous methods are used to incorporate bioactive adhesion molecules into hydrogels (Slaughter and Fisher, 2009). We believe that our simple and cost-effective protocol can be exploited for hydrogel modification with collagen-like proteins, other functional ECM molecules, or bioactive components such as growth factors, without modifying the chemical structure of the hydrogels and without using toxic cross linkers. These composite hydrogels should be useful in tissue engineering and cell culture applications.

Chapter 4 Modification of hydroxyapatite and RGD functionalised hydrogels with Osteoclast- Associated Receptor (OSCAR)

4.1 Introduction

The crucial role of the cytokine RANKL in osteoclastogenesis has been reviewed in section 1.4.2. RANKL stimulates OC differentiation by binding to its receptor RANK, which is expressed on the surface of OC precursor cells (Boyce and Xing, 2007; Nedeva *et al.*, 2021). However, although RANKL/RANK is the leading pathway for OC differentiation, there is evidence for the existence of costimulatory pathways that support and co-operate with the RANKL-mediated osteoclastogenesis (Nedeva *et al.*, 2021). Koga *et al*, for instance, showed that OC differentiation factors were present even though the RANKL/RANK pathway was impaired (Koga *et al.*, 2004). These authors used genetically modified mice that were lacking important mediators of the RANKL/RANK signalling. Nevertheless, following RANKL stimulation a normal number of osteoclasts and only a mild form of osteopetrosis were observed (Zou and Teitelbaum, 2015; Humphrey and Nakamura, 2016). These results suggest that, even though the main signalling was impaired, pathways downstream of RANK were activated regardless, suggesting the presence of costimulatory pathways that act alongside

the main RANKL/RANK pathway, potentially leading to OC differentiation (Nedeva *et al.*, 2021).

The differentiation of OCs requires, alongside to the RANKL/RANK pathway, the presence of costimulatory receptor signalling through the activation of adaptors that contain immunoreceptor tyrosine-based activation motifs (ITAMs), such as Fc receptor common γ-chain (FcRγ). However, little is still known about the mechanism of activation of these ITAM-containing receptors and their potential ligands (Barrow *et al.*, 2011).

It has been hypothesized that the osteoclast–associated receptor (OSCAR) is also involved in OC differentiation as a costimulatory pathway. OSCAR is mainly detected in bone tissue and interacts with OBs-released factors. Thus, it is considered to promote the differentiation of OC precursors into mature OCs via FCRγ, alongside the RANKL/RANK pathway (Kim *et al.*, 2002; Nedeva *et al.*, 2021).

The identities of all possible OSCAR ligands are still under investigation. It has been reported that OSCAR may interact with fibrillar collagens released to the ECM from the bone surfaces in which OCs undergo maturation and terminal differentiation *in vivo* (Barrow *et al.*, 2011). The interaction between OSCAR and collagen is also important during normal bone development, maintenance and repair, and could be important in many diseases where either collagen or OC

function is impaired (Zhou *et al.*, 2016). For example, in rheumatoid arthritis, it has been shown that OSCAR is overexpressed into the synovial fluid and in the joints, where the exposed collagen is abundant. In fact the overexpression of OSCAR maximizes cytokine levels, thus contributing to the pro-inflammatory environment of the disease (Schultz *et al.*, 2016).

In order to understand more the mechanism of interaction between OSCAR and collagen during osteoclastogenesis, the crystal structure of OSCAR ectodomain in complex with a collagen-like peptide (CLP) was determined (Haywood *et al.*, 2016; Zhou *et al.*, 2016).

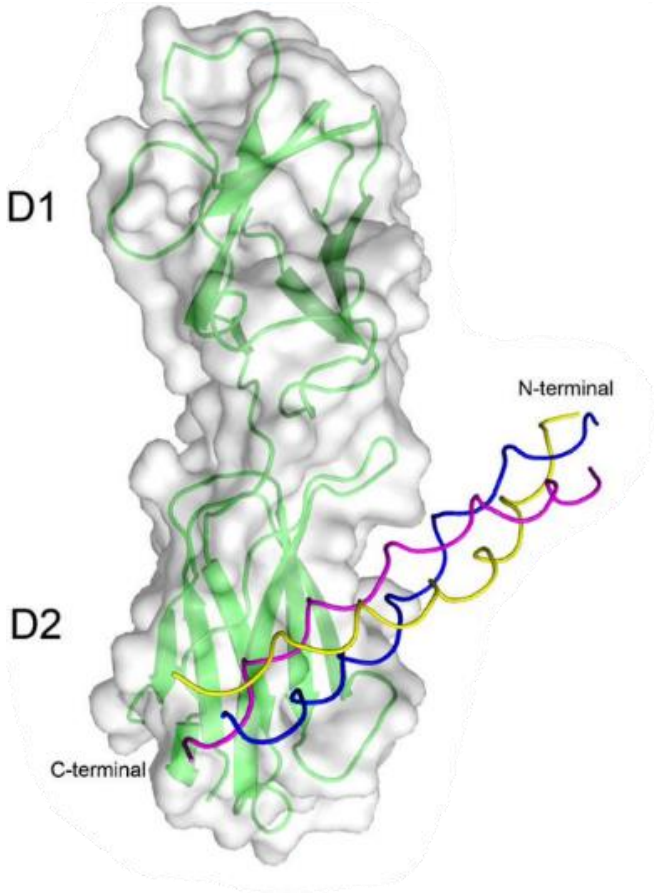

Figure 38 X-ray crystal structure of human OSCAR ectodomain in complex with a collagen triple helical peptide. Ribbon diagram of OSCAR (green) showing the two Ig domains D1 and D2 in a semi-transparent surface. The collagen triple helical peptide is shown as three chains coloured blue, yellow and magenta. Adapted from (Haywood *et al.*, 2016).

OSCAR belongs to the Ig-like family of receptors. Its ectodomain contains two Ig domains named D1 and D2, arranged at an angle with respect to each other (**Figure 38**). The primary collagen-binding site is in a groove in the D2 domain although a low affinity site is also present on the D1 domain (Zhou *et al.*, 2016). Zhou *et al* hypothesized that OSCAR binds collagen through a two-phase process involving a low affinity interaction at the beginning (mediated by D1), followed by a strong interaction mediated by the D2 domain (Zhou *et al.*, 2016).

Different groups have investigated the interaction between OSCAR and collagen to assess whether this contributes to osteoclastogenesis *in vitro*. By using a library of triple-helical collagen peptides, Barrow et *al.* (Barrow *et al.*, 2011) managed to identify the minimum collagen sequence that binds OSCAR as GPOGPX'GFX' (OSC^{pep}), where O is 4-hydroxyproline, X' is a variable amino acid, and each proline residue can be substituted by alanine. Next, they assessed whether peptides containing this binding motif could promote differentiation of OCs. They cultured mouse Bone Marrow isolated Macrophages (BMMs) on two peptides containing the OSC^{pep} minimal binding sequence, $(GPP)_5$-GPOGPAGFOGAO-$(GPP)_5$ and $(GPP)_5$-GAOGPAGFA-$(GPP)_5$. They detected the formation of giant TRAP-positive OCs as well as an increased expression of typical OC proteases such as MMP9 and CTSK, confirming the involvement of the OSCAR-collagen interaction during osteoclastogenesis.

Following on the work reported in Chapter 2 and to further investigate the role of OSCAR in osteoclastogenesis, the aim of this fourth Chapter was to combine OSCAR-binding collagen peptides with the newly developed Hap-decorated RGD-functionalised hydrogel (as described in Chapter 2) to assess whether this composite hydrogel had a positive or detrimental effect on the differentiation of Raw 264.7 cells. Collagen binding to OSCAR was first assessed *via* Surface Plasmon Resonance to measure the affinity of the receptor-ligand interaction. Next, a newly designed recombinant protein containing the OSCAR-binding

motif was engineered by using the recombinant collagen technology that is well established in our laboratory (see section 3.1.1). Once characterized, proteins and peptides were combined with the Hap-decorated Fmoc-FF/S/RGD hydrogels (Chapter 2) by using the protocol described in Chapter 3. Finally these composite hydrogels were used to culture the pre-osteoclast cell line Raw 264.7. Differentation of Raw 264.7 cells into OCs was assessed by analysing cell morphology and viability as previously described in Chapter 2.

The specific aims of this Chapter were:

1. To design collagen-like peptides and a recombinant collagen-like protein containing the OSCAR-collagen binding motif.
2. To produce this recombinant collagen-like protein using a bacterial expression system and to purify it by chromatographic methods.
3. To characterise the collagen secondary structure of the collagen-like peptides and recombinant protein using Circular Dichroism spectroscopy.
4. To assess their binding to OSCAR.
5. To combine them with the Hap-decorated Fmoc-FF/S/RGD hydrogel.
6. To culture (2D) Raw 264.7 cells on this composite hydrogel and to investigate their differentiation into mature OC cells.

4.2 Materials and methods

4.2.1 OSCAR- binding collagen-like peptides, recombinant collagen-like proteins, and Fmoc-based hydrogels

A 27-amino acid collagen-like peptide containing the OSCAR-binding motif GAOGPAGFA was designed with nine-residue $(GPO)_3$ segments flanking it at each side and with N-terminal acetylation and C-terminal amidation. Its overall sequence is shown in **Table 6**. A second collagen-like peptide was designed by replacing the hydroxyproline on the OSCAR-binding motif of the first peptide with proline (GAPGPAGFA) and following the same design principles (Table 6). Synthesis and purification of both peptides, hereafter referred as OP1 and OP1* respectively, was outsourced to GenScript (UK). Purity was assessed by Genscript using HPLC. OP1 (Batch Nº U0503EK140_1) was 95.3% pure and $OP1^*$ (Batch Nº U0503EK140_3) was 95.0% pure. Both peptides were supplied in freeze-dried form and were stored at -80°C until used. A recombinant collagen-like protein, hereafter named OCol1, was designed with the potential OSCAR-binding sequence GPPGPQGFQ and a domain architecture identical to that of the recombinant protein DCol1 (section 3.2.2) (**Figure 39)**, with a C-terminal PfC trimerization domain (Ghosh *et al.*, 2012a) (**Figure 27**) and an N-terminal hexahistidine tag $(His)_6$ for purification purposes. The amino acid sequence of OCol1 is shown in Table 6. Gene synthesis, subcloning to a pET28c vector, expression in *E. coli* and purification by nickel-affinity chromatography was carried out by GenScript (UK). The final purity of OCol1 (Batch No.

U6699HA190-1_OCol1) was assessed by GenScript *via* SDS-PAGE and it was estimated at 85%. The proteins were shipped in dry ice in storage buffer (50 mM Tris-HCl, 150 mM NaCl, 10 % Glycerol, pH 8.0) and stored at -80 °C upon arrival until used.

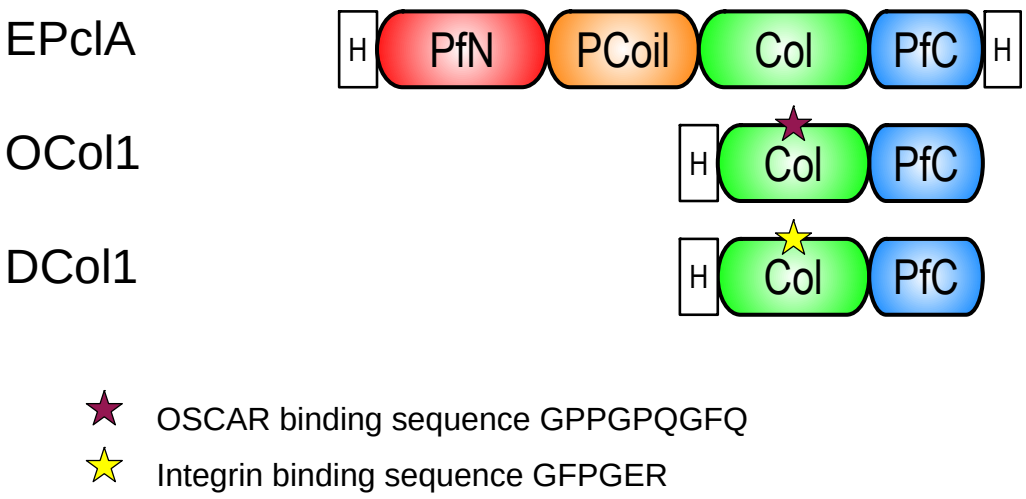

Figure 39 Domain architectures of the recombinant proteins OCol1, DCol1 and the parent recombinant collagen EPclA (Ghosh *et al.*, 2012a). Key to domain names and colors: **PfN** (red) – phage fiber N terminal capping domain; **PfC** (blue) – phage fiber C terminal capping domain; **PCoil** (orange) – phage trimeric coiled-coil domain; **H** – hexa-histidine tag (His_6). The red and yellow stars indicate approximate positions of OSCAR and integrin binding sites.

Table 6 Collagen-like peptides and recombinant protein used to modify Hap-decorated, Fmoc-FF/S/RGD hydrogels. Amino acid sequences shown in standard single-letter code, plus O for 4-hydroxyproline. Known or potential OSCAR binding sites in green bold type. Ac-, N-terminal acetylation; -NH_2, C-terminal amidation.

Molecule	**Sequence**	**Amino acids**	**Monomer M_w (kDa)**	**Trimer M_w (kDa)**
OP1 peptide	Ac-GPOGPOGPO**GAOGPAGFA**GPOGPOGPO-NH_2	27	2.4	7.2
OP1* peptide	Ac-GPOGPOGPO**GAPGPAGFA**GPOGPOGPO-NH_2	27	2.4	7.2
OCol1 protein	MGSHHHHHHSGLVPRGSGPPGPPGPQGPAGPRGEPGPAGPKGEPG PA**GPPGPQGFQ**GPPGPQGPAGPIGPKGEPGPIGPQGPKGDPGETQI RFRLGPASIIETNSNGWFPDTDGALITGLTFLAPKDATRVQGFFQHLQV RFGDGPWQDVKGLDEVGSDTGRTGE			

The secondary structures of the OP1 and OP1* peptides and the OCol1 protein were analysed by circular dichroism (CD) spectroscopy using a Jasco® J-810 spectropolarimeter equipped with a Peltier temperature controller as described in the previous chapter (section 3.2.4). OP1 and OP1* were resuspended up to a concentration of 0.5 mg/ml in CD buffer (10 mM K_2HPO_4, 10 mM KH_2PO_4, 150 mM KF, pH 7.4) (Norma J. Greenfield, 2007), 24 h in advance of the measurements to allow the collagen triple helix to form. OCol1 was thawed and buffer-exchanged to CD buffer by using a PD10 disposable desalting column (GE17-0851-01, Merck, UK). Briefly, the column was equilibrated with 5× column volumes of CD buffer before addition of OCol1. After flow through collection, 0.500 mL fractions were collected into Eppendorf tubes and analysed by CD. Parameters and settings are described in section 3.2.3. Additionally, the thermal stability of all the constructs was analysed. Thermal transition profiles were recorded between 4°C and 70°C at 222 nm with a data pitch of 0.5 nm, bandwidth of 1 nm, detector response time of 32 sec and temperature slope of 1°C/min. Samples were cooled back to 4°C after the different transitions and final spectra were recorded at that temperature. Ellipticity in millidegrees were converted to mean residue molar ellipticity (degree cm^2 $dmol^{-1}$) by normalizing for the number of residues and molecular weight of each peptide or protein.

4.2.2 Surface Plasmon Resonance (SPR) for protein-protein interaction

SPR analyses were carried out on a Biacore™ T200 (Cytiva) using a Series S CM5 sensor chip with an assay running buffer of 10 mM PBS, 150 mM NaCl, 0.05% Tween20, pH7.4. Reference and active flow cells were activated by injecting 70 µl of a 1:1 mixture of 0.2 M 1-ethyl-3-(3-dimethylaminopropyl)-carbodiimide (EDC) and 0.1 M N-hydroxysuccinimide (NHS) at 10 µL/min. OSCAR FC-receptor protein was immobilised onto the active flow cell at 20µg/ml in 10 mM Sodium Acetate pH 5.0 at 10 µL/min to 6880 response units (RU). Reference and active flow cells were blocked using 1 M ethanolamine, pH 8 at a flow rate of 10 µL/min. For kinetic and equilibrium binding analysis peptides were flowed overactive and reference flow cells at 30 µL/min in assay running buffer at peptide concentrations of 5000 – 0 nM and 40,000 – 0 nM, for OP1 and OP1* respectively, using a two-fold dilution series. Analysis temperature was set at 25 ◦C. Surfaces were regenerated with a 10 second injection of 0.1 M Glycine, pH 2.0. Data sets were analysed using the appropriate fitting algorithm within the BiaEvaluation software. Models used for analysis were the Langmuir 1:1 Binding model and the Steady State Analysis model. Data presented are the mean and standard error of the mean (SEM) of triplicate runs.

4.2.3 Raw 264.7 cell adhesion assay

Raw 264.7 cells were maintained in cultured and passaged as described in the second chapter, section 2.2.9. Cell adhesion to OP1 and OP1* was assessed as

shown by Barrow *et al* (Barrow *et al.*, 2011). Briefly, 48 well plate was coated with 10 µg/mL of OSCAR peptides overnight at 4 °C. Excess of protein was then removed by washing with PBS before addition of 1% BSA to block the nonspecific interaction for 1h at RT. Meanwhile, Raw 264.7 were resuspended at concentration of 2 x 10^5 cell/mL and added to the well. Cells were cultured with different concentration of hRANKL (Peprotech, UK) (0-100 ng/ml) for up to 5 days to assess the contribution of OSCAR to the differentiation of Raw 264.7 towards mature OCs.

4.2.4 TRAP staining

Successful differentiation of OCs was demonstrated by staining of TRAP activity. After 5 days post culture, Raw 264.7 were fixed in 4% PFA for 15 min at RT and detection of TRAP was assessed by following the manufacturer's protocol (Acid Phosphatase, Leukocyte (TRAP) Kit; Sigma–Aldrich, USA and evaluated by light microscopy (ThermoFisher, UK). Multinucleated TRAP+ cells containing more than three nuclei were scored as mature osteoclasts.

4.2.5 Gene Expression

Gene expression of OCs markers was evaluated as described in Chapter 2, section 2.2.13. By using a StepOne™ Real-Time PCR System (Applied Biosystems, UK) using TaqMan probes with the universal PCR Master Mix (Life Technologies, 4304437) in a total volume of 10 µL. The TaqMan probe for Trap and OSCAR were: Mm00475698_m1 and Mm01338227_g1. Data were analysed using the

$2^{-\Delta Ct}$ method and normalised to the endogenous house-keeping gene GAPDH (Mm99999915_g1). Experiments were performed in triplicates.

4.2.6 Incorporation of OSCAR-collagen into Hap-decorated hydrogels

In order to incorporate OSCAR-collagen binding protein into the newly developed Hap-decorated RGD-functionalised Fmoc-hydrogels, the same protocol described in Chapter 3 was used (section 3.2.5).

Hap-decorated hydrogels were prepared as described in the Chapter 2. Briefly, 0.0142 g of Fmoc-FF/S/RGD (final concentration 15 mM) were dissolved into 1 mL of d_2H_2O w/wo 1 mg/mL of Hap, respectively. Then, hydrogels were pipetted into a 24-well plate containing 100 µg/ml of OCol1. Due to the short molecular weight, OP1 and OP1* were not used to demonstrate the protocol of incorporation and the same behaviour of GFOGER peptide, described in the previous chapter, was assumed. Finally, protein incorporation was assessed by SDS-PAGE as described in Chapter 3, section 3.2.3.

4.2.7 Hydrogel cell culture

Hap-decorated hydrogels were tested in combination with OP1, OP1* and OCol1 to evaluate the contribution of OSCAR as costimulatory pathway for OCs differentiation. Hydrogels were prepared 24 h in advance as described in Chapter 2, section 2.2.2. OP1, OP1* and OCol1 were resuspended in PBS up to 100 µg/ml and dispensed on the surface of the Pre-gel with and without Hap. Hydrogels were left to crosslink overnight at 4°C. The day after, 2 mL of Raw 264.7 (cell density

of 4 x 10^5 cell/mL) were seeded on top of all the different formulation of hydrogels. 10 ng/ml of hRANKL were added to the cell media in order to differentiate OCs. Cells were cultured for up to 7 days and media was replenished every other day.

4.2.8 F-actin staining

Cell differentiation was also assessed by measuring the difference in morphology between OSCAR-modified and OSCAR-free hydrogels. Cell diameter, cell multinucleation and presence of typical OCs features were observed by using an F-actin staining. Cells cytoskeleton and nuclei were imaged as described in Chapter 2, section 2.2.4.

4.2.9 LIVE/DEAD cell viability assay

After 7 days, cell viability on the OSCAR-modified Hap-decorated hydrogels was evaluated by using a LIVE/DEAD assay. For experimental details, please refer to Chapter 2, section 2.2.3.

4.2.10 Statistical analysis

All quantitative values are presented as mean ± standard deviation. All experiments were performed using at least three replicates. Data were plotted using Origin 2019b and compared using an unpaired *t* test, unless stated otherwise. Two levels of significance were used: 0.005 (**) and 0.001 (***).

4.3 Results and Discussion

4.3.1 Protein and peptide characterization

OSCAR is a costimulatory receptor that has been show to contribute to the differentiation of OCs precursors to mature, bone resorbing osteoclasts by binding the collagen exposed in the bone (Nedeva *et al.*, 2021). For this reason, we wanted to combine peptides and protein containing OSCAR-collagen binding motif to Hap-decorated, Fmoc-based peptide hydrogel scaffold (described in Chapter 2) to assess the effect during osteoclastogenesis *in vitro*. Two peptides, namely OP1 and OP1* were designed based on the results described by Barrow *et al* (Barrow *et al.*, 2011). Both peptides contained the minimal binding motif of collagen for OSCAR recognition GA**X**GPAGFA (where X stands for hydroxyproline or proline, accordingly). Similarly, a recombinant version of these peptides was designed to contain the OSCAR-collagen binding motif presenting the proline amino acid. In order to analyse the collagen triple helix secondary structure, all of the constructs were characterised by CD. Both OP1 and OP1* and OCol1 showed a band of positive ellipticity with a maximum at around 220 nm, and a deep band of negative ellipticity with a minimum around 198 nm (Kelly and Price, 2005; Norma J Greenfield, 2007; Drzewiecki *et al.*, 2016). As described previously, these features are associated with the typical conformation of collagen triple helix. Moreover, the triple helical features disappeared from the CD spectrum when the temperature was increased to 70°C as shown in **Figure 40**. Interestingly, upon cooling to 4°C again, the collagen

samples almost completely recovered their triple helical structure (**Figure 40**) confirming that the increase in temperature did not affect their initial collagen structure. In particular, compared to OP1 and OP1* that showed partial recovery of the collagen structure, the effect was much more evident in OCol1 with a CD spectrum practically indistinguishable from the initial one. This is due to the presence of the PfC trimerization domain in the OCol1 structure that aids the triple helix to form (Ghosh *et al.*, 2012a).

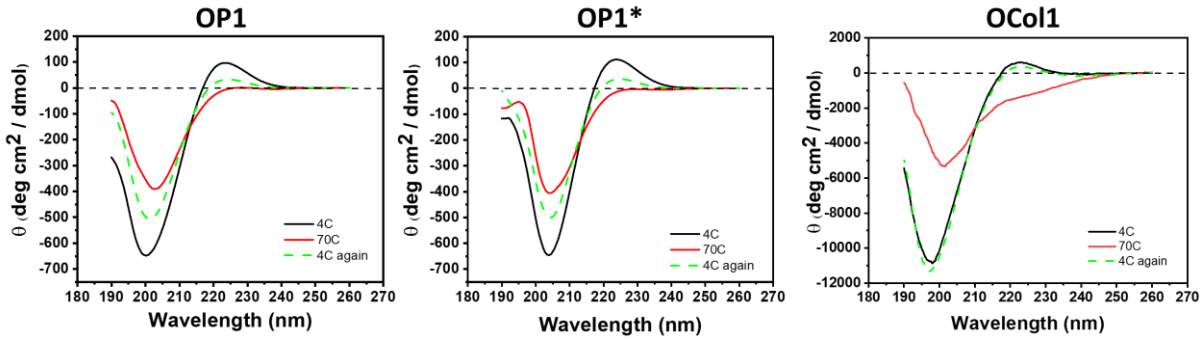

Figure 40 CD spectra at 4°C (black line), 70°C (red line) and 4°C after denaturation (green dashed line) for OP1, OP1* and OCol1. The vertical axis measures mean residue ellipticity θ in degrees cm2 dmol−1. CD data were collected between 190 and 260 nm.

In order to assess thermal stability of the collagen peptides, denaturation of the collagen triple helix was monitored at 220 nm as a function of continuously increasing temperature, from 4°C to 70°C. The thermal curve showed a single transition, which typically corresponds to the decrease of ellipticity at 220 nm and loss of collagen triple helical structure (**Figure 41**). Both OP1 and OP1* showed a transition from trimer to monomer at ~ 37°C and ~ 27 °C, respectively. Less thermal stability was already expected due to OP1* not presenting the

hydroxyproline in the structure. In fact, it has been demonstrated that the presence of hydroxyproline helps stabilise the collagen triple helical structure (Jenkins *et al.*, 2003; Brinckmann, 2005; Bella, 2016). As for OCol1, thermal denaturation showed a single, sharp transition that occurred at ~ 56 °C. As described above, the higher thermal stability is caused by the presence of the PfC trimerization domain (Ghosh *et al.*, 2012a).

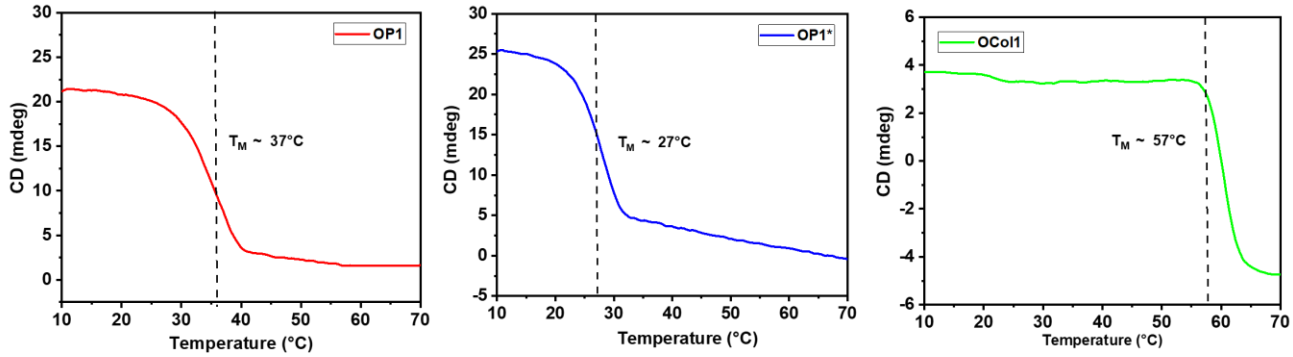

Figure 41 Thermal denaturation of the OP1, OP1* and OCo1, monitored by CD at 220 nm as a function of increasing temperature between 4°C and 70°C, with a protein concentration of 0.5 mg/ml in CD Buffer pH 7.4, and a heating rate of 1°C/min.

4.3.2 Analysis of Binding Interactions

SPR was used to determine the binding affinity between OP1 and OP1* and FC-OSCAR chimeric receptor. To establish affinity of this interaction, kinetic analysis of immobilised OSCAR FC-receptor with OP1 and OP1* as analytes was performed. The Langmuir 1:1 model was used to perform the kinetic analysis. The Langmuir 1:1 model is based on a simple interaction between ligand and analyte where a 1:1 molar complex is formed at equilibrium i.e. A+B↔AB as determined by the association (*k*a) and dissociation (*k*d) rate-constants. The overall affinity constant (KD) is given by KD= *k*d/*k*a (Jonsson *et al.*, 1991).

Figure 42 shows the sensograms from the OSCAR: OP1 interaction illustrating the relative response shown (red line) with experimental curve-fitting (black line).

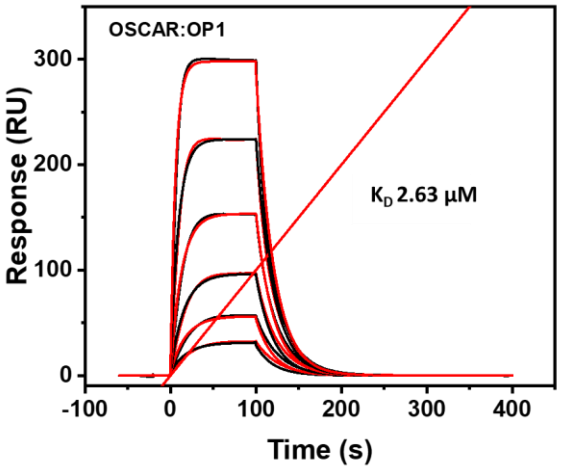

K_D (M)	k_a (1/Ms)	k_d (1/s)
Mean	Mean	Mean
2.63 X 10^{-6}	10049.85	0.0042

Figure 42 SPR multi-cycle kinetic analysis of OSCAR-OP1 interaction. OSCAR was immobilised onto a CM5 sensor chip surface and OP1s was flowed over the surface in assay running buffer of 10 mM PBS, 150 mM NaCl, 0.05% Tween20, pH 7.4.at a concentration series 5000 – 0 nM . Sensograms were analysed using the Langmuir 1:1 model and relative responses shown (red) with theoretical fit (black) overlaid. Experiments were performed in duplicate and sensograms presented representative of data obtained.

As shown from the association and dissociation phases the OP1 showed a progressive binding phase to the receptor with a slow release at all the concentrations tested. From the Langmuir 1:1 analysis the affinity constant (K_D) was determined as 2.63 µM, suggesting that OP is a high affinity binding partner for OSCAR Fc-receptor. On the other hand, OP1* sensograms (**Figure 43A**) showed that both association and dissociation phases occurred very quickly. For this reason, a weak interaction was assumed for that between OSCAR and OP1*. As such, steady state analysis (SSA) was used to measure the affinity, (**Figure**

43B). From SSA, K_D was calculated to be 19.5 µM suggesting a much lower affinity for the OSCAR receptor than OP1.

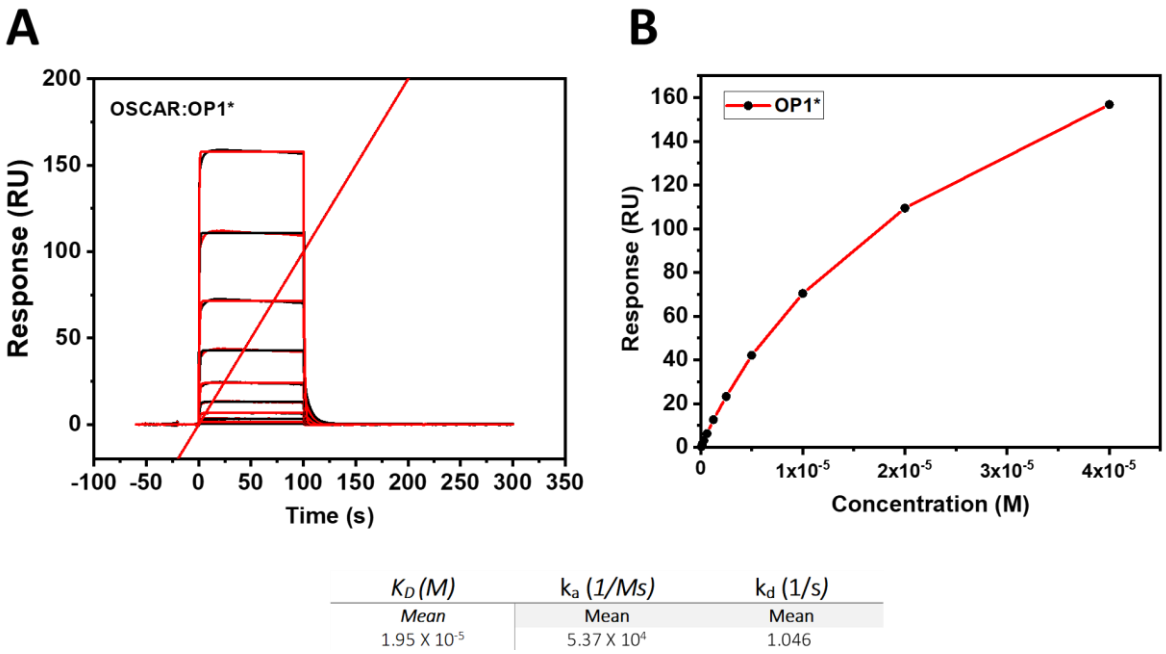

Figure 43 SPR multi-cycle kinetic analysis of OSCAR-OP1* interaction. Panel **A** shows sensograms of OSCAR-OP1*, analysed using the Langmuir 1:1 model and relative responses shown (red) with theoretical fit (black). Panel **B** showed steady state analysis as a measure of affinity vs OP1* concentration.

Based on these results, it is believed that hydroxyproline contributes to a more stable OP and therefore a much higher affinity for the OSCAR FC-receptor.

4.3.3 OSCAR contributes to differentiation of Raw 264.7 cells towards osteoclasts

In order to assess the involvement of OSCAR during osteoclastogenesis Raw 264.7 cells were cultured in presence of OP1 and OP1*. OCol1 was not used for this set of experiments as it contained the same binding motif of OP1*.

Figure 44 shows TRAP staining of Raw 264.7 cells after 5 days culture. As expected, Raw 264.7 cells showed typical OCs features when cultured in the presence of 100 ng/mL of hRANKL for both OP1 and OP1*. In fact, cells were larger in diameter than the counterpart treated with lower concentration of hRANKL showing the presence of an actin ring surrounding more than 3 nuclei (highlighted by the purple colour). In this case, the effect of the OPs could not be seen due to the high concentration of hRANKL that masked any costimulatory pathway.

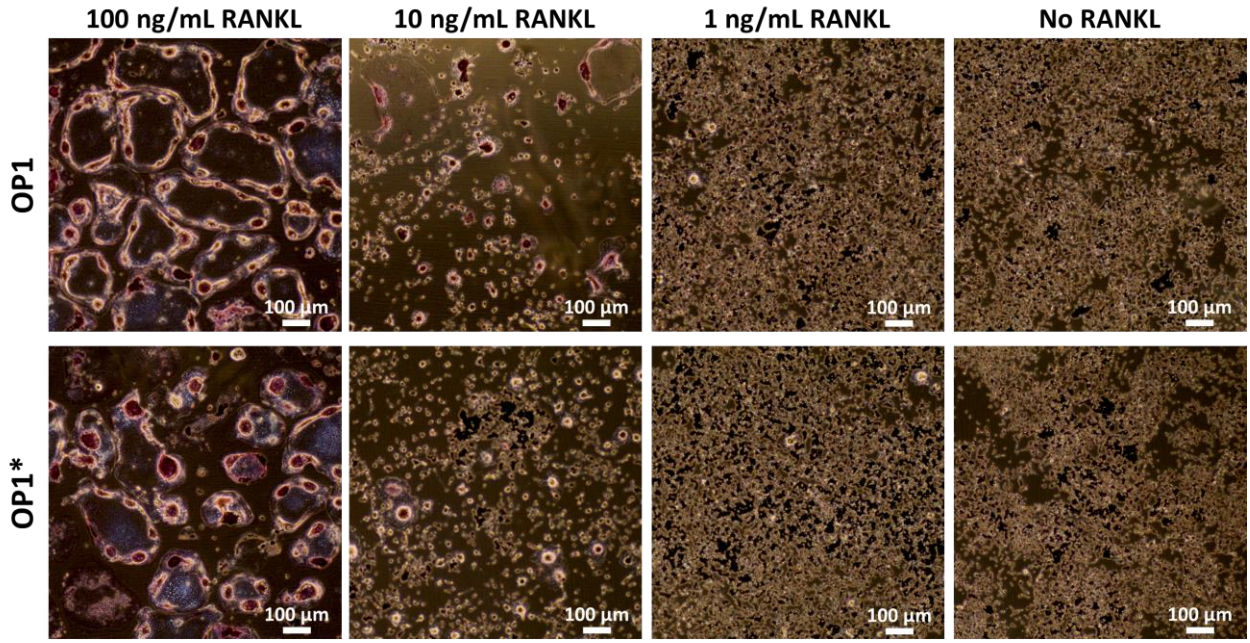

Figure 44 TRAP straining of Raw 264.7 cells cultured for up to 5 days on OP1/OP1* coated 24-well plate. Different concentrations (0-100 ng/ml) of hRANKL were used.

However, when cultured with 10 ng/mL of hRANKL, although less change in morphology was noticed, Raw 264.7 cells still showed differentiation to OCs. In particular, the effect was more evident when cultured on OP1 with more cells showing OC-like features compared to those cultured on OP1*. No differentiation

effect was seen when Raw 264.7 cells were cultured with 1 ng/mL of hRANKL. Additionally, OP1 and OP1* were not able to trigger any differentiation on their own (no hRANKL added) as shown by the absence of TRAP staining (**Figure 44)**.

Differentiation of OCs and presence of any costimulatory pathway was also assessed by analysing typical OCs markers *via* qRT-PCR (**Figure 45**).

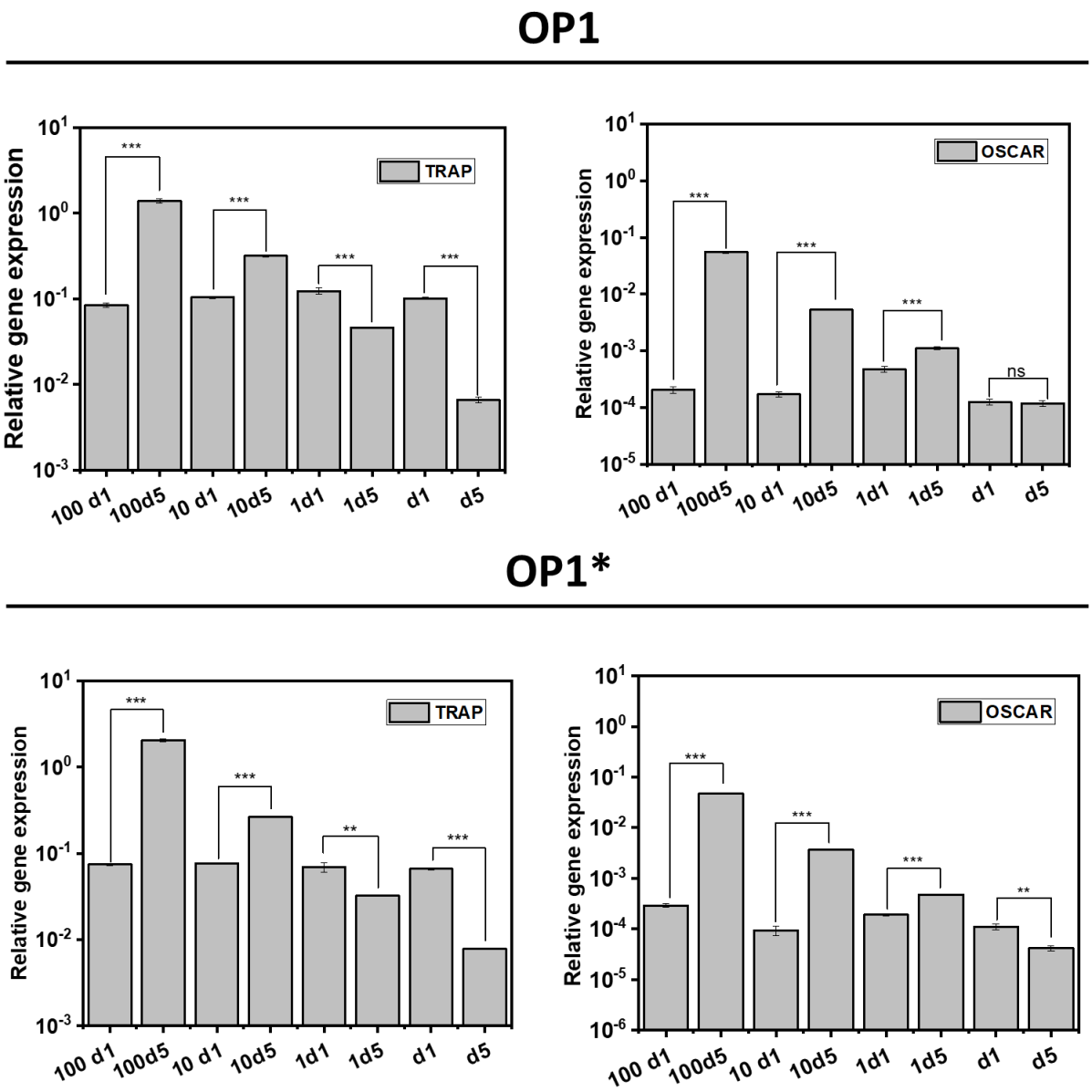

Figure 45 Gene expression of TRAP and OSCAR relative to GAPDH by Raw 264.7 cells (n = 3) after 24h and five (d5) days cultured on OP1 and OP1* with different concentration of hRANKL (0-100 ng/ml). (Data shown as mean ± SD; ∗∗∗p < 0.001; ∗∗p < 0.05).

As expected, gene expression data confirmed OSCAR involvement during the differentiation of Raw 264.7 cells. In fact, compared to day 1, the level of TRAP expression was significantly higher for both OP1 and OP1* after 5 days when cells were treated with 100 ng/mL of hRANKL. Similarly, OSCAR expression

was also significantly higher compared to day 1, indicating that the cells were potentially interacting with the OP1 and OP1* through OSCAR. A similar pattern of expression was observed when the cells were treated with a lower concentration of hRANKL (10 ng/ml). Indeed, although TRAP expression was lower than the counterpart treated with a higher concentration of cytokine, OSCAR gene expression was still significantly higher for both OP1 and OP1*. This suggests that not only were cells able to differentiate to OCs, as confirmed by the TRAP expression but also that OSCAR was involved during the differentiation. On the other hand, when cells were treated with a minimum dose of hRANKL (0-1 ng/mL), both TRAP and OSCAR gene were either expressed at lower amounts or that there was no significant change in gene expression.

Despite the differences in stability and binding affinity observed between OP1 and OP1*, both peptides showed a positive effect on the differentiation when used as a substrate to culture of Raw 264.7 cells. In fact, the collagen equilibrium in solution (as in SPR experiment) may not be the same as the collagen equilibrium on TCPS and therefore the local saturation of OP1* in the well may still be able to provide cell adhesion and therefore stimulate differentiation.

For this reason, Raw 264.7 cells were able to grow and differentiate to mature OCs on both OP1 and OP1* when treated with a high concentration of hRANKL (100 ng/ml). Similarly, differentiation of Raw 264.7 cells was still observed with lower concentration of hRANKL, although the effect was much more evident on

OP1. In order to assess the effect of OSCAR as a costimulatory pathway for OCs differentiation, 10 ng/mL of hRANKL was chosen as the concentration for further as a higher concentration of protein may masks the effect of secondary pathways.

4.3.4 OSCAR-collagen peptide incorporation into Hap-decorated Fmoc-RGD hydrogels

The same protocol described in Chapter 3 was used to incorporate OCol1 into the newly developed Hap-decorated Fmoc-based self-assembling peptide hydrogels described in Chapter 2. SDS-PAGE was used to check the successful incorporation of OCol1 into hydrogels. Similar to that described in Chapter 3, OCol1 was successfully incorporated within Fmoc-FF/S/RGD with and without Hap, as shown from the protein appearing at the correct MW in the SDS-PAGE gel. However, as illustrated in **Figure 46**, compared to the control lane, OCol1 had a much darker bands when incorporated into the Hap-decorated Fmoc-FF/S/RGD than the Hap free hydrogels. Indeed, a lighter dark band appeared in lane 11 for Fmoc-FF/S/RGD, indicating a lower incorporation of OCol1.These results suggest that the OCol1 incorporation was more efficient in the Hap-decorated hydrogel than the naked Fmoc-FF/S/RGD.

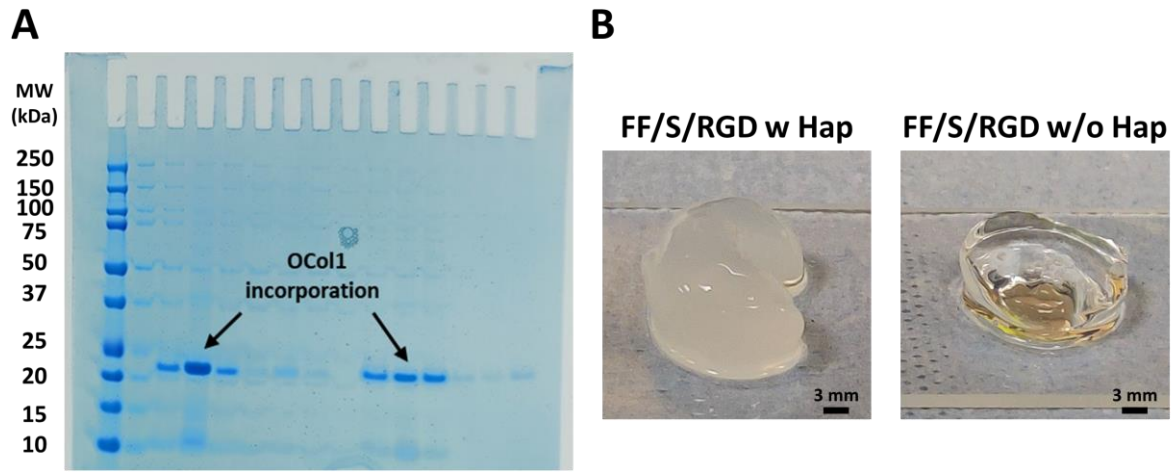

Figure 46 OCol1 incorporation into Fmoc-FF/S/RGD with and without Hap. Panel **A** shows SDS-PAGE of OCol1 incorporated into hydrogels. Lane composition (from left to right): Molecular weight markers; 3, 4, 5 and 10, 11, 12 protein stock solution; protein incorporated into the hydrogel; remaining protein into the well, respectively. Panel **B**, photograph of Fmoc-FF/S/RGD with and without Hap incorporating OCol1.

Additionally, it was also noticed that Hap-decorated hydrogels that incorporated OCol1 retained the structure better than the Hap-free hydrogels. In fact, as seen in **Figure 47**, undecorated hydrogels lost his shape whilst the Hap-decorated hydrogels maintained their structures.

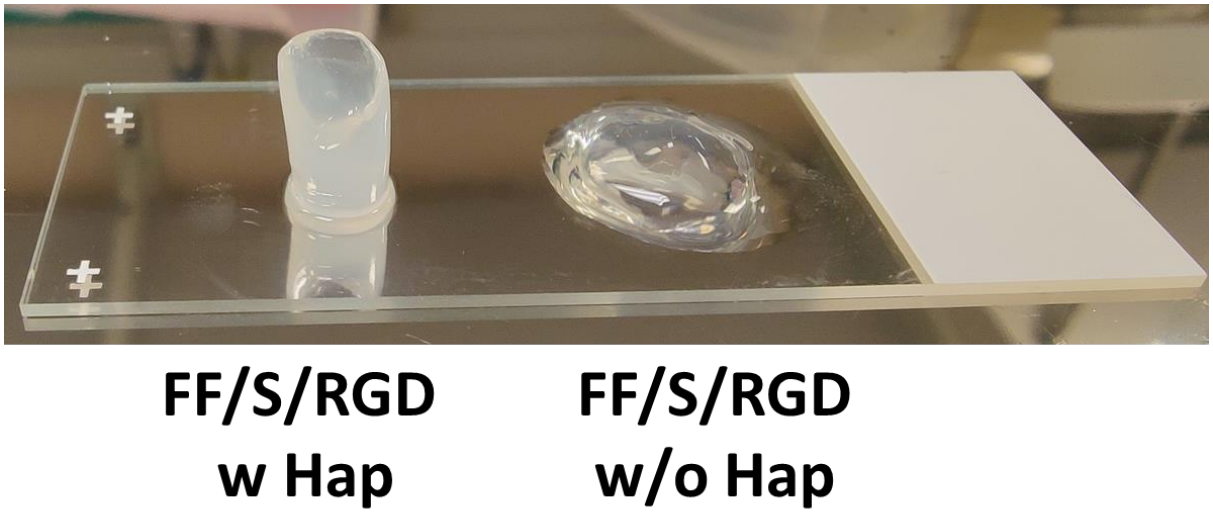

Figure 47 Fmoc-FF/S/RGD with and without Hap incorporating OCol1.

For this reason, due to the loss of shape and considering the remaining protein in the well, it is plausible that Fmoc-FF/S/RGD without Hap is not able to retain large amounts of protein and therefore the structure collapsed over time.

4.3.5 OSCAR-modified Hap-decorated hydrogels for OCs culture and differentiation

In order to test the effect of OSCAR during the differentiation of Raw 264.7 cells to mature OCs, Hap-decorated Fmoc-FF/S/RGD hydrogels, described in Chapter 2, were used as platform to culture cells. Based on the results described in these chapters a few conditions were applied to this hydrogel platform:

1- Only Fmoc-FF/S/RGD hydrogels decorated with Hap were used as most suitable scaffold to differentiate OCs as well as to successfully incorporate OSCAR-collagen peptides/protein;
2- Hydrogels were modified with 100 µg/ml of OP1/OP1* and OCol1, respectively;

3- A low dosage of hRANKL (10 ng/ml) was used to trigger OCs differentiation and analyse OSCAR costimulatory effect;

Similar to that described in the Chapter 2, cells were cultured for up to 7 days and OC-like features were assessed. Results are presented in comparison with the "naked" Fmoc-FF/S/RGD that incorporates Hap (called FF/S/RGD for simplicity), in order to assess whether the addition of OSCAR-collagen binding peptides has a positive or detrimental effect on the differentiation of OCs.

As can be seen from the staining in **Figure 48**, Raw 264.7 cells showed OC-like morphology with a prominent cytoplasm which is surrounded by an F-actin-rich structure (actin ring). This area contains densely packed podosomes (**Figure 48A**) that generates focal adhesion with the hydrogel matrix. This is a typical OC feature as extensively described in literature (Lakkakorpi and Väänänen, 1991; Roscher *et al.*, 2016). Moreover, the actin ring surrounded more than 3 nuclei in all the formulation tested. As explained before, this is usually associated with the morphology of mature OCs (Pierce, Lindskog and Hammarström, 1991; Boyle, Simonet and Lacey, 2003).

Multinucleation was also assessed by counting number of nuclei/cell and depicted as a violin plot. **Figure 48B** illustrates that, compared to the naked FF/S/RGD, violin plots highlight a broader distribution of nuclei (between 3-5) in all the combinations tested apart from those cultured on OP1*. However, of all the

OSCAR-modified hydrogels, only those incorporating OP1, produced a significantly different distribution (ANOVA, non-parametric $p<0.05$).

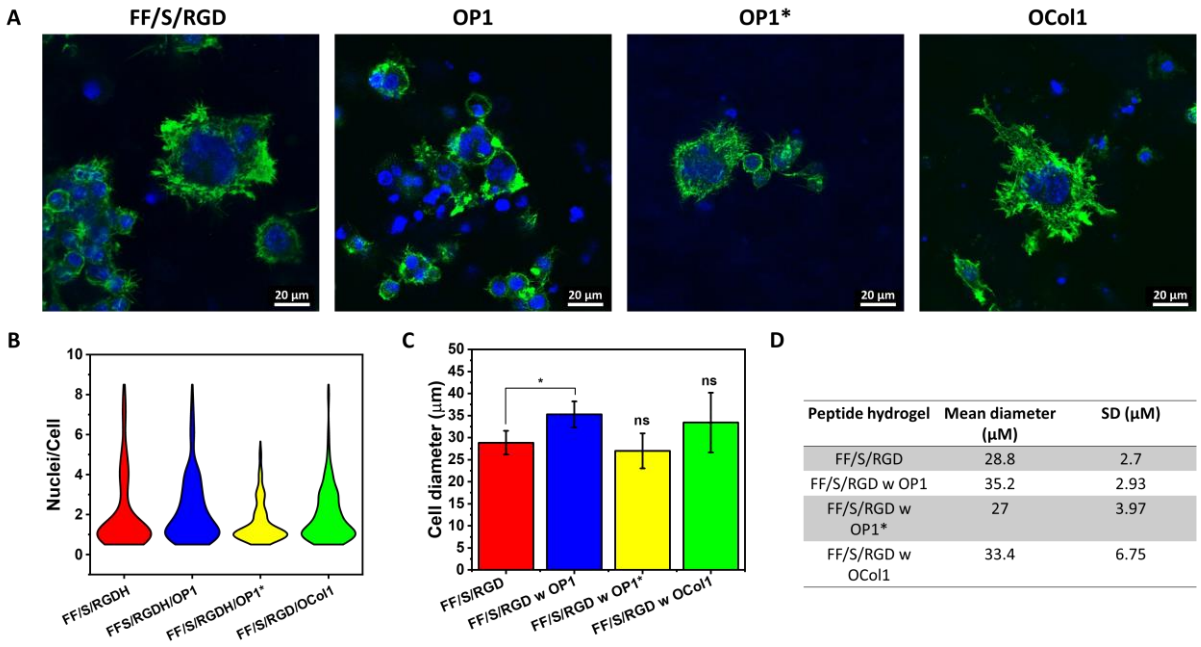

Peptide hydrogel	Mean diameter (µM)	SD (µM)
FF/S/RGD	28.8	2.7
FF/S/RGD w OP1	35.2	2.93
FF/S/RGD w OP1*	27	3.97
FF/S/RGD w OCol1	33.4	6.75

Figure 48 (**A**) Analysis of Raw 264.7 cells after seven days culture on FF/S/RGD and OSCAR-collagen modified hydrogels (green: F-actin, Alexa Fluor 488 phalloidin; blue: Nuclei, Hoechst 33342; scale bars 20 µm). (**B**) Analysis of multinucleation by a violin distribution plot (data shown as number of nuclei per cell, N = 100). (**C**) Measurements of cell diameter (data shown as mean ± SD, N = 43, ∗∗$p < 0.05$). (**D**) Table summarising the mean diameter of the cells cultured on the OSCAR modified hydrogels.

Of all the combination tested, only cells cultured on FF/S/RGD with OP1 showed a statistically significant increase in diameter (**Figure 48C**). Raw 264.7 cells cultured on OP1* showed a decreased diameter compared to unmodified hydrogels (although not statistically significant).

Cells cultured here on different OSCAR-modified hydrogels showed typical features of mature OCs. These results are in line to those described by Barrow *et*

al where they showed that OPs were able to act as costimulatory pathway for OCs differentiation (Barrow *et al.*, 2011). Although all the collagen peptides tested seemed to trigger the differentiation of Raw 264.7 cells, the effect was more evident with OP1. However, these results are coherent to what was observed so far in this chapter. In fact, OP1 has shown to interact more efficiently with OSCAR (**Figure 42**) and to have a higher thermostability (**Figure 41**) due to the presence of hydroxyproline in the OP1 sequence. For this reason, Raw 264.7 may have a stronger affinity for OP1 and therefore the differentiation effect (as shown by OCs features in **Figure 48**) may be more evident (Berg and Prockop, 1973).

Furthermore, viability of Raw 264.7 cells cultured on the OSCAR modified hydrogels was analysed *via* LIVE/Dead assay. Viability was assessed only at day 3 (day that supposedly the differentiation starts) and at end point (day 7).

As illustrated in **Figure 49**, at day 3, cells were mainly viable with a majority of live cells over dead cells (green vs red). At day 7 of culture, a predominance of live cells was still observed but, interestingly, similarly to what shown in Chapter 2, larger cells (indicated by white arrows) were visible throughout the fields of view.

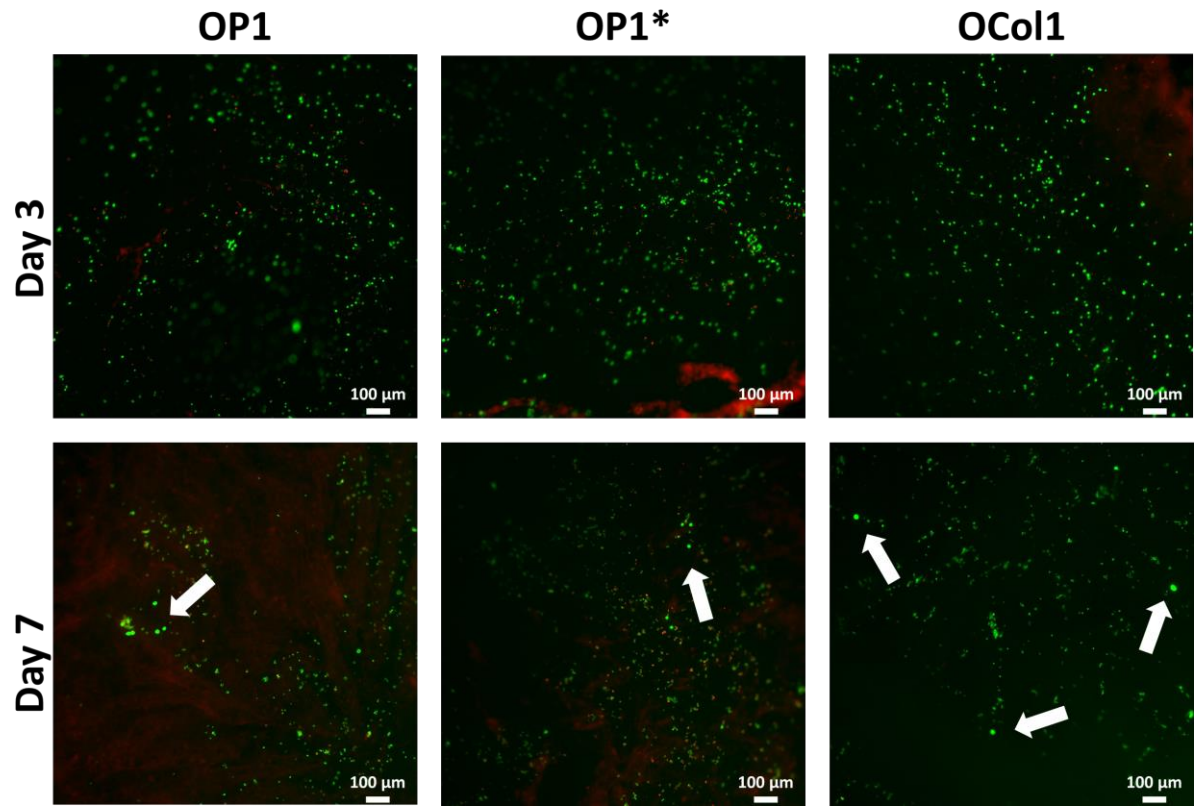

Figure 49 Analysis of viability of Raw 264.7 cells cultured on OSCAR modified Fmoc-FF/S/RGD at day 3 and day 7 using a LIVE/DEAD assay (green: viable cells, calcein AM; red: dead cells, ethidium homodimer-1).

According to this, OSCAR-modified hydrogels were able to maintain cell viability of Raw 264.7 cells over time as well as support the differentiation *in vitro* to mature OCs.

To confirm the gene expression of typical OCs markers as well as the involvement of OSCAR during the osteoclastogenesis of Raw 264.7 cells cultured on the OSCAR-modified hydrogels, qRT-PCR was used. Expression of TRAP and OSCAR was analysed at day 3 and day 7.

As can be seen in **Figure 50**, TRAP expression was significantly higher ($p < 0.001$) at day 7 compared to day 3, when cells were cultured on OP1 and OCol1.

As for OP1*, although cells showed typical OC-like features, TRAP expression at day 7 was not higher than day 3. On the other hand, OSCAR expression was detected, and it was significantly higher for all of the modified hydrogels on day 7 compared to day 3.

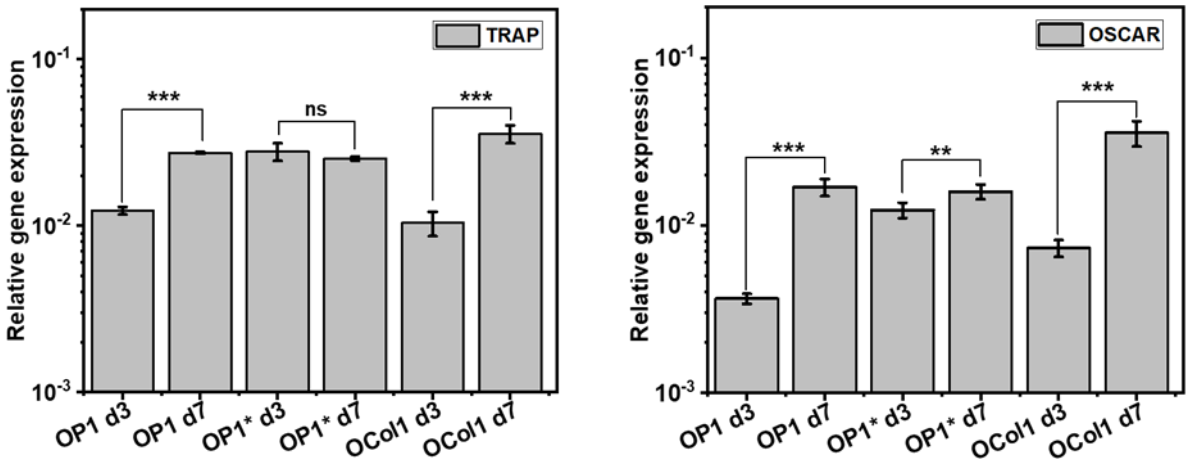

Figure 50 Gene expression of TRAP and OSCAR relative to GAPDH by Raw 264.7 cells (n = 3) after day three (d3) and seven (d7) days cultured on OSCAR-modified hydrogels with different concentration of 10ng/ml of hRANKL. (Data shown as mean ± SD; ∗∗∗p < 0.001; ∗∗p < 0.05).

According to these results, OP1 and OCol-1 incorporated within the Fmoc-FF/S/RGD hydrogel can efficiently bind OSCAR and therefore, after a minimal stimulation with hRANKL (10 ng/ml), Raw 264.7 cells are fully committed to OC, as shown by F-actin staining results and nuclei distribution (**Figure 48A** and **B**). Due to the poorer/ reduced interaction with OP1* (as demonstrated by the SPR results in **Figure 43**), it is reasonable to believe that the signalling pathway is somehow interrupted or becomes hindered when the protein is incorporated into the hydrogels, and it is not free as seen in TCPS results (**Figure 44**). Taking

into consideration the changes in Raw 264.7 cell morphology, the increase of multinucleation, and the increase in expression of the OC-typical marker TRAP/OSCAR it can be concluded that OP1 and OCol-1 have a positive effect when incorporated into the Hap-decorated Fmoc-FF/S/RGD developed in Chapter 2.

4.4 Conclusion

In this chapter, OSCAR-binding collagen peptides have been combined to Fmoc-FF/S/RGD incorporating Hap to test the effect of collagen during the osteoclastogenesis of OCs. In fact, it has been previously demonstrated that collagen can bind OSCAR and act as a costimulatory receptor during the differentiation of OCs *in vitro* (Kim *et al.*, 2002; Barrow *et al.*, 2011; Nedeva *et al.*, 2021). Collagen peptides, presenting the minimum OSCAR binding motif, were designed and characterised in order to be used as potential ligand for this receptor. The protocol described in the third chapter was used to combine OPs with Fmoc-FF/S/RGD.

Here are presented the major finding of this chapter:

- CD characterisation of OP1, OP1* and OCol1 showed that all of the collagen peptides tested presented collagen-like features showing triple helix conformation as well as thermal stability (T_m 37°C, 27°C, 57°C for OP1, OP1* and OCol1, respectively).
- OP1 and OCol1 were stable at RT with a much higher Tm for OCol1 due to the protein being synthesised *via* recombinant techniques and presenting the trimerization domain that helps with higher thermostability (Ghosh *et al.*, 2012a). The lower Tm observed for OP1* could be due to the absence of hydroxyproline in the Col domain, as this has been proven to affect the

overall stability of the collagen triple helix (Berg and Prockop, 1973; Jenkins *et al.*, 2003; Shoulders and Raines, 2009).

- SPR results confirmed the higher affinity of OP1 for OSCAR. In fact, OP1 showed a higher binding affinity to OSCAR compared to OP1* (KD was 2.63 µM vs 19.5 µM).
- Although presenting a lower affinity to OSCAR, OP1* still had a costimulatory effect to Raw 264.7 cell differentiation when cultured on TCPS. In fact, cells seeded on both peptides and treated with different dose of hRANKL (0-100 ng/ml), showed OC-like features and both TRAP and OSCAR expression were observed (as demonstrated by TRAP staining and qPCR results).
- Both OP1, OP1* and OCol1 were used to be incorporated within the Fmoc-FF/S/RGD modified with Hap. Incorporation was successful and showed that the scaffold was able to incorporate OCol1 (as demonstrated by much darker band in SDS-PAGE) as well as retain the hydrogel structure over time.
- When cultured on OPs-modified hydrogels, Raw 264.7 showed improved OC-like features compared to the unmodified scaffolds.
- OP1 and OCol1 showed a greater scaffold improvement (i.e. higher nuclei/cell distribution, increased cell diameter…) although only OP1 was statistically significant.

- OPs were able to support the viability of Raw 264.7 over time. However, only OP1 and OCol1-modified hydrogels caused a significantly higher expression of typical OC markers such as TRAP and OSCAR.

All of these results taken together confirms that the incorporation of OPs to Fmoc-FF/S/RGD SAPH did not have a detrimental effect to the Raw 264.7 but actually the addition of OSCAR-collagen binding peptides promoted an enhanced differentiation of pre-OC towards mature OCs.

Chapter 5 Conclusion and Future work

5.1 Summary and General Conclusions

Peptide-based hydrogels have proven to be an excellent tool to study cell-cell interactions and cell differentiation (Worthington, Pochan and Langhans, 2015; Caliari and Burdick, 2016; MacPherson *et al.*, 2021). Due to their high content of water, tuneable mechanical stiffness, and biocompatibility these biomaterials can mimic the natural ECM offering a more appropriate scaffold to culture cells than TCPS (Li *et al.*, 2019). However, despite the promising results obtained with peptide-based hydrogels, low mechanical strength, long-term stability, viability issues are still challenges that need to be to overcome in order to obtain a suitable scaffold for many TE applications. For these reasons, hydrogels are often combined with nanoparticles (such as minerals) that serve as *nanofillers*, to improve the overall properties of the scaffolds (e.g. enhanced mechanical properties, improved cell adhesion and bioactivity) (Gaharwar, Peppas and Khademhosseini, 2014).

The overall objective of this thesis was to develop new customised hydrogels to culture and differentiate OCs. OCs are the cells responsible for bone resorption and their activity is aberrant in several bone diseases (Teitelbaum, 2000b; Soysa and Alles, 2016). At the same time, whilst the OBs activity has extensively been explored and bone deposition activity is paramount when developing a new

scaffold for BTE, the OCs activity, interaction with biomaterials as well as effective way to culture and differentiate them are often overlooked.

For this reason, in the **Chapter 2**, the main goal was to develop a SAPH able to successfully support OC precursor' viability and differentiation to mature OCs. Following that, the focus of **Chapter 3** was to develop a protocol to successfully incorporate collagen into these SAPH without affecting the "bulk" properties of the resulting scaffolds, whilst providing cell binding motifs. Finally, in **Chapter 4**, the main results of the two previous chapters were combined to develop a collagen-modified hydrogel nanocomposite that incorporated OSCAR-collagen binding peptides to investigate the effect of a potential costimulatory pathway on osteoclastogenesis.

From these studies, the following major findings were reported:

1- Hap nanoparticles were successfully incorporated into an Fmoc-based RGD functionalised SAPH. Hydrogels were homogeneous with increased mechanical properties compared to the undecorated hydrogels;
2- Hap nanoparticles can "decorate" the Fmoc-FF/S/RGD peptide fibres in a repeated pattern;
3- This developed system resembles the typical OC-bone interface: OCs interact with a biomineralised peptide surface in an active way through OC-typical RGD-integrin binding (integrin $\alpha v\beta_3$);

4- Significantly, these Hap-decorated hydrogels support osteoclastogenesis *in vitro* and do not require the presence of inducing factors such as RANKL to generate mature OCs;
5- A new, quick and simple, yet effective protocol of incorporation of collagen proteins into SAPH has been developed. This protocol does not require any prior chemical modification of the proteins and/or the hydrogels.
6- Incorporation of collagen is driven mainly by diffusion and does not affect the "bulk" properties of the composite gels whilst still providing cell binding motifs.
7- OSCAR-collagen binding peptides were successfully incorporated into the Hap-decorated SAPH. OPs were shown to be able to bind OSCAR, to some extent.
8- Of all the constructs tested, OP1-modified hydrogels provided a positive effect on the differentiation of Raw 264.7 cells improving the overall OC-like features of the cells.

5.2 Future work

The work described in this thesis provides the foundation for future lines of research. However, a few questions remained unanswered. Future work would focus on exploring the bone-resorbing activity of the OCs obtained using these scaffolds. In fact, while TRAP staining and gene expression confirmed the actual

differentiation of the Raw 264.7 cells, their ability to resorb bone has not been assessed. A common way of demonstrating this is to culture cells on dentine discs to assess their resorption activity (Marino *et al.*, 2014). These could be embedded in the Hap-decorated scaffolds and cells cultured on them should be able to resorb the dentine discs, once differentiated. This would strengthen the findings of this work suggesting that these scaffolds not only are able to differentiate OCs precursors but that the differentiated cells are indeed functional.

Furthermore, the presence or absence of a ruffled borders should be investigated. In fact, ruffled borders are widely recognised as OCs features as they are only present when OCs are mature and grown on surface that recognise as degradable (e.g. on bone, but not on plastic or glass) (Stenbeck, 2002). Unfortunately, presence of ruffled borders could not be detected just with an F-actin staining (as performed throughout this work) as the ruffled border is located "under" the OC, between the cell and the underlying mineralised surface. However this could be investigated *via* Transmission Electron Microscopy (TEM) on slices of hydrogels on which cells are grown (Holtrop and King, 1977). This could confirm the presence of mature bone-resorbing OCs as they can sense the presence of a biomineralised surface that can be resorbed.

Furthermore, these results could be validated using PBMCs. In fact, testing these hydrogels with primary cells, would provide more physiological (and therefore relevant to the *in vivo* environment) effect.

The work could be also broadened by developing a co-culture system with OBs. In fact, one of the advantages of these Fmoc-hydrogels is that they can be shaped into different settings. Therefore, by using ThinCert well inserts pre-OCs could be seeded on Hap-decorated hydrogels in the upper part of the insert the while OB, sitting at the bottom of the multiwell, would provide the right amount of hRANKL. This would provide several advantages: 1) more reliable mechanism of differentiation as closely mimic the bone microenvironments where OB are releasing hRANKL; 2) interplay between OCs and OBs could be investigated by using this type of settings.

Moreover, recent advantages in immunology provide the opportunity to develop mAb that targets specific antigens (e.g. antibody drug-conjugates, nanobodies…) (Chau, Steeg and Figg, 2019). These can be incorporated within these scaffolds and by providing a slow, controlled released they could affect the differentiation of OCs by blocking the RANKL/RANK pathway, for instance. By doing so, this system could be used to develop more efficient pharmacological treatments to tackle excessive bone degradation, as it occurs in osteoporosis, osteoarthritis, and cancers (Aderibigbe, 2017).

Finally, this improved system could be useful for BTE application, to some extent. In fact, hydrogels could be implanted at the defect site by using minimally invasive surgery and provide support for both OBs and OCs to enable the

interactive process of bone remodelling, ensuring scaffold resorption and new bone formation at the same time.

Chapter 6 References

Aderibigbe, B. (2017) Design and biological evaluation of delivery systems containing bisphosphonates, *Pharmaceutics*. MDPI AG. https://doi.org/10.3390/pharmaceutics9010002.

Agrawal, S. and Srivastava, R. (2020) Osteoinductive and osteoconductive biomaterials, in *Racing for the Surface: Antimicrobial and Interface Tissue Engineering*. Springer International Publishing, pp. 355–395. https://doi.org/10.1007/978-3-030-34471-9_15.

Ahmed, E.M. (2015) Hydrogel: Preparation, characterization, and applications: A review, *Journal of Advanced Research*, 6(2), pp. 105–121. https://doi.org/10.1016/j.jare.2013.07.006.

Alge, C.S. *et al.* (2006) Differential protein profiling of primary versus immortalized human RPE cells identifies expression patterns associated with cytoskeletal remodeling and cell survival, *Journal of Proteome Research*, 5(4), pp. 862–878. https://doi.org/10.1021/pr050420t.

Alnaeeli, M., Penninger, J.M. and Teng, Y.-T.A. (2006) Immune Interactions with CD4+ T Cells Promote the Development of Functional Osteoclasts from Murine CD11c+ Dendritic Cells, *The Journal of Immunology*, 177(5), pp. 3314–3326. https://doi.org/10.4049/jimmunol.177.5.3314.

Amini, A.R., Laurencin, C.T. and Nukavarapu, S.P. (2012) Bone tissue engineering: Recent advances and challenges, *Critical Reviews in Biomedical Engineering*, 40(5), pp. 363–408. https://doi.org/10.1615/CritRevBiomedEng.v40.i5.10.

Andersen, T.L. *et al.* (2004) A scrutiny of matrix metalloproteinases in osteoclasts: Evidence for heterogeneity and for the presence of MMPs synthesized by other cells, *Bone*, 35(5), pp. 1107–1119. https://doi.org/10.1016/j.bone.2004.06.019.

Anderson, D.M. *et al.* (1997) A homologue of the TNF receptor and its ligand enhance T-cell growth and dendritic-cell function, *Nature*, 390(6656), pp. 175–179. https://doi.org/10.1038/36593.

ATCC (2018) *RAW 264.7 (ATCC® TIB-71™), American Type Culture Collection*. Available at: https://www.atcc.org/~/ps/TIB-71.ashx.

Bai, X. *et al.* (2018) Bioactive hydrogels for bone regeneration, *Bioactive Materials*, 3(4), pp. 401–417. https://doi.org/10.1016/j.bioactmat.2018.05.006.

Baillargeon, A.L. and Mequanint, K. (2014) Biodegradable polyphosphazene biomaterials for tissue engineering and delivery of therapeutics, *BioMed Research International*. https://doi.org/10.1155/2014/761373.

Baldwin, P. *et al.* (2019) Autograft, Allograft, and Bone Graft Substitutes: Clinical Evidence and Indications for Use in the Setting of Orthopaedic Trauma Surgery, *Journal of Orthopaedic Trauma*, 33(4), pp. 203–213. https://doi.org/10.1097/BOT.0000000000001420.

Ballanti, P. *et al.* (1997) Tartrate-resistant acid phosphate activity as osteoclastic marker: Sensitivity of cytochemical assessment and serum assay in comparison with standardized osteoclast histomorphometry, *Osteoporosis International*, 7(1), pp. 39–43. https://doi.org/10.1007/BF01623458.

Bar-Shavit, Z. (2007) The osteoclast: A multinucleated, hematopoietic-origin, bone-resorbing osteoimmune cell, *Journal of Cellular Biochemistry*, pp. 1130–1139. https://doi.org/10.1002/jcb.21553.

Barrow, A.D. *et al.* (2011) OSCAR is a collagen receptor that costimulates osteoclastogenesis in DAP12-deficient humans and mice, *Journal of Clinical Investigation*, 121(9), pp. 3505–3516. https://doi.org/10.1172/JCI45913.

Bella, J. (2016) Collagen structure: new tricks from a very old dog, *Biochemical Journal*, 473(8), pp. 1001–1025. https://doi.org/10.1042/BJ20151169.

Benoit, D.S.W. *et al.* (2008) Small functional groups for controlled differentiation of hydrogel-encapsulated human mesenchymal stem cells,

Nature Materials, 7(10), pp. 816–823. https://doi.org/10.1038/nmat2269.
Berg, R.A. and Prockop, D.J. (1973) The thermal transition of a non-hydroxylated form of collagen. Evidence for a role for hydroxyproline in stabilizing the triple-helix of collagen, *Biochemical and Biophysical Research Communications*, 52(1), pp. 115–120. https://doi.org/10.1016/0006-291X(73)90961-3.
Bi, H. *et al.* (2017) Key triggers of osteoclast-related diseases and available strategies for targeted therapies: A review, *Frontiers in Medicine*. Frontiers Media S.A., p. 234. https://doi.org/10.3389/fmed.2017.00234.
BioRender (no date). Available at: https://biorender.com/ (Accessed: 25 July 2022).
Blokhuis, T.J. and Arts, J.J.C. (2011) Bioactive and osteoinductive bone graft substitutes: Definitions, facts and myths, *Injury*, 42(2). https://doi.org/10.1016/j.injury.2011.06.010.
Boateng, S.Y. *et al.* (2005) RGD and YIGSR synthetic peptides facilitate cellular adhesion identical to that of laminin and fibronectin but alter the physiology of neonatal cardiac myocytes, *American Journal of Physiology - Cell Physiology*, 288(1 57-1). https://doi.org/10.1152/ajpcell.00199.2004.
Bonewald, L.F. (2011) The amazing osteocyte, *Journal of Bone and Mineral Research*, 26(2), pp. 229–238. https://doi.org/10.1002/jbmr.320.
Boskey, A.L. (2013) Bone composition: relationship to bone fragility and antiosteoporotic drug effects, *BoneKEy Reports*, 2. https://doi.org/10.1038/bonekey.2013.181.
Botelho, C.M. *et al.* (2006) Differentiation of mononuclear precursors into osteoclasts on the surface of Si-substituted hydroxyapatite, *Journal of Biomedical Materials Research - Part A*, 78(4), pp. 709–720. https://doi.org/10.1002/jbm.a.30726.
Boyce, B.F. and Xing, L. (2007) The RANKL / RANK / OPG Pathway,

Epidemiology and Pathophysiology Accessory, 5, pp. 98–104.
Boydston, J.A. *et al.* (2005) Orientation within the exosporium and structural stability of the collagen-like glycoprotein BclA of Bacillus anthracis, *Journal of Bacteriology*, 187(15), pp. 5310–5317. https://doi.org/10.1128/JB.187.15.5310-5317.2005.
Boyle, W.J., Simonet, W.S. and Lacey, D.L. (2003) Osteoclast differentiation and activation, *Nature*, 423(6937), pp. 337–342. https://doi.org/10.1038/nature01658.
Brinckmann, J. (2005) Collagens at a glance, *Topics in Current Chemistry*, pp. 1–6. https://doi.org/10.1007/b103817.
Brodsky, B. and Kaplan, D.L. (2013) Shining light on collagen: Expressing collagen in plants, *Tissue Engineering - Part A*, 19(13–14), pp. 1499–1501. https://doi.org/10.1089/ten.tea.2013.0137.
Brodsky, O. and Cronin, C.N. (2006) Economical parallel protein expression screening and scale-up in Escherichia coli, *Journal of Structural and Functional Genomics*, 7(2), pp. 101–108. https://doi.org/10.1007/s10969-006-9013-0.
Caliari, S.R. and Burdick, J.A. (2016) *A practical guide to hydrogels for cell culture*, *Nature Methods*. https://doi.org/10.1038/nmeth.3839.
Cancer Research UK (2020) *Treatment for secondary bone cancer*. Available at: https://www.cancerresearchuk.org/about-cancer/secondary-cancer/secondary-bone-cancer/treatment (Accessed: 25 February 2022).
Capito, R.M. *et al.* (2008) Self-assembly of large and small molecules into hierarchically ordered sacs and membranes, *Science*, 319(5871), pp. 1812–1816. https://doi.org/10.1126/science.1154586.
Capulli, M., Paone, R. and Rucci, N. (2014) Osteoblast and osteocyte: Games without frontiers, *Archives of Biochemistry and Biophysics*, pp. 3–12. https://doi.org/10.1016/j.abb.2014.05.003.
Castillo, L.M., Guerrero, C.A. and Acosta, O. (2017) Expression of typical

osteoclast markers by PBMCs after PEG-induced fusion as a model for studying osteoclast differentiation, *Journal of Molecular Histology*, 48(3), pp. 169–185. https://doi.org/10.1007/s10735-017-9717-4.

Cenci, S. *et al.* (2000) Estrogen deficiency induces bone loss by enhancing T-cell production of TNF-α, *Journal of Clinical Investigation*, 106(10), pp. 1229–1237. https://doi.org/10.1172/JCI11066.

Chambers, T.J. *et al.* (1984) Resorption of bone by isolated rabbit osteoclasts, *Journal of Cell Science*, VOL. 66, pp. 383–399. https://doi.org/10.1242/jcs.66.1.383.

Chau, C.H., Steeg, P.S. and Figg, W.D. (2019) Antibody–drug conjugates for cancer, *The Lancet*. Lancet Publishing Group, pp. 793–804. https://doi.org/10.1016/S0140-6736(19)31774-X.

Chen, F. *et al.* (2019) Effects of hydroxyapatite surface nano/micro-structure on osteoclast formation and activity, *Journal of Materials Chemistry B*, 7(47), pp. 7574–7587. https://doi.org/10.1039/c9tb01204d.

Chiesa, I. *et al.* (2020) Modeling the Three-Dimensional Bioprinting Process of β-Sheet Self-Assembling Peptide Hydrogel Scaffolds, *Frontiers in Medical Technology*, 2, p. 4. https://doi.org/10.3389/fmedt.2020.571626.

Chiu, L.H. *et al.* (2011) Differential effect of ECM molecules on re-expression of cartilaginous markers in near quiescent human chondrocytes, *Journal of Cellular Physiology*, 226(8), pp. 1981–1988. https://doi.org/10.1002/jcp.22530.

Ciapetti, G. *et al.* (2017) Osteoclast differentiation from human blood precursors on biomimetic calcium-phosphate substrates, *Acta Biomaterialia*, 50, pp. 102–113. https://doi.org/10.1016/j.actbio.2016.12.013.

Collin-Osdoby, P. and Osdoby, P. (2012) RANKL-Mediated Osteoclast Formation from Murine RAW 264.7 cells, in *Bone Research Protocols*. Totowa, NJ: Humana Press, pp. 187–202.

Copp, D.H. and Shim, S.S. (1963) The homeostatic function of bone as a

mineral reservoir, *Oral Surgery, Oral Medicine, Oral Pathology*, 16(6), pp. 738–744. https://doi.org/10.1016/0030-4220(63)90081-1.
Costa, D.O. *et al.* (2013) The differential regulation of osteoblast and osteoclast activity bysurface topography of hydroxyapatite coatings, *Biomaterials*, 34(30), pp. 7215–7226. https://doi.org/10.1016/j.biomaterials.2013.06.014.
Crockett, J.C. *et al.* (2011) New knowledge on critical osteoclast formation and activation pathways from study of rare genetic diseases of osteoclasts: Focus on the RANK/RANKL axis, *Osteoporosis International*. Springer, pp. 1–20. https://doi.org/10.1007/s00198-010-1272-8.
Currey, J.D. (2003) How well are bones designed to resist fracture?, *Journal of Bone and Mineral Research*, pp. 591–598. https://doi.org/10.1359/jbmr.2003.18.4.591.
D'Amelio, P. *et al.* (2008) Estrogen deficiency increases osteoclastogenesis up-regulating T cells activity: A key mechanism in osteoporosis, *Bone*, 43(1), pp. 92–100. https://doi.org/10.1016/j.bone.2008.02.017.
Davis, M.E. *et al.* (2005) Injectable self-assembling peptide nanofibers create intramyocardial microenvironments for endothelial cells, *Circulation*, 111(4), pp. 442–450. https://doi.org/10.1161/01.CIR.0000153847.47301.80.
Delloye, C. *et al.* (2007) Bone allografts. What they can offer and what they cannot, *Journal of Bone and Joint Surgery - Series B*. J Bone Joint Surg Br, pp. 574–579. https://doi.org/10.1302/0301-620X.89B5.19039.
Detsch, R. and Boccaccini, A.R. (2015) The role of osteoclasts in bone tissue engineering, *Journal of Tissue Engineering and Regenerative Medicine*. John Wiley and Sons Ltd, pp. 1133–1149. https://doi.org/10.1002/term.1851.
Detsch, R., Mayr, H. and Ziegler, G. (2008) Formation of osteoclast-like cells on HA and TCP ceramics, *Acta Biomaterialia*, 4(1), pp. 139–148. https://doi.org/10.1016/j.actbio.2007.03.014.
Diaferia, C., Morelli, G. and Accardo, A. (2019) Fmoc-diphenylalanine as a

suitable building block for the preparation of hybrid materials and their potential applications, *Journal of Materials Chemistry B*, 7(34), pp. 5142–5155. https://doi.org/10.1039/c9tb01043b.

Dimitriou, R. *et al.* (2011) Bone regeneration: Current concepts and future directions, *BMC Medicine*. BMC Med. https://doi.org/10.1186/1741-7015-9-66.

Disser, N.P. *et al.* (2020) Musculoskeletal Consequences of COVID-19, *Journal of Bone and Joint Surgery - American Volume*. Lippincott Williams and Wilkins, pp. 1197–1204. https://doi.org/10.2106/JBJS.20.00847.

Dosier, C.R. *et al.* (2015) Effect of cell origin and timing of delivery for stem cell-based bone tissue engineering using biologically functionalized hydrogels, *Tissue Engineering - Part A*, 21(1–2), pp. 156–165. https://doi.org/10.1089/ten.tea.2014.0057.

Doyle, M.E. and Jan de Beur, S.M. (2008) The skeleton: Endocrine regulator of phosphate homeostasis, *Current Osteoporosis Reports*. Springer, pp. 134–141. https://doi.org/10.1007/s11914-008-0024-6.

Drury, J.L. and Mooney, D.J. (2003) Hydrogels for tissue engineering: Scaffold design variables and applications, *Biomaterials*, pp. 4337–4351. https://doi.org/10.1016/S0142-9612(03)00340-5.

Drzewiecki, K.E. *et al.* (2016) Circular Dichroism Spectroscopy of Collagen Fibrillogenesis: A New Use for an Old Technique, *Biophysical Journal*, 111(11), pp. 2377–2386. https://doi.org/10.1016/j.bpj.2016.10.023.

Elsdale, T. and Bard, J. (1972) Collagen substrata for studies on cell behavior, *Journal of Cell Biology*, 54(3), pp. 626–637. https://doi.org/10.1083/jcb.54.3.626.

Von Euw, S. *et al.* (2019) Bone mineral: new insights into its chemical composition, *Scientific Reports*, 9(1), pp. 1–11. https://doi.org/10.1038/s41598-019-44620-6.

Farndale, S.H. and R.W. (2014) Integrin Recognition Motifs in the Human

Collagens, *I Domain Integrins*, 819(800), pp. 41–60. https://doi.org/10.1007/978-94-017-9153-3.

Fatouros, D.G. *et al.* (2014) Lipid-like self-assembling peptide nanovesicles for drug delivery, *ACS Applied Materials and Interfaces*, 6(11), pp. 8184–8189. https://doi.org/10.1021/am501673x.

Felding-Habermann, B. and Cheresh, D.A. (1993) Vitronectin and its receptors, *Current Opinion in Cell Biology*, 5(5), pp. 864–868. https://doi.org/10.1016/0955-0674(93)90036-P.

Feng, X. (2009) Chemical and Biochemical Basis of Cell-Bone Matrix Interaction in Health and Disease, *Current Chemical Biology*, 3(2), pp. 189–196. https://doi.org/10.2174/187231309788166398.

Ferguson, J.L. and Turner, S.P. (2018) Bone cancer: Diagnosis and treatment principles, *American Family Physician*, 98(4), pp. 205–213.

Findlay, D.M. and Atkins, G.J. (2011) Relationship between serum RANKL and RANKL in bone, *Osteoporosis International*, 22(10), pp. 2597–2602. https://doi.org/10.1007/s00198-011-1740-9.

Florencio-Silva, R. *et al.* (2015) Biology of Bone Tissue: Structure, Function, and Factors That Influence Bone Cells, *BioMed Research International*. Hindawi Publishing Corporation. https://doi.org/10.1155/2015/421746.

Gaharwar, A.K., Peppas, N.A. and Khademhosseini, A. (2014) Nanocomposite hydrogels for biomedical applications, *Biotechnology and Bioengineering*, 111(3), pp. 441–453. https://doi.org/10.1002/bit.25160.

Gazit, M.R. and E. (2009) Casting Metal Nanowires Within Discrete Self-Assembled Peptide Nanotubes.pdf, *J. Chem. Phys*. JAI Press, p. 3.

Ghosh, K. *et al.* (2007) Cell adaptation to a physiologically relevant ECM mimic with different viscoelastic properties, *Biomaterials*, 28(4), pp. 671–679. https://doi.org/10.1016/j.biomaterials.2006.09.038.

Ghosh, M. *et al.* (2017a) Arginine-Presenting Peptide Hydrogels Decorated

with Hydroxyapatite as Biomimetic Scaffolds for Bone Regeneration, *Biomacromolecules*, 18(11), pp. 3541–3550. https://doi.org/10.1021/acs.biomac.7b00876.
Ghosh, M. *et al.* (2017b) Arginine-Presenting Peptide Hydrogels Decorated with Hydroxyapatite as Biomimetic Scaffolds for Bone Regeneration, *Biomacromolecules*, 18(11), pp. 3541–3550. https://doi.org/10.1021/acs.biomac.7b00876.
Ghosh, M. *et al.* (2019) Injectable alginate-peptide composite Hydrogel as a scaffold for bone tissue regeneration, *Nanomaterials*, 9(4). https://doi.org/10.3390/nano9040497.
Ghosh, N. *et al.* (2012a) Collagen-like proteins in pathogenic E. coli strains, *PLoS ONE*, 7(6). https://doi.org/10.1371/journal.pone.0037872.
Ghosh, N. *et al.* (2012b) Collagen-like proteins in pathogenic E. coli strains, *PLoS ONE*, 7(6), pp. 1–5. https://doi.org/10.1371/journal.pone.0037872.
Gkioni, K. *et al.* (2010) Mineralization of hydrogels for bone regeneration, *Tissue Engineering - Part B: Reviews*, 16(6), pp. 577–585. https://doi.org/10.1089/ten.teb.2010.0462.
Gordon, M.K. and Hahn, R.A. (2010) Collagens, *Cell and Tissue Research*. Cell Tissue Res, pp. 247–257. https://doi.org/10.1007/s00441-009-0844-4.
Green, H. *et al.* (2018) RGD-presenting peptides in amphiphilic and anionic β-sheet hydrogels for improved interactions with cells, *RSC Advances*, 8(18), pp. 10072–10080. https://doi.org/10.1039/c7ra12503h.
Greenfield, Norma J (2007) Analysis of the kinetics of folding of proteins and peptides using circular dichroism, *Nature Protocols*, 1(6), pp. 2891–2899. https://doi.org/10.1038/nprot.2006.244.
Greenfield, Norma J. (2007) Using circular dichroism spectra to estimate protein secondary structure, *Nature Protocols*, 1(6), pp. 2876–2890. https://doi.org/10.1038/nprot.2006.202.

Guler, M.O. *et al.* (2006) Presentation of RGDS epitopes on self-assembled nanofibers of branched peptide amphiphiles, *Biomacromolecules*, 7(6), pp. 1855–1863. https://doi.org/10.1021/bm060161g.

Gulsen, D. and Chauhan, A. (2005) Dispersion of microemulsion drops in HEMA hydrogel: A potential ophthalmic drug delivery vehicle, *International Journal of Pharmaceutics*, 292(1–2), pp. 95–117. https://doi.org/10.1016/j.ijpharm.2004.11.033.

Hale, L. V, Ma, Y.F. and Santerre, R.F. (2000) Semi-quantitative fluorescence analysis of calcein binding as a measurement of in vitro mineralization, *Calcified Tissue International*, 67(1), pp. 80–84. https://doi.org/10.1007/s00223001101.

Hanada, R. *et al.* (2011) RANKL/RANK-beyond bones, *Journal of Molecular Medicine*, 89(7), pp. 647–656. https://doi.org/10.1007/s00109-011-0749-z.

Haraguchi, K. and Takehisa, T. (2002) Nanocomposite hydrogels: A unique organic-inorganic network structure with extraordinary mechanical, optical, and swelling/De-swelling properties, *Advanced Materials*, 14(16), pp. 1120–1124. https://doi.org/10.1002/1521-4095(20020816)14:16<1120::AID-ADMA1120>3.0.CO;2-9.

Hayman, A. (2008) Tartrate-resistant acid phosphatase (TRAP) and the osteoclast/immune cell dichotomy, *Autoimmunity*, 41(3), pp. 218–223. https://doi.org/10.1080/08916930701694667.

Haywood, J. *et al.* (2016) Structural basis of collagen recognition by human osteoclast-associated receptor and design of osteoclastogenesis inhibitors, *Proceedings of the National Academy of Sciences*, 113(4), pp. 1038–1043. https://doi.org/10.1073/pnas.1522572113.

Helfrich, M.H. (2005) Osteoclast diseases and dental abnormalities, *Archives of Oral Biology*, 50, pp. 115–122. https://doi.org/10.1016/j.archoralbio.2004.11.016.

Hellmund, K.S. and Koksch, B. (2019) Self-assembling peptides as extracellular matrix mimics to influence stem cell's fate, *Frontiers in Chemistry*. Front Chem. https://doi.org/10.3389/fchem.2019.00172.
Holster, T. *et al.* (2007) Loss of assembly of the main basement membrane collagen, type IV, but not fibril-forming collagens and embryonic death in collagen prolyl 4-hydroxylase i null mice, *Journal of Biological Chemistry*, 282(4), pp. 2512–2519. https://doi.org/10.1074/jbc.M606608200.
Holtrop, M.E. and King, G.J. (1977) The ultrastructure of the osteoclast and its functional implications., *Clinical orthopaedics and related research*, 123(123), pp. 177–196. https://doi.org/10.1097/00003086-197703000-00062.
Hu, J. *et al.* (2016) A detailed study of homogeneous agarose/hydroxyapatite nanocomposites for load-bearing bone tissue, *International Journal of Biological Macromolecules*, 82, pp. 134–143. https://doi.org/10.1016/j.ijbiomac.2015.09.077.
Hu, Y. *et al.* (2017) Biomimetic mineralized hierarchical hybrid scaffolds based on in situ synthesis of nano-hydroxyapatite/chitosan/chondroitin sulfate/hyaluronic acid for bone tissue engineering, *Colloids and Surfaces B: Biointerfaces*, 157, pp. 93–100. https://doi.org/10.1016/j.colsurfb.2017.05.059.
Huang, L.K. and Wang, M.J.J. (1995) Image thresholding by minimizing the measures of fuzziness, *Pattern Recognition*, 28(1), pp. 41–51. https://doi.org/10.1016/0031-3203(94)E0043-K.
Hulley, P.A., Papadimitriou-Olivgeri, I. and Knowles, H.J. (2020) Osteoblast–Osteoclast Coculture Amplifies Inhibitory Effects of FG-4592 on Human Osteoclastogenesis and Reduces Bone Resorption, *JBMR Plus*, 4(7), p. e10370. https://doi.org/10.1002/jbm4.10370.
Humphrey, M.B. and Nakamura, M.C. (2016) A Comprehensive Review of Immunoreceptor Regulation of Osteoclasts, *Clinical Reviews in Allergy and Immunology*. Humana Press Inc., pp. 48–58. https://doi.org/10.1007/s12016-

015-8521-8.
Humphries, M.J. (1998) Cell-Substrate adhesion assay, *Current protocols in Cell Biology*, 9.1.1, pp. 9.1.1-9.1.11. https://doi.org/10.1007/978-1-59745-413-1_14.
Lo Iacono, N. *et al.* (2012) Osteopetrosis rescue upon RANKL administration to Rankl-/-mice: A new therapy for human RANKL-dependent ARO, *Journal of Bone and Mineral Research*, 27(12), pp. 2501–2510. https://doi.org/10.1002/jbmr.1712.
Imere, A. *et al.* (2021) Engineering a cell-hydrogel-fibre composite to mimic the structure and function of the tendon synovial sheath, *Acta Biomaterialia*, 119, pp. 140–154. https://doi.org/10.1016/j.actbio.2020.11.017.
Inaoka, T. *et al.* (1995) Molecular cloning of human cDNA for cathepsin K: Novel cysteine proteinase predominantly expressed in bone, *Biochemical and Biophysical Research Communications*, pp. 89–96.
Ingber, D.E. (2006) Cellular mechanotransduction: putting all the pieces together again, *The FASEB Journal*, 20(7), pp. 811–827. https://doi.org/10.1096/fj.05-5424rev.
Inostroza-Brito, K.E. *et al.* (2015) Co-Assembly, spatiotemporal control and morphogenesis of a hybrid protein-peptide system, *Nature Chemistry*, 7(11), pp. 897–904. https://doi.org/10.1038/nchem.2349.
Jacome-Galarza, C.E. *et al.* (2019) Developmental origin, functional maintenance and genetic rescue of osteoclasts, *Nature*, 568(7753), pp. 541–545. https://doi.org/10.1038/s41586-019-1105-7.
Jain, R. and Roy, S. (2020) Controlling Neuronal Cell Growth through Composite Laminin Supramolecular Hydrogels, *ACS Biomaterials Science and Engineering*, 6(5), pp. 2832–2846. https://doi.org/10.1021/acsbiomaterials.9b01998.
Jayawarna, Vineetha *et al.* (2006) Nanostructured hydrogels for three-

dimensional cell culture through self-assembly of fluorenylmethoxycarbonyl-dipeptides, *Advanced Materials*, 18(5), pp. 611–614. https://doi.org/10.1002/adma.200501522.
Jayawarna, V. *et al.* (2006) Nanostructured Hydrogels for Three-Dimensional Cell Culture Through Self-Assembly of Fluorenylmethoxycarbonyl–Dipeptides, *Advanced Materials*, 18(5), pp. 611–614. https://doi.org/10.1002/adma.200501522.
Jayawarna, V. *et al.* (2009) Introducing chemical functionality in Fmoc-peptide gels for cell culture, *Acta Biomaterialia*, 5(3), pp. 934–943. https://doi.org/10.1016/j.actbio.2009.01.006.
Jenkins, C.L. *et al.* (2003) Effect of 3-hydroxyproline residues on collagen stability, *Journal of the American Chemical Society*, 125(21), pp. 6422–6427. https://doi.org/10.1021/ja034015j.
Jeong, J. *et al.* (2019) Bioactive calcium phosphate materials and applications in bone regeneration, *Biomaterials Research*. BioMed Central, pp. 1–11. https://doi.org/10.1186/s40824-018-0149-3.
Jonsson, U. *et al.* (1991) Real-time biospecific interaction analysis using surface plasmon resonance and a sensor chip technology, *BioTechniques*, 11(5).
Kajiya, H. (2012) Calcium signaling in osteoclast differentiation and bone resorption, *Advances in Experimental Medicine and Biology*, 740, pp. 917–932. https://doi.org/10.1007/978-94-007-2888-2_41.
Kattimani, V.S., Kondaka, S. and Lingamaneni, K.P. (2016) Hydroxyapatite–-Past, Present, and Future in Bone Regeneration, *Bone and Tissue Regeneration Insights*, 7, p. BTRI.S36138. https://doi.org/10.4137/btri.s36138.
Kelly, S. and Price, N. (2005) The Use of Circular Dichroism in the Investigation of Protein Structure and Function, *Current Protein & Peptide Science*, 1(4), pp. 349–384. https://doi.org/10.2174/1389203003381315.
Kenkre, J.S. and Bassett, J.H.D. (2018) The bone remodelling cycle, *Annals of*

Clinical Biochemistry. SAGE Publications Ltd, pp. 308–327. https://doi.org/10.1177/0004563218759371.

Khan, R. and Khan, M.H. (2013) Use of collagen as a biomaterial: An update, *Journal of Indian Society of Periodontology*, 17(4), pp. 539–542. https://doi.org/10.4103/0972-124X.118333.

Kim, J.H. and Kim, N. (2016) Signaling Pathways in Osteoclast Differentiation, *Chonnam Medical Journal*, 52(1), p. 12. https://doi.org/10.4068/cmj.2016.52.1.12.

Kim, N. *et al.* (2002) A Novel Member of the Leukocyte Receptor Complex Regulates Osteoclast Differentiation, *The Journal of Experimental Medicine*, 195(2), pp. 201–209. https://doi.org/10.1084/jem.20011681.

Kisiday, J. *et al.* (2002) Self-assembling peptide hydrogel fosters chondrocyte extracellular matrix production and cell division: Implications for cartilage tissue repair, *Proceedings of the National Academy of Sciences*, 99(15), pp. 9996–10001. https://doi.org/10.1073/pnas.142309999.

Knight, C.G. *et al.* (1998) Identification in collagen type I of an integrin α2β1-binding site containing an essential GER sequence, *Journal of Biological Chemistry*, 273(50), pp. 33287–33294. https://doi.org/10.1074/jbc.273.50.33287.

Knight, C.G. *et al.* (2000) The collagen-binding a-domains of integrins α1/β1 and α2/β1 recognize the same specific amino acid sequence, GFOGER, in native (triple- helical) collagens, *Journal of Biological Chemistry*, 275(1), pp. 35–40. https://doi.org/10.1074/jbc.275.1.35.

Koga, T. *et al.* (2004) Costimulatory signals mediated by the ITAM motif cooperate with RANKL for bone homeostasis, *Nature*, 428(6984), pp. 758–763. https://doi.org/10.1038/nature02444.

Kölliker, A. von (1873) *Die normale Resorption des Knochengewebes und ihre Bedeutung für die Entstehung der typischen Knochenformen*. Edited by Voger.

Available at: http://archive.org/details/b22392610.
Koutsopoulos, S. *et al.* (2009) Controlled release of functional proteins through designer self-assembling peptide nanofiber hydrogel scaffold, *Proceedings of the National Academy of Sciences of the United States of America*, 106(12), pp. 4623–4628. https://doi.org/10.1073/pnas.0807506106.
Kovacs, E.J. (2001) *Wheater's Functional Histology: A Text and Colour Atlas*, *Archives of Pathology & Laboratory Medicine*. https://doi.org/10.5858/2001-125-708b-wfhata.
Kwon, T. and Sung, B.J. (2018) Effects of nanoparticles on the stability of polymer fibers, *Physical Review E*, 98(4), pp. 1–9. https://doi.org/10.1103/PhysRevE.98.042503.
Lakkakorpi, P.T. *et al.* (1991) Vitronectin receptor has a role in bone resorption but does not mediate tight sealing zone attachment of osteoclasts to the bone surface, *Journal of Cell Biology*, 115(4), pp. 1179–1186. https://doi.org/10.1083/jcb.115.4.1179.
Lakkakorpi, P.T. and Väänänen, K.H. (1991) Kinetics of the osteoclast cytoskeleton during the resorption cycle in vitro, *Journal of Bone and Mineral Research*, 6(8), pp. 817–826. https://doi.org/10.1002/jbmr.5650060806.
Lau, H.K. and Kiick, K.L. (2015) Opportunities for multicomponent hybrid hydrogels in biomedical applications, *Biomacromolecules*, 16(1), pp. 28–42. https://doi.org/10.1021/bm501361c.
Laurencin, C., Khan, Y. and El-Amin, S.F. (2006) Bone graft substitutes, *Expert Review of Medical Devices*. Expert Rev Med Devices, pp. 49–57. https://doi.org/10.1586/17434440.3.1.49.
Lee, K.Y. and Mooney, D.J. (2001) Hydrogels for tissue engineering, *Chemical Reviews*, pp. 1869–1879. https://doi.org/10.1021/cr000108x.
Li, J. *et al.* (2019) Recent advances of self-assembling peptide-based hydrogels for biomedical applications, *Soft Matter*. The Royal Society of Chemistry, pp.

1704–1715. https://doi.org/10.1039/C8SM02573H.
Li, X. *et al.* (2013) Nanostructured scaffolds for bone tissue engineering, *Journal of Biomedical Materials Research*, 101 A(8), pp. 2424–2435. https://doi.org/10.1002/jbm.a.34539.
Ligorio, C. *et al.* (2021) TGF-β3-loaded graphene oxide - self-assembling peptide hybrid hydrogels as functional 3D scaffolds for the regeneration of the nucleus pulposus, *Acta Biomaterialia*, 127, pp. 116–130. https://doi.org/10.1016/j.actbio.2021.03.077.
Lin, C.C. and Anseth, K.S. (2009) PEG hydrogels for the controlled release of biomolecules in regenerative medicine, *Pharmaceutical Research*. Pharm Res, pp. 631–643. https://doi.org/10.1007/s11095-008-9801-2.
Lindsey, W.H. *et al.* (1996) Nasal reconstruction using an osteoconductive collagen gel matrix, *Archives of Otolaryngology - Head and Neck Surgery*, 122(1), pp. 37–40. https://doi.org/10.1001/archotol.1996.01890130031004.
Ljusberg, J. *et al.* (2005) Proteolytic excision of a repressive loop domain in tartrate-resistant acid phosphatase by cathepsin K in osteoclasts, *Journal of Biological Chemistry*, 280(31), pp. 28370–28381. https://doi.org/10.1074/jbc.M502469200.
Lu, D. *et al.* (2018) LRP1 Suppresses Bone Resorption in Mice by Inhibiting the RANKL-Stimulated NF-κB and p38 Pathways During Osteoclastogenesis, *Journal of Bone and Mineral Research*, 33(10), pp. 1773–1784. https://doi.org/10.1002/jbmr.3469.
Luo, T. *et al.* (2022) A Review on the Design of Hydrogels With Different Stiffness and Their Effects on Tissue Repair, *Frontiers in Bioengineering and Biotechnology*. Frontiers Media S.A., p. 39. https://doi.org/10.3389/fbioe.2022.817391.
Luxenburg, C. *et al.* (2007) The architecture of the adhesive apparatus of cultured osteoclasts: From podosome formation to sealing zone assembly, *PLoS*

ONE. Edited by N. Cordes, 2(1), p. e179. https://doi.org/10.1371/journal.pone.0000179.

Ma, X. *et al.* (2016) Preparation of collagen/hydroxyapatite/alendronate hybrid hydrogels as potential scaffolds for bone regeneration, *Colloids and Surfaces B: Biointerfaces*, 143, pp. 81–87. https://doi.org/10.1016/j.colsurfb.2016.03.025.

MacPherson, D. *et al.* (2021) Peptide-based scaffolds for the culture and maintenance of primary human hepatocytes, *Scientific Reports*, 11(1), p. 6772. https://doi.org/10.1038/s41598-021-86016-5.

Maia, F.R. *et al.* (2018) Differentiation of osteoclast precursors on gellan gum-based spongy-like hydrogels for bone tissue engineering, *Biomedical Materials*, 13(3). https://doi.org/10.1088/1748-605X/aaaf29.

Manias, E. (2007) Nanocomposites: Stiffer by design, *Nature Materials*, pp. 9–11. https://doi.org/10.1038/nmat1812.

Manolagas, S.C. (2000) Birth and Death of Bone Cells: Basic Regulatory Mechanisms and Implications for the Pathogenesis and Treatment of Osteoporosis, *Endocrine Reviews*, 21(2), pp. 115–137. https://doi.org/10.1210/edrv.21.2.0395.

Marino, S. *et al.* (2014) Generation and culture of osteoclasts, *BoneKEy Reports*, 3, pp. 1–9. https://doi.org/10.1038/bonekey.2014.65.

Markey, A. *et al.* (2017) Peptide hydrogel in vitro non-inflammatory potential, in *Journal of Peptide Science*. J Pept Sci, pp. 148–154. https://doi.org/10.1002/psc.2940.

Mart, R.J. *et al.* (2006) Peptide-based stimuli-responsive biomaterials, *Soft Matter*, 2(10), pp. 822–835. https://doi.org/10.1039/b607706d.

McDonald, M.M. *et al.* (2021) Osteoclasts recycle via osteomorphs during RANKL-stimulated bone resorption, *Cell*, 184(5), pp. 1330-1347.e13. https://doi.org/10.1016/j.cell.2021.02.002.

Moroi, A. *et al.* (2022) Effects of ultraviolet irradiation on beta-tricalcium

phosphate as a bone graft substitute, *Odontology*, 1, pp. 1–15. https://doi.org/10.1007/s10266-022-00704-w.
Muscle and Bone Diseases | NIAMS (no date). Available at: https://www.niams.nih.gov/health-topics/muscle-bone-diseases.
Nagai, Y. *et al.* (2006) Slow release of molecules in self-assembling peptide nanofiber scaffold, *Journal of Controlled Release*, 115(1), pp. 18–25. https://doi.org/10.1016/j.jconrel.2006.06.031.
Nagase H, Visse R, M.G. (2006) Structure and function of matrix metalloproteinases and TIMPs, *Cardiovascular Research*, 69(3), pp. 562–573. https://doi.org/10.1016/j.cardiores.2005.12.002.
Nakagawa, N. *et al.* (1998) RANK is the essential signaling receptor for osteoclast differentiation factor in osteoclastogenesis, *Biochemical and Biophysical Research Communications*, 253(2), pp. 395–400. https://doi.org/10.1006/bbrc.1998.9788.
Narducci, P. and Nicolin, V. (2009) Differentiation of activated monocytes into osteoclast-like cells on a hydroxyapatite substrate: An in vitro study, *Annals of Anatomy - Anatomischer Anzeiger*, 191(4), pp. 349–355. https://doi.org/10.1016/j.aanat.2009.02.009.
Nedeva, I.R. *et al.* (2021) Role of OSCAR Signaling in Osteoclastogenesis and Bone Disease, *Frontiers in Cell and Developmental Biology*. Frontiers Media S.A., p. 641162. https://doi.org/10.3389/fcell.2021.641162.
NHS (2019) Osteoporosis - NHS, *NHS website*, p. 1. Available at: https://www.nhs.uk/conditions/osteoporosis/ (Accessed: 25 February 2022).
Nijweide, P.J., Burger, E.H. and Feyen, J.H.M. (1986) Physiological Reviews Cells of Bone: Proliferation, Differentiation, and Hormonal Regulation, *The American Physiological Society*, (4)66. Available at: www.physiology.org/journal/physrev (Accessed: 19 October 2018).
Novack, D.V. and Mbalaviele, G. (2016) Osteoclasts—Key Players in Skeletal

Health and Disease, *Microbiology Spectrum*. Edited by S. Gordon, 4(3). https://doi.org/10.1128/microbiolspec.mchd-0011-2015.
O'Keefe, R.J. and Mao, J. (2011) Bone tissue engineering and regeneration: From discovery to the clinic-an overview, *Tissue Engineering - Part B: Reviews*. Mary Ann Liebert, Inc., pp. 389–392. https://doi.org/10.1089/ten.teb.2011.0475.
Ono, T. and Nakashima, T. (2018) Recent advances in osteoclast biology, *Histochemistry and Cell Biology*, 149, pp. 325–341. https://doi.org/10.1007/s00418-018-1636-2.
OriginLab - Origin and OriginPro - Data Analysis and Graphing Software (no date). Available at: http://www.originlab.com/.
Pan, C. *et al.* (2009) Comparative Proteomic Phenotyping of Cell Lines and Primary Cells to Assess Preservation of Cell Type-specific Functions, *Molecular & Cellular Proteomics*, 8(3), pp. 443–450. https://doi.org/10.1074/mcp.m800258-mcp200.
Park, J.H., Lee, N.K. and Lee, S.Y. (2017) Current understanding of RANK signaling in osteoclast differentiation and maturation, *Molecules and Cells*, pp. 706–713. https://doi.org/10.14348/molcells.2017.0225.
Patterson, J. *et al.* (2010) Hyaluronic acid hydrogels with controlled degradation properties for oriented bone regeneration, *Biomaterials*, 31(26), pp. 6772–6781. https://doi.org/10.1016/j.biomaterials.2010.05.047.
Peppas, Nicholas A. *et al.* (2006) Hydrogels in biology and medicine: From molecular principles to bionanotechnology, *Advanced Materials*. John Wiley & Sons, Ltd, pp. 1345–1360. https://doi.org/10.1002/adma.200501612.
Peppas, N. A. *et al.* (2006) Hydrogels in Biology and Medicine: From Molecular Principles to Bionanotechnology, *Advanced Materials*, 18(11), pp. 1345–1360. https://doi.org/10.1002/adma.200501612.
Petite, H. *et al.* (2000) Tissue-engineered bone regeneration, *Nature*

Biotechnology, 18, pp. 959–963.
Phan, T.C.A., Xu, J. and Zheng, M.H. (2004) Interaction between osteoblast and osteoclast: impact in bone disease, *Histology and Histopathology*, 19, pp. 1325–1344.
Pierce, A.M., Lindskog, S. and Hammarström, L. (1991) Osteoclasts: Structure and function, *Electron Microscopy Reviews*. Pergamon, pp. 1–45. https://doi.org/10.1016/0892-0354(91)90015-5.
ProteoGenix (no date). Available at: https://www.proteogenix.science/.
Qi, Y. *et al.* (2018) Injectable Hexapeptide Hydrogel for Localized Chemotherapy Prevents Breast Cancer Recurrence, *ACS Applied Materials and Interfaces*, 10(8), pp. 6972–6981. https://doi.org/10.1021/acsami.7b19258.
Raimondi, L. *et al.* (2015) Involvement of multiple myeloma cell-derived exosomes in osteoclast differentiation, *Oncotarget*, 6(15), pp. 13772–13789. https://doi.org/10.18632/oncotarget.3830.
Rajan, N. *et al.* (2007) Preparation of ready-to-use, storable and reconstituted type I collagen from rat tail tendon for tissue engineering applications, *Nature Protocols*, 1(6), pp. 2753–2758. https://doi.org/10.1038/nprot.2006.430.
Ralston, S.H. (2013) *Bone structure and metabolism*, *Calcium and bone*.
Ralston, S.H. (2018) Davidson's principles and practice of medicine (23rd ed.). Elsevier Health Sciences., p. 6. Available at: https://www.uk.elsevierhealth.com/davidsons-principles-and-practice-of-medicine-9780702070280.html%0Ahttps://www.eu.elsevierhealth.com/davidsons-principles-and-practice-of-medicine-9780702070280.html?isbn=9780702070280&campid=CKB_book (Accessed: 25 February 2022).
Ramos, E. *et al.* (2016) Carbonic Anhydrase II Plays a Major Role in Osteoclast Differentiation and Bone Resorption by Effecting the Steady State Intracellular

pH and Ca2⩽, *Journal of Law, Medicine and Ethics*, 44(1), pp. 205–215. https://doi.org/10.1177/1073110516644211.
Raschke, W.C. *et al.* (1978) Functional macrophage cell line transformed by Abelson leukemia virus, *Cell*, 15(1), pp. 261–267.
Reches, M. and Gazit, E. (2003) Casting metal nanowires within discrete self-assembled peptide nanotubes, *Science*, 300(5619), pp. 625–627. https://doi.org/10.1126/science.1082387.
Remington, S.J. (2011) Green fluorescent protein: A perspective, *Protein Science*. John Wiley & Sons, Ltd, pp. 1509–1519. https://doi.org/10.1002/pro.684.
Reznikov, N., Shahar, R. and Weiner, S. (2014) Bone hierarchical structure in three dimensions, in *Acta Biomaterialia*. Elsevier Ltd, pp. 3815–3826. https://doi.org/10.1016/j.actbio.2014.05.024.
Riedhammer, C., Halbritter, D. and Weissert, R. (2015) Peripheral blood mononuclear cells: Isolation, freezing, thawing, and culture, *Methods in Molecular Biology*, 1304, pp. 53–61. https://doi.org/10.1007/7651_2014_99.
Rivas, M. *et al.* (2019) Peptide self-assembly into hydrogels for biomedical applications related to hydroxyapatite, *Gels*, 5(1), pp. 1–29. https://doi.org/10.3390/gels5010014.
Roscher, A. *et al.* (2016) The F-actin modulator SWAP-70 controls podosome patterning in osteoclasts, *Bone Reports*, 5, pp. 214–221. https://doi.org/10.1016/j.bonr.2016.07.002.
Ruggiero, F. and Koch, M. (2008) Making recombinant extracellular matrix proteins, *Methods*, 45, pp. 75–85. https://doi.org/10.1016/j.ymeth.2008.01.003.
Russell, R.G.G. *et al.* (2007) Bisphosphonates: An update on mechanisms of action and how these relate to clinical efficacy, in *Annals of the New York Academy of Sciences*. John Wiley & Sons, Ltd, pp. 209–257. https://doi.org/10.1196/annals.1402.089.

Sabir, M.I., Xu, X. and Li, L. (2009) A review on biodegradable polymeric materials for bone tissue engineering applications, *Journal of Materials Science*, 44(21), pp. 5713–5724. https://doi.org/10.1007/s10853-009-3770-7.

Saftig, P. *et al.* (2000) Functions of Cathepsin K in Bone Resorption, in *Adv Exp Med Biol*, pp. 293–303. Available at: http://link.springer.com/10.1007/0-306-46826-3_32.

Saiani, A. *et al.* (2009) Self-assembly and gelation properties of α-helix versus β-sheet forming peptides, *Soft Matter*, 5(1), pp. 193–202. https://doi.org/10.1039/b811288f.

Salinas, C.N. and Anseth, K.S. (2008) The influence of the RGD peptide motif and its contextual presentation in PEG gels on human mesenchymal stem cell viability, *Journal of Tissue Engineering and Regenerative Medicine*, 2(5), pp. 296–304. https://doi.org/10.1002/term.95.

Saravanan, S. *et al.* (2019) A review on injectable chitosan/beta glycerophosphate hydrogels for bone tissue regeneration, *International Journal of Biological Macromolecules*. Elsevier, pp. 38–54. https://doi.org/10.1016/j.ijbiomac.2018.10.014.

Sassi, A.P., Blanch, H.W. and Prausnitz, J.M. (1996) Phase Equilibria for Aqueous Protein/ Polyelectrolyte Gel Systems, *AIChE Journal*, 42(8), pp. 2335–2353. https://doi.org/10.1002/aic.690420823.

Schindelin, J. *et al.* (2012) Fiji: An open-source platform for biological-image analysis, *Nature Methods*. Nature Publishing Group, pp. 676–682. https://doi.org/10.1038/nmeth.2019.

Schultz, H.S. *et al.* (2016) OSCAR-collagen signaling in monocytes plays a proinflammatory role and may contribute to the pathogenesis of rheumatoid arthritis, *European Journal of Immunology*, 46(4), pp. 952–963. https://doi.org/10.1002/eji.201545986.

Shadduck, R.K. *et al.* (1993) Preparation of a monoclonal antibody directed

against the receptor for murine colony-stimulating factor-1., *Experimental hematology*, 21(4), pp. 515–20. Available at: http://www.ncbi.nlm.nih.gov/pubmed/8462660 (Accessed: 31 October 2018).
Shimada, T. *et al.* (2004) FGF-23 is a potent regulator of vitamin D metabolism and phosphate homeostasis, *Journal of Bone and Mineral Research*, 19(3), pp. 429–435. https://doi.org/10.1359/JBMR.0301264.
Shimomura, O., Johnson, F.H. and Saiga, Y. (1962) Extraction, purification and properties of aequorin, a bioluminescent, *Journal of cellular and comparative physiology*, 59, pp. 223–239. https://doi.org/10.1002/jcp.1030590302.
Shoulders, M.D. and Raines, R.T. (2009) Collagen structure and stability, *Annual Review of Biochemistry*. Annu Rev Biochem, pp. 929–958. https://doi.org/10.1146/annurev.biochem.77.032207.120833.
Sims, N.A. and Martin, T.J. (2014) Coupling the activities of bone formation and resorption: a multitude of signals within the basic multicellular unit, *BoneKEy Reports*, 3. https://doi.org/10.1038/bonekey.2013.215.
Sims, N.A. and Vrahnas, C. (2014) Regulation of cortical and trabecular bone mass by communication between osteoblasts, osteocytes and osteoclasts, *Archives of Biochemistry and Biophysics*. Academic Press, pp. 22–28. https://doi.org/10.1016/j.abb.2014.05.015.
Singh, A. and Peppas, N.A. (2014) Hydrogels and scaffolds for immunomodulation, *Advanced materials*. NIH Public Access, pp. 6530–6541. https://doi.org/10.1002/adma.201402105.
Slaughter, B. V. *et al.* (2009) Hydrogels in regenerative medicine, *Advanced Materials*. John Wiley & Sons, Ltd, pp. 3307–3329. https://doi.org/10.1002/adma.200802106.
Slaughter, B. V and Fisher, O.Z. (2009) Hydrogels in regenerative medicine, *Advanced materials*, 21(0), pp. 3307–3329. https://doi.org/10.1002/adma.200802106.Hydrogels.

Soille, P. and Vincent, L.M. (1990) Determining watersheds in digital pictures via flooding simulations, in *Visual Communications and Image Processing '90: Fifth in a Series*. SPIE, pp. 240–250. https://doi.org/10.1117/12.24211.
Soysa, N.S. and Alles, N. (2016) Osteoclast function and bone-resorbing activity: An overview, *Biochemical and Biophysical Research Communications*, 476(3), pp. 115–120. https://doi.org/10.1016/j.bbrc.2016.05.019.
Sreerama, N. and Woody, R.W. (1994) Poly(Pro)II Helices in Globular Proteins: Identification and Circular Dichroic Analysis, *Biochemistry*, 33(33), pp. 10022–10025. https://doi.org/10.1021/bi00199a028.
Sridharan, R. *et al.* (2019) Material stiffness influences the polarization state, function and migration mode of macrophages, *Acta Biomaterialia*, 89, pp. 47–59. https://doi.org/10.1016/j.actbio.2019.02.048.
Steele, D.G. and Bramblett, C.A. (1990) The Anatomy and Biology of the Human Skeleton, *Journal of Field Archaeology* [Preprint]. https://doi.org/10.2307/530029.
Stenbeck, G. (2002) Formation and function of the ruffled border in osteoclasts, *Seminars in Cell and Developmental Biology*, 13(4), pp. 285–292. https://doi.org/10.1016/S1084952102000587.
Storrie, H. *et al.* (2007) Supramolecular crafting of cell adhesion, *Biomaterials*, 28(31), pp. 4608–4618. https://doi.org/10.1016/j.biomaterials.2007.06.026.
Styner, M. *et al.* (2017) Exercise Decreases Marrow Adipose Tissue Through ß-Oxidation in Obese Running Mice, *Journal of Bone and Mineral Research*, 32(8), pp. 1692–1702. https://doi.org/10.1002/jbmr.3159.
Suda, T. *et al.* (1999) Modulation of osteoclast differentiation and function by the new members of the tumor necrosis factor receptor and ligand families, *Endocrine Reviews*, 20(3), pp. 345–57.
Suvarnapathaki, S. *et al.* (2020) Hydroxyapatite-Incorporated Composite Gels Improve Mechanical Properties and Bioactivity of Bone Scaffolds,

Macromolecular Bioscience, 20(10), p. 2000176. https://doi.org/10.1002/mabi.202000176.
Tang, A. *et al.* (2016) Self-assembling bisphosphonates into nanofibers to enhance their inhibitory capacity on bone resorption, *Nanoscale*, 8(20), pp. 10570–10575. https://doi.org/10.1039/c6nr00843g.
Tavafoghi Jahromi, M., Yao, G. and Cerruti, M. (2013) The importance of amino acid interactions in the crystallization of hydroxyapatite, *Journal of the Royal Society Interface*, 10(80). https://doi.org/10.1098/rsif.2012.0906.
Tavafoghi Jahromi, M., Yao, G and Cerruti, M. (2013) The importance of amino acid interactions in the crystallization of hydroxyapatite, *Journal of the Royal Society Interface*, 10(80).
Tavafoghi, M. *et al.* (2016) Hydroxyapatite formation on graphene oxide modified with amino acids: Arginine versus glutamic acid, *Journal of the Royal Society Interface*, 13(114). https://doi.org/10.1098/rsif.2015.0986.
Taylor, J.C. *et al.* (no date) In vitro osteoclast resorption of bone substitute biomaterials used for implant site augmentation: a pilot study., *The International journal of oral & maxillofacial implants*, 17(3), pp. 321–30.
Teitelbaum, S.L. (2000a) Bone resorption by osteoclasts, *Science*. Science, pp. 1504–1508. https://doi.org/10.1126/science.289.5484.1504.
Teitelbaum, S.L. (2000b) Bone resorption by osteoclasts, *Science*. American Association for the Advancement of Science, pp. 1504–1508. https://doi.org/10.1126/science.289.5484.1504.
Teitelbaum, S.L. and Ross, F.P. (2003) Genetic regulation of osteoclast development and function, *Nature Reviews Genetics*. Nat Rev Genet, pp. 638–649. https://doi.org/10.1038/nrg1122.
Terzi, A. *et al.* (2020) Sub- and Supramolecular X-Ray Characterization of Engineered Tissues from Equine Tendon, Bovine Dermis, and Fish Skin Type-I Collagen, *Macromolecular Bioscience*. John Wiley & Sons, Ltd, p. 2000017.

https://doi.org/10.1002/mabi.202000017.
Timothy John Eyes (2014) *PhD dissertation*. University of Manchester.
Toman, P.D. *et al.* (2000) Production of recombinant human type I procollagen trimers using a four-gene expression system in the yeast Saccharomyces cerevisiae, *Journal of Biological Chemistry*, 275(30), pp. 23303–23309. https://doi.org/10.1074/jbc.M002284200.
Tozzi, G. *et al.* (2016) Composite hydrogels for bone regeneration, *Materials*. MDPI AG, p. 267. https://doi.org/10.3390/ma9040267.
Tsai, S.W. *et al.* (2020) Collagen scaffolds containing hydroxyapatite-CaO fiber fragments for bone tissue engineering, *Polymers*, 12(5). https://doi.org/10.3390/POLYM12051174.
Tsukamoto, J. *et al.* (2017) Efficacy of a self-Assembling peptide hydrogel, spg-178-gel, for bone regeneration and three-dimensional osteogenic induction of dental pulp stem cells, *Tissue Engineering - Part A*, 23(23–24), pp. 1394–1402. https://doi.org/10.1089/ten.tea.2017.0025.
Tuck, S.P. *et al.* (2017) Adult Paget's disease of bone: A review, *Rheumatology (United Kingdom)*, 56(12), pp. 2050–2059. https://doi.org/10.1093/rheumatology/kew430.
Tuckwell, D. *et al.* (1995) Integrin alpha 2 I-domain is a binding site for collagens., *Journal of cell science*, 108, pp. 1629–37. https://doi.org/10.1074/jbc.M110.142992.
Tuckwell, D., Smith, L. and Korda, M. (2000) Monoclonal antibodies identify residues 199-216 of the integrin alpha2 vWFA domain as a functionally important region within alpha2beta1., *Biochemical …*, 350 Pt 2, pp. 485–493. Available at: http://www.ncbi.nlm.nih.gov/pubmed/10947963%5Cnhttp://www.ncbi.nlm.nih.gov/pmc/articles/PMC1221276/.
Tuckwell, D.S. *et al.* (1996) The A-domain of integrin α2 binds specifically to a

range of collagens but is not a general receptor for the collagenous motif, *European Journal of Biochemistry*, 241(3), pp. 732–739. https://doi.org/10.1111/j.1432-1033.1996.00732.x.

Turner, C.H., Wang, T. and Burr, D.B. (2001) Shear strength and fatigue properties of human cortical bone determined from pure shear tests, *Calcified Tissue International*, 69(6), pp. 373–378. https://doi.org/10.1007/s00223-001-1006-1.

U.S. Department of Health and Human Services. (2004) *Prevention and Treatment for Those Who Have Bone Diseases*, *Bone Health and Osteoporosis: A Report of the Surgeon General.* Available at: https://www.ncbi.nlm.nih.gov/books/NBK45501/ (Accessed: 25 February 2022).

Ulery, B.D., Nair, L.S. and Laurencin, C.T. (2011) Biomedical applications of biodegradable polymers, *Journal of Polymer Science, Part B: Polymer Physics*. J Polym Sci B Polym Phys, pp. 832–864. https://doi.org/10.1002/polb.22259.

Ulijn, R. V. and Smith, A.M. (2008) Designing peptide based nanomaterials, *Chemical Society Reviews*, 37(4), pp. 664–675. https://doi.org/10.1039/b609047h.

Ulijn, R. V and Smith, A.M. (2008) Designing peptide based nanomaterials, *Chemical Society Reviews*, 37(4), pp. 664–675. https://doi.org/10.1039/b609047h.

Ulubayram, K. *et al.* (2002) Cytotoxicity evaluation of gelatin sponges prepared with different cross-linking agents, *Journal of Biomaterials Science, Polymer Edition*, 13(11), pp. 1203–1219. https://doi.org/10.1163/156856202320892966.

Väänänen, H.K. *et al.* (2000) The cell biology of osteoclast function, *J Cell Sci*, 113, pp. 377–81.

Veis Novack, D. and Mbalaviele, G. (2017) Osteoclasts-key players in skeletal health and disease, *Myeloid Cells in Health and Disease: A Synthesis*, 4(3), pp.

235–255. https://doi.org/10.1128/9781555819194.ch13.
Viguet-Carrin, S., Garnero, P. and Delmas, P.D. (2006) The role of collagen in bone strength, *Osteoporosis International*, 17(3), pp. 319–336. https://doi.org/10.1007/s00198-005-2035-9.
Vitale, M. *et al.* (2022) Hydroxyapatite-decorated Fmoc-hydrogel as a bone-mimicking substrate for osteoclast differentiation and culture, *Acta Biomaterialia*, 138, pp. 144–154. https://doi.org/10.1016/j.actbio.2021.11.011.
Wada, T. *et al.* (2006) RANKL-RANK signaling in osteoclastogenesis and bone disease, *Trends in Molecular Medicine*, 12(1), pp. 17–25. https://doi.org/10.1016/j.molmed.2005.11.007.
Wahl, D.A. and Czernuszka, J.T. (2006) Collagen-hydroxyapatite composites for hard tissue repair, *European Cells and Materials*. Eur Cell Mater, pp. 43–56. https://doi.org/10.22203/eCM.v011a06.
Wan, S. *et al.* (2016) Self-assembling peptide hydrogel for intervertebral disc tissue engineering, *Acta Biomaterialia*, 46, pp. 29–40. https://doi.org/10.1016/j.actbio.2016.09.033.
Weilbaecher, K.N., Guise, T.A. and McCauley, L.K. (2011a) Cancer to bone: A fatal attraction, *Nature Reviews Cancer*, pp. 411–425. https://doi.org/10.1038/nrc3055.
Weilbaecher, K.N., Guise, T.A. and McCauley, L.K. (2011b) Cancer to bone: A fatal attraction, *Nature Reviews Cancer*, pp. 411–425. https://doi.org/10.1038/nrc3055.
Weiner, S. and Traub, W. (1992) Bone structure: from ångstroms to microns, *The FASEB Journal*, 6(3), pp. 879–885. https://doi.org/10.1096/fasebj.6.3.1740237.
Wojtowicz, A.M. *et al.* (2010) Coating of biomaterial scaffolds with the collagen-mimetic peptide GFOGER for bone defect repair, *Biomaterials*, 31(9), pp. 2574–2582. https://doi.org/10.1016/j.biomaterials.2009.12.008.

Worthington, P., Pochan, D.J. and Langhans, S.A. (2015) Peptide hydrogels - versatile matrices for 3D cell culture in cancer medicine, *Frontiers in Oncology*. Frontiers Media SA. https://doi.org/10.3389/fonc.2015.00092.

Wu, X. *et al.* (2020) Mineralization of biomaterials for bone tissue engineering, *Bioengineering*. Multidisciplinary Digital Publishing Institute (MDPI), pp. 1–24. https://doi.org/10.3390/bioengineering7040132.

Xavier, J.R. *et al.* (2015) Bioactive nanoengineered hydrogels for bone tissue engineering: A growth-factor-free approach, *ACS Nano*, 9(3), pp. 3109–3118. https://doi.org/10.1021/nn507488s.

Xing, J.Z. *et al.* (2017) RANKL release from self-assembling nanofiber hydrogels for inducing osteoclastogenesis in vitro, *Acta Biomaterialia*, 49, pp. 306–315. https://doi.org/10.1016/j.actbio.2016.12.006.

Xu, Y. *et al.* (2002) Streptococcal Scl1 and Scl2 proteins form collagen-like triple helices, *Journal of Biological Chemistry*, 277(30), pp. 27312–27318. https://doi.org/10.1074/jbc.M201163200.

Yahara, Y. *et al.* (2020) Erythromyeloid progenitors give rise to a population of osteoclasts that contribute to bone homeostasis and repair, *Nature Cell Biology*, 22(1), pp. 49–59. https://doi.org/10.1038/s41556-019-0437-8.

Yan, C. and Pochan, D.J. (2010) Rheological properties of peptide-based hydrogels for biomedical and other applications, *Chemical Society Reviews*, 39(9), pp. 3528–3540. https://doi.org/10.1039/b919449p.

Yang, Z. *et al.* (2004) Small molecule hydrogels based on a class of antiinflammatory agents, *Chemical Communications*, 4(2), pp. 208–209. https://doi.org/10.1039/b310574a.

Yasuda, H. (2021) Discovery of the RANKL/RANK/OPG system, *Journal of Bone and Mineral Metabolism*. Springer, pp. 2–11. https://doi.org/10.1007/s00774-020-01175-1.

Yeo, C. *et al.* (2009) Ficoll-paque™ versus lymphoprep™: A comparative study

of two density gradient media for therapeutic bone marrow mononuclear cell preparations, *Regenerative Medicine*, 4(5), pp. 689–696. https://doi.org/10.2217/rme.09.44.

Yoon, H.H. *et al.* (2014) Dual roles of graphene oxide in chondrogenic differentiation of adult stem cells: Cell-adhesion substrate and growth factor-delivery carrier, *Advanced Functional Materials*, 24(41), pp. 6455–6464. https://doi.org/10.1002/adfm.201400793.

Young, B., Woodford, P. and O'Dowd, G. (2014) *Wheater's Functional Histology: A Color Text and Atlas*.

Yu, Z. *et al.* (2014) Bacterial collagen-like proteins that form triple-helical structures, *Journal of Structural Biology*, 186(3), pp. 451–461. https://doi.org/10.1016/j.jsb.2014.01.003.

Yue, S. *et al.* (2020) Hydrogel as a biomaterial for bone tissue engineering: A review, *Nanomaterials*, pp. 1–25. https://doi.org/10.3390/nano10081511.

Zehnder, T., Boccaccini, A.R. and Detsch, R. (2017) Biofabrication of a co-culture system in an osteoid-like hydrogel matrix, *Biofabrication*, 9(2). https://doi.org/10.1088/1758-5090/aa64ec.

Zhang, S. (2003) Fabrication of novel biomaterials through molecular self-assembly, *Nature Biotechnology*, 21(10), pp. 1171–1178. https://doi.org/10.1038/nbt874.

Zhang, Y. *et al.* (2021) Hydrogel: A potential therapeutic material for bone tissue engineering, *AIP Advances*. AIP Publishing LLCAIP Publishing, p. 010701. https://doi.org/10.1063/5.0035504.

Zhao, D. *et al.* (2021) Poly(lactic-co-glycolic acid)-based composite bone-substitute materials, *Bioactive Materials*. Elsevier, pp. 346–360. https://doi.org/10.1016/j.bioactmat.2020.08.016.

Zhao, X. and Zhang, S. (2007) Designer self-assembling peptide materials, *Macromolecular Bioscience*. Macromol Biosci, pp. 13–22.

https://doi.org/10.1002/mabi.200600230.
Zhou, H. and Lee, J. (2011) Nanoscale hydroxyapatite particles for bone tissue engineering, *Acta Biomaterialia*. Elsevier, pp. 2769–2781. https://doi.org/10.1016/j.actbio.2011.03.019.
Zhou, L. *et al.* (2016) Structural basis for collagen recognition by the immune receptor OSCAR, *Blood*, 127(5), pp. 529–537. https://doi.org/10.1182/blood-2015-08-667055.
Zhou, M. *et al.* (2009) Self-assembled peptide-based hydrogels as scaffolds for anchorage-dependent cells, *Biomaterials*, 30(13), pp. 2523–2530. https://doi.org/10.1016/j.biomaterials.2009.01.010.
Zhuang, J. *et al.* (2012) Osteoclasts in Multiple Myeloma Are Derived from Gr-1+CD11b+Myeloid-Derived Suppressor Cells, *PLoS ONE*, 7(11), p. 48871. https://doi.org/10.1371/journal.pone.0048871.
Zou, W. and Teitelbaum, S.L. (2015) Absence of Dap12 and the αvβ3 integrin causes severe osteopetrosis, *Journal of Cell Biology*, 208(1), pp. 125–136. https://doi.org/10.1083/jcb.201410123.

Appendix A

In the following pages, the version of **Chapter 2** published on *Acta Biomaterialia* as M.Vitale *et al.* Acta Biomaterialia, 138 (2021), 144-154. https://doi.org/10.1016/j.actbio.2021.11.011 is reported. The paper has been reprinted with permission, Copyright ©, 2019, Elsevier.

Appendix B

In the following pages, the version of **Chapter 3** published on *Gels* as M. Vitale *et al.* (2022), 8, 254, https://doi.org/10.3390/gels8050254 is reported. The paper has been reprinted with permission, Copyright ©, 2019, Elsevier.